ISTANBUL TECHNICAL UNIVERSITY ★ GRADUATE SCHOOL OF SCIENCE ENGINEERING AND TECHNOLOGY

THE INFLUENCE OF UNSTEADINESS DEGREE ON HYDRAULIC CHARACTERISTICS IN OPEN CHANNEL FLOW

M.Sc. THESIS

Eryılmaz ERDOG

Department of Civil Engineering

Hydraulics and Water Resources Engineering Programme

MAY 2014

ISTANBUL TECHNICAL UNIVERSITY ★ GRADUATE SCHOOL OF SCIENCE ENGINEERING AND TECHNOLOGY

THE INFLUENCE OF UNSTEADINESS DEGREE ON HYDRAULIC CHARACTERISTICS IN OPEN CHANNEL FLOW

M.Sc. THESIS

Eryılmaz ERDOG
(501121508)

Department of Civil Engineering

Hydraulics and Water Resources Engineering Programme

Thesis Advisor: Assoc. Prof. Oral YAĞCI

MAY 2014

İSTANBUL TEKNİK ÜNİVERSİTESİ ★ FEN BİLİMLERİ ENSTİTÜSÜ

AÇIK KANAL AKIMLARINDA KARARSIZLIK DERECESİNİN HİDROLİK KARAKTERİSTİKLER ÜZERİNE ETKİSİ

YÜKSEK LİSANS TEZİ

Eryılmaz ERDOG
(501121508)

İnşaat Mühendisliği Anabilim Dalı

Hidrolik ve Su Kaynakları Mühendisliği Programı

Tez Danışmanı: Doç. Dr. Oral YAĞCI

MAYIS 2014

Eryılmaz ERDOG, a **M.Sc.** student of ITU **Graduate School of Science Engineering and Technology** student ID **501121508**, successfully defended the **thesis** entitled "**THE INFLUENCE OF UNSTEADINESS DEGREE ON HYDRAULIC CHRACTERISTICS IN OPEN CHANNEL FLOW**", which he prepared after fulfilling the requirements specified in the associated legislations, before the jury whose signatures are below.

Thesis Advisor :	**Assoc. Prof. Oral YAĞCI** İstanbul Technical University	.....
Jury Members :	**Prof. Dr. Şevket ÇOKGÖR** İstanbul Technical University	.....
	Prof. Dr. Yalçın YÜKSEL Yıldız Technical University	.....

Date of Submission : 05 May 2014
Date of Defense : 28 May 2014

To my mother and father,

FOREWORD

This master thesis was prepared at the Hydraulic Laboratory of Istanbul Technical University under the supervision of Assoc. Prof. Oral Yagcı. I can never repay him for his motivation and guidance, not only for academic pursuits but also throughout my life. He has always been much more than a supervisor to me and I would like to express my sincere thanks to him for being such an important piece of my life.

I would also like to thank Assoc. Prof. V. Ş. Özgür Kırca for his supports through all stages of this study. His willingness to share all of is wisdom and joyful support to me will never be forgotten and I'll always cherish those moments my entire life. I would like to express my heartfull thanks to him for showing me how great academic pursuits can be.

I wish to thank my jury members of my committee, Prof. Dr. Yalçın Yüksel and Prof. Dr. Şevket Çokgör for their precious support and encouragements.

I would very much like to thank my cousin Dr. İlker Comak, my dearest friend Ozgur Turan, my colleague Kadir Yılmaz for their endless help and support throughout the study.

Last but not least my sincere thanks to my mother and father. Their endless support and love kept me going throughout all stages of this study. I want express my heartfull thanks to them for being at my side no matter what.

This work has been funded by the contribution of Scientific Research Foundation of Istanbul Technical University under the project title of "Bir Taşkına Ait Hidrografın Kabarma ve Çekilme Eğrisi Kısımlarında Hidrolik Karakteristiklerin Zamansal Değişimi ".

May 2014

Eryılmaz ERDOG
(Civil Engineer)

TABLE OF CONTENTS

Page

ABBREVIATIONS

TKE **:** Turbulence Kinetic Energy
USGCRP **:** United States Global Change Research Program

LIST OF TABLES

Page

LIST OF FIGURES

Page

THE INFLUENCE OF UNSTEADINES DEGREE ON HYDRAULIC CHARACTERISTICS IN OPEN CHANNEL FLOW

SUMMARY

Due to climate change, and intese rainfall events unsteady flow and flood occurs more frequently globally in recent years. The unsteady conditions changes all the formulas created by single value approach and injustifies it. The unsteady flow conditions and its efects on hydraulic characteristics is investigated in the present study.

The hysterisis effects are very significant features of unsteady flows. The hysterisis of hydraulic characteristics and the relationship between unsteadiness and hysterisis pattern is observed for different types of flow conditions.

In this experimetal study, different types of hydrographs are generated under controlled laboratory conditions with a globe valve and a control unit. The flow velocities were measured with two ADVs and with two acoustic sensors water depth values were simultaneous recorded troughout the each experiment.

The experimental data is analyzed and the variation of hydraulic characteristics during the passage of an unsteady flow is calculated. The variaton of flow parameters with respect to both time and water depth calculated and represented in the study. For each experiment, all of the hydraulic parameters showed an hysterical pattern. This clearly showed the influence of unsteadiness on hydraulic characterisitcs in unsteady flows.

A quantification for hysteresis is made by an dimensionless number which represent the size of the hysterical loop. Based on this quantification the realtionship between hysterisis and unsteadiness degree is observed. The results clearly showed that for increasing values of unsteadiness degree, hysteresis effects also increases.

A criterion was derived to decide about whether the flow condition is unsteady or not. Based on this creteria is decided that if the unsteadiness degree is under the interval of 0.01-0.02 the flow can be considered as steady and single value approach can be applicable. But for the flows having a larger unsteadiness degree than this treshold value, the flow definitely should be considered as unsteady and hysterical effects are not neglectable.

AÇIK KANAL AKIMLARINDA KARARSIZLIK DERECESİNİN HİDROLİK KARAKTERİSTİKLER ÜZERİNE ETKİSİ

ÖZET

Doğada karşılaşılan akımların büyük bir çoğunluğu karasız özellik sergilerler. Son yıllarda yaşanan iklim değişiklikleri nehir akımlarını büyük ölçüde etkilmiştir. Şiddetli ve ani yağışlar taşkınlara sebebiyet vermekte ve bu sebeple bir taşkının veya değişken bir akımın geçişi sırasında hidrolik özelliklerinin ne derecede değiştiğinin saptanması büyük önem kazanmıştır.

Kararsız akımlar belli bir bölgede hidrolik özelliklerin zaman içerisinde değiştiği akım tipleridir. Bu tip akımların hidrolik olarak incelenmesi zor olması sebebiyle genel olarak çoğu hidrolik mühendislik formülü kararlı akım kabulü ile çıkarılmıştır. Her ne kadar bu kabül faydalı ve kullanışlı olsa da değişken akım koşullarını tanımlamak konsusunda yeterli olamazlar. Bu sebeple hidrolik formüllerin kararsız akım koşullarına göre düzeltilmeleri gerekmektedir.

Kararsız akımların hidrolik özellikler üzerinde en önemli etkilerinden biri histerik etkilerdir. Histerik etkiler bir hidrolik özelliğin, aynı derinlik ve koşullar altında farklı özelliker göstermesi durumudur. Histerik etkilerin incelenmesi, bu çalışmada önemli amaçlarından biridir.

Bir akım ortamında değişken bir akımın geçişi ele alındığında, bu durum seviyenin yükselmesi ve seviyenin alçalması olarak iki evreden oluşmaktadır. Histerik etkiler bu akım koşullarında çok net olarak gözlenir. Değişken akımın geçişi boyunca su seviyesi-debi grafiği çizilecek olduğunda aynı su derinliği için seviyenin yükselmesi evresinde daha yüksek, seviyenin alçama evresinde ise daha düşük debi gözlenir.

Bu çalışmada değişken akımların hidrolik özellikleri nasıl ve ne seviyede etkilediğini araştırmak amaçlanmıştır. Bu sebeple İstanbul Teknik Üniversitesi, Hidrolik Laboratuvarında deneyler yapılmıştır. 26 m uzunluğunda ve 1 m genişliğinde bir kanalda akım deneyleri gerçekleştirilmiştir. Bu deneyler iki setten oluşup ilk set 20 cm eşik derinliği ile ikinci set ise 14 cm eşik derinliğinde gerçekleştirilmiştir. Kontrol edilebilir vana sayesinde debi regüle edilerek farklı tiplerde hidrograflar oluşturacak akımlar yaratılmıştır.

Deneyler boyunca hız ve su derinliği ölçümleri alınmıştır. Hız ölçümleri ADV cihazları, su derinliği ölçümleri ise akıma temas etmenden ölçüm alabilen akustik sensörler ile 100 Hz freakansla yapılmıştır. İki hız ölçüm cihazı ile hem taban hem de serbest su yüzü için hız değerleri alınmıştır. İki akustik sensör biri hız ölçüm aletlerinden menba tarafında diğeri ise mansap kısmında olacak şekilde yerleştirilmiştir. Bütün ölçüm aletleri birbiri ile senkronize edilmiş ve tüm aletler aynı anda ölçüm almaya başalatılarak deneyler gerçekleştirilmiştir.

Alınan veriler bilgisayar ortamında incelenmiştir. ADV hız ölçüm cihazları her ne kadar kullanışlı ve isabetli sonuç veren cihazlar olasalarda bazı sebeplerden aykırı değerler verebilmektdir. Bu sebeple, verilerde bir gerçek dışı gözlem oluşmaması için ilk olarak veriler literatürde sıkça kullanılan bir metod ile aykırı değerlerden arındırılmıştır.

Temizlenen veri setleri analiz edilmiştir. Analizler için ilk olarak hız ve su derinliği ölçümlerinin zamansal ortalamaları alınmıştır. Bu sayede hız değerleri ortalama ve çalkantı bileşenleri olarak ikiye ayrılmış ve çalışmanın önemli kısımlarından biri olan türbülans bileşenleri hesaplanabilir hale gelmiştir.

Zamansal olarak ortalamaları alınan tabandan serbest su seviyesi kadar olan noktalar her an için tabandan su seviyesine kadar birleşitirilerek anlık hız profilleri elde edilmiştir. Hız profilleri derinlik boyunca integre edilerek anlık debi değerleri bulunmuştur. Bulunan debi su derinliğine bölünerek derinlik boyunca ortalama hız elde edilmiştir. Derinlik boyunca ortalama hızın elde edilmesi akım özelliklerini tanımlayıcı Reynols ve Froude sayıları hesaplanmıştır.

Hidrolik parametrelerin bulunması ile tüm hidrolik parametrelerin değişken akımın geçişi boyunca su derinliğine göre nasıl değiştiğini gözlemlenmiştir. Yapılan tüm deneyler için bütün hidrolik değerler histerik etkiler gösterdiği görülmüştür.

Akımın çalkantı bileşini kullanılarak, değişken akımın geçişi süresince türbülans kinetik enerjisi hesaplanmıştır. Bulunan değer taban akışı için elde edilmiş olan türbülans kinetik enerjisine bölünerek birimsiz hale getirilmiştir. Bu aşamadan sonra su derinliği makisimum su derinliğine bölünerek boyutsuz hale getirilmiş ve bu iki boyutsuz değer bir grafiğe çizilmiştir. Diğer tüm hidrolik parametreler gibi türbülans da değişken akım boyunca histerik karakteristik göstermiştir.

Çalışma kapsamında histerik etkilerin ne ölçüde değiştiğini gözlemlemek için histerik etkiler boyutsuz olarak sayısallaştırılmıştır. Bunun için bir döngü şeklinde olan histerik grafiklerin dikey ve yatay olarak genişlikleri çarpılmış ve bu boyutsuz sayıyla göre histerik etki tanımlanmıştır. Bu sayı ne kadar büyük olursa histeri o kadar fazla etkin ve ne kadar küçük olursa histeri o kadar etkisiz olarak değerlendirilmiştir. Geniş diyagrama sahip olan grafikler dolayısıyla daha büyük histeriye sahip olup dar diyagramlar etkisiz histeriye sahip olacaktır.

Bu düşünceden yola çıkarak histerik etkilerin sayısallaştırılması kıyaslanmalarını sağlamıştır. Bu sayede her zamansal değişkenlik derecesine karşılık gelen histeriklik değeri bir grafiğe çizilmiştir. Bu grafikler açıkça göstermiştir ki artan kararsızlık dereceleri histerik değerleri net bir şekilde arttırmaktadır.

Çalışmanın bir başka önemli sonucu ise akımların kararlı ya da kararsız olarak tanımlanmasını sağlayacak bir kriterin geliştirilmiş olmasıdır. Histerik etkiler ve kararsızlık derecesinin aynı grafiğe çizilmesinin ardından değerler bir eğilim çizgisi ile birleştirilmiştir. Bu eğilim çizgilerinin grafiğin kararsızlık derecesini kestiği yer histerinin sıfır olduğu yer olması sebebiyle ile bu noktaya kararsızlık etkilerinin belirginleşmeye başladığı yer denmiştir. Bu nokta kararsılık derecesinin 0.01-0.02 arasındaki bölgeye denk gelmektedir.

Çalışma göstermiştirki kararsızlığın etkili olmaya başladığı değerden yüksek kararsızlağa sahip akımlar kararsız akım olarak değerlendirilip formüller ona göre düzeltilmelidir. Bu değerin altına kararsızlığa sahip olan akımlar ise kararlı olarak kabul edilip kararlı akım formülleri geçerli olarak kullanılabilir.

1. INTRODUCTION

1.1 Definition and Significance of the Topic

In natural streams most of the flow has an unsteady character. The flows which occur as a result of intensive precipitation with short duration, tends to create flow with unsteady character, i.e. infrequent floods. This flow types exhibits a destructive and disastrous effects on human made structures. Also for self formed natural channels, channel forming discharges has unsteady character in a great extent.

Wheras flood have catastrophic effects on human made structures as stated above, on the other hand these flows with spiky hydrographs have a vital function in ecosystem. A flood affect ecology by rearranging the streambed habitats, scouring away aquatic plants and increasing the drift of insects (Gordon et. al. , 2004).

Due to the increasing climate change effect, in recent years temporal distribution of precipitations has changed at a considerable degree. Today, owing to this effect the rainfall characteristics has altered and intense precipitation with short duration cause to more spiky hydrographs compared that of it used to be. More specifically, according to USGCRP, 2009, the quantity of rain falling during the most intense 1% of storms increased by almost 20% in the last 50 years.

In addition to varying precipitation characterisitcs recently, in the rivers located in semi-arid zones, these afferomentioned channel forming sudden and sporadic flow conditions (i.e. ephemeral hydrographs) take part more markedly. Desert streams and steep confined valley streams are mostly subject to infrequent flashy flow condition, so the channel-forming flow conditions are taking place predominantly during the passage of ephemeral hydrographs for these streams. These floods with spiky hydrographs are in the unsteady flow character and they have a great capability of changing the conveyance capacity of the main channel as well as the floodplain characteristics.

The hysterisis of flow parameters causes a major concern for unsteady flows. The existence of this hysterical pattern makes it harder to describe the flow properties in

unsteady flows. In unsteady cases the assumption of flowrate will be the function of only water depth will not be justified. For the same water depth value, discharge generally takes different values during the rising and the falling limps of a typical hydrograph (Holtan and Overton, 1964).

1.2 Objective and Scope of the Study

As mentioned above, for unsteady flows hysterical effects plays a significant role on hydraulic characteristics during the passage of the sudden flows. In other words, for a given channel the same discharge does not generates the same water depth due to the hysterical effect. Yet, most of the hydraulic formulas such as Manning-Strcikler and Chezy were developed on the basis of single-value concept. These equations do not take the hysterical effects into account. At this stage, the main goal of this study is to bring a better understanding to the influence of unsteadiness degree of hydrograph on the hydraulic characteristics.

Since it's known that the hysterical effect injustify single value concept, an understanding between unstadiness and hystresis is needed. In which unsteadiness condition what level of hysterical patterns occur on some main flow and turbulence components ? The influence of unsteadiness on hysterical effects is investigated.

Another major goal of this study is creating an understanding of steady and unsteady state alteration. It has been said that for unsteady flow the hysterical effects should be taken into account. But most of the time these effects can be negligibly small. A criterion is needed to state from which point hysteresis cannot be neglected. Which flows can be considered as steady and which flows cannot be? To state a quantitative criterion that defines the threshold above which unsteadiness should be taken into account was another objective of this study.

In second chapter, the literature review on unsteady flow and hysterical effects is presented. The definition of unsteady flow and it effects on basic governing equations is given. Saint-Venant equation and its basic implactions and the hysterical loops of water depth-discharge are presented. The role of unsteadiness in streambed and armoring processes is pointed. The effects of hysteresis patterns on hydraulic parameters are closely investigated through the literature.

In third chapter, the experimental setup is given. The laboratory conditions and flume properties are presented. The measurement devices and their utilizations in this study are demonstrated abased on some definition sketch.

In chapter four, the method of analysis is described. The used formulas and their derivations are briefly presented to make a better understeanding on the carried out analysis in this study.

In chapter five, results of the carried out analysis are given. By the light of the given results discussion are made to get the answers of questions presented above. The effect of hysteresis patterns on hydraulics parameter investigated to state a cretira that defines which flows are steady or unsteady.

In last chapter, conclusions of discussion on main questions are given. To main drives of this study, namely, hysterical effects of spiky hydrographs on the variation of hydraulic characteristics in open channel flow and stating a quantitative criterion that defines the threshold above which the unsteadiness should be taken into account are concluded.

1.3 Method

To attain the afferomentioned objective above of the study a laboratory experiment has been undertaken under controlled conditions. During the experiments unsteady flow conditions each having different unsteadiness degree were generated. Specially dense and temporally frequent velocity measurements were conducted throughout the passage of the unsteady flow. It is aimed to acquire mean flow and turbulence characteristics during the rising falling limbs of the hydrograph.

2. LITARATURE REVIEW

2.1 Basics of Unsteady Flow and Governing Equations

2.1.1 Unsteady flow

Vast majority of flows in hydraulic problems show an unsteasy character in nature. A flow can be classified as unsteady if flow properties such as velocity and depth changes with time. In many cases it is necessary to study the flow only under steady conditions. But when the change in flow conditions with respect to time is a major of concern, then the flow should be treated as unsteady (Chow,1959). By its definition for unsteady flows

$$\frac{\partial u}{\partial t} \neq 0 \tag{2.1}$$

in which *u* is velocity and *t* is time(Sumer et al., 2007). In this situation, acceleration and force formulizations in steady flows will be invalid and new adjustments will be needed.

2.1.2 Governing equations

When adjusting the formulas for unsteady conditions, fisrt observation will be the changes in friction effects. For an open channel, shear stess can be formulated like

$$\tau_0 = \gamma \cdot R \cdot S_f \tag{2.2}$$

in which S_f is friction slope. For steady conditions friction slope is equal to enegy slope, $\partial H/\partial x$, but under unsteady conditions local acceleretions dictate an alteration in this formula.

$$\frac{\partial H}{\partial x} = \frac{\partial}{\partial x}(h + \frac{u^2}{2g}) \tag{2.3}$$

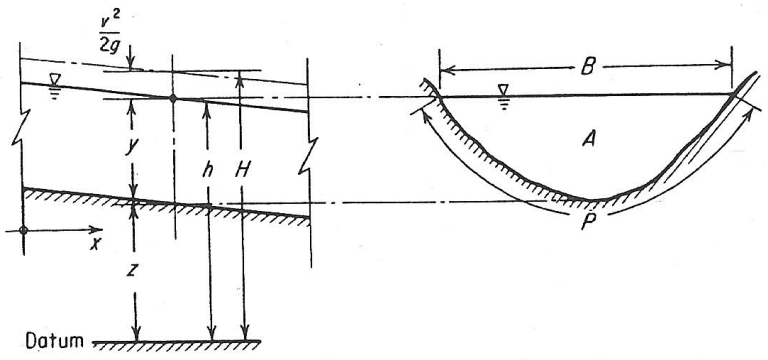

Figure 2.1 : Definition Sketch for the Equations of Motion (Henderson,1996).

To allow variation with time, acceleration can be written as

$$a_x = u\frac{\partial u}{\partial x} + \frac{\partial u}{\partial t} \tag{2.4}$$

which creates a more general expression. Therefore the equation of motion becomes

$$-\gamma A\Delta h - \tau_0 P\Delta x = \rho A\Delta x(u\frac{\partial u}{\partial x} + \frac{\partial u}{\partial t}) \tag{2.5}$$

$$\tau_0 = -\gamma R\left(\frac{\partial u}{\partial x} + \frac{v}{g}\frac{\partial u}{\partial x} + \frac{1}{g}\frac{\partial u}{\partial t}\right) \tag{2.6}$$

$$\tau_0 = -\gamma R\left(\frac{\partial H}{\partial x} + \frac{1}{g}\frac{\partial u}{\partial t}\right) \tag{2.7}$$

from **(1.3)** (Henderson,1966). A more radical rearrangement can be made by expressing energy slope by taking in consederation that $h = z + y$ and friction slope is $S_0 = -\partial z/\partial x$, which leads to

$$\frac{\partial H}{\partial x} = -S_0 + \frac{\partial u}{\partial x} + \frac{u}{g}\frac{\partial u}{\partial x} \tag{2.8}$$

Hence, friction slope S_f is

$$\underbrace{\underbrace{\underbrace{S_f = \overbrace{S_0}^{\text{steady}}}_{\text{uniform flow}} - \frac{\partial y}{\partial x}}_{\text{steady nonuniform flow}} - \frac{u}{g}\frac{\partial u}{\partial x}}_{\text{unsteady nonuniform flow}} - \frac{1}{g}\frac{\partial u}{\partial t}\frac{u}{g}\frac{\partial u}{\partial x} \tag{2.9}$$

(1.9) clearly show how nonuniformatiy and unsteadines introduce extra terms into the dynamic equation (Henderson,1966).

The equation of continuity for an unsteady flow is

$$\frac{\partial Q}{\partial x} + B\frac{\partial y}{\partial t} = 0 \qquad \textbf{(2.10)}$$

In which B is the surface width as in **Figure. 2.1**. The subsutation of $Q = u \cdot A$ leads **(1.8)** to

$$A\frac{\partial u}{\partial x} + u\frac{\partial A}{\partial x} + B\frac{\partial y}{\partial t} = 0 \qquad \textbf{(2.11)}$$

In which this three well known terms as prism storage, wedge storage and and rate-of-rise terms respectively. This significant terms, which describes storage in open channel in a very reasonable level, will be detailed in next chapter.

2.2 Flood Routing

The procedure of determining flow properties of an unknown point from a known hydrogpah at one point is called *flow routing*. If the flow is a flood then the procedure is specifically called *flood rooting* (Chow,1959). Two types of models can be used in studying this phenomenon, namely these are hydraulic methods and hydrologic methods. Hydraulic models are based on continuity and momentum equations while hydrologic models are using continuity equations only (Bayazıt,2003).

2.2.1 Hydraulic models for flood rooting

Changes in flow properties with respect to both time and space are taken in consideration by hydraulic models. Hence, they use not only continuity equations but also momentum equations. Through this model floodplains can be taken under protection by determining changes in velocity and water depth along the river. Hydraulic models are also widely use for determining rain and snow water effects to the downstream.

2.2.1.1 Saint Venant Equations and Reynolds Transport Theorem

Rivers are an example for an unsteady flow. When modeling in such zones with respect to time and space, Saint Venant Equations are highly used. This equations are introduced by Barre de Saint-Venant in 1871. This equations consist 6 assumptions:

1) The flow is one dimensional.
2) Flow is assumed to vary gradually along the channel.
3) The longitudinal axis of the channel is approximated as a straight line.
4) The effects of scour and deposition are negligible.
5) Manning's Equation can be used to describe resistance effects.
6) The fluid is incompressible.

By using Reynolds Transport Theorem with this 6 assumptions Saint-Vennat equations are derived.

While making calculations in a control volume (Eulerian approach) Reynolds Transport Theorem is widely used. This theorem distinguishes two types of flow properties, namely these are *extensive* properties, whose values depend on the amount of mass present, and *intensive* properties, which are independent of mass (Chow,1959). In this theorem for any extensive propery *B*, a corresponding intensive property β can be defined as

$$\beta = \frac{dB}{dm} \tag{2.12}$$

(2.12) is rearranged by integrating over a control volume by substuting $dm = \rho d\forall$

$$B = \iiint \beta \rho d\forall \tag{2.13}$$

in which $d\forall$ is a shaded element of volume. In this formula *B* can be any extensive property. Any change in *B* with respect to is given as

$$\frac{dB}{dt} = \frac{d}{dt}\dot{\iiint}_{c.v} \beta \rho d\forall + \dot{\iint}_{c.s} \beta \rho \mathbf{V} \cdot \mathbf{dA} \tag{2.14}$$

In **2.14**, product of velocity vector and normal area vector donetoed by $\mathbf{V} \cdot \mathbf{dA}$. Reynolds Transport Theorem state that total change of an extensive property is equals to *total rate of change of extensive propert stored in the control volume* plus *the net outflow of extensive property trough the control surface* (Chow,1959).

When deriving the continuity formulations for Saint Venant Equations, Reynolds Trasnport Theorem is used. If extensive property *B* is chosed as mass "*m*" then the continuity equation will be found by Reynolds Transport Theroem. By the law of conservation of mass

$$\beta = \frac{dB}{dm} = \frac{dm}{dm} = 1 \qquad \frac{dB}{dt} = \frac{dm}{dt} = 0 \tag{2.15}$$

Substuting the foundings in **2.15** to Reynolds Transport Theorem

$$0 = \frac{d}{dt} \dot{\iiint}_{c.v} \rho d\forall + \dot{\iint}_{c.s} \rho \mathbf{V} \cdot \mathbf{dA} \tag{2.16}$$

gives the continuity equation. For deriving Saint Venant Equations for continuity, **2.16** is rearranged with necessary adjustments. In a flow envoriment such described like **Figure 2.2** , there will be inflows both coming from upstream which is denoted by *Q* and lateral inflow which denoted by *q*. When inflow and outflow of the control volume formulated separately

$$\dot{\iint}_{inflow} \rho \mathbf{V} \cdot \mathbf{dA} = -\rho(Q + qdx) \tag{2.17}$$

$$\dot{\iint}_{\text{çıkan}} \rho \mathbf{V} \cdot \mathbf{dA} = \rho \left(Q + \frac{\partial Q}{\partial x} dx \right) \tag{2.18}$$

The rate of change mass stored within the control volume is

$$\frac{d}{dt} \dot{\iiint}_{c.v} \rho d\forall = \frac{\partial(\rho A dx)}{\partial t} \tag{2.19}$$

Where the partial derivatie is used because the control volume is fixed in size. Finally the putting all together the calculations in **2.17**, **2.18** and **2.19** and also

reminding that the fluid is incompressible so density is constant Saint- Venant continuity equations will appear like

$$\frac{\partial Q}{\partial x} + \frac{\partial A}{\partial t} - q = 0 \qquad \textbf{(2.20)}$$

after necessary reaarengments. This equation is valid for both prismatic and nonprismatic channels.

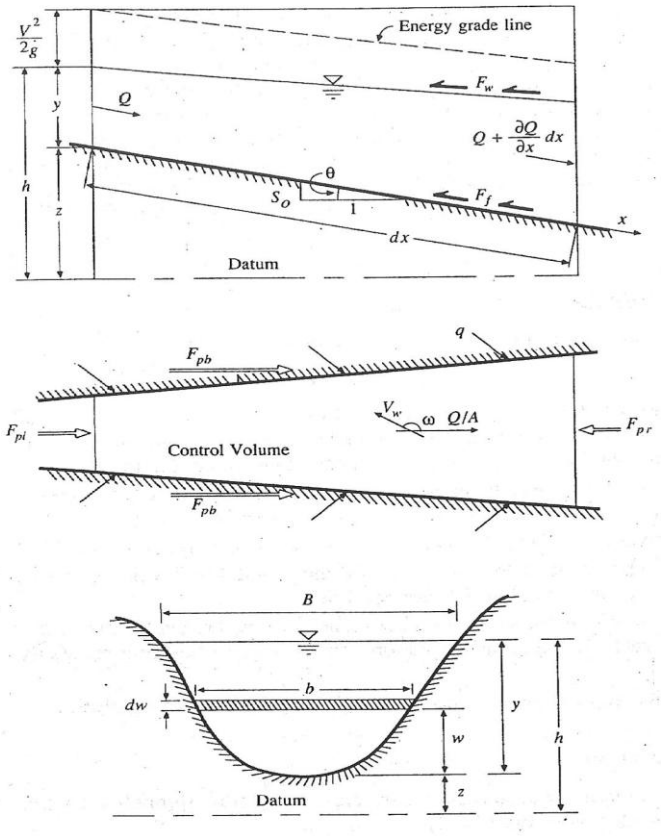

Figure 2.2 : Channel for the derivation of Saint-Venant Equations (Chow,1959).

Saint-Venant Momentum equations are also derived with Reynolds Transport Theorem. If the extensive property *B* is taken as momentum by Newton's second law

$$B = m \cdot \boldsymbol{V} \;\rightarrow\; \beta = \boldsymbol{V} \;\rightarrow\; \frac{dB}{dt} = \frac{d(mV)}{dt} = \Sigma F \qquad \textbf{(2.21)}$$

. Substuting the foundings in **2.21** to Reynolds Transport Theorem

$$\Sigma F = \frac{d}{dt} \dot{\iiint}_{c.v} \mathbf{V} \rho d\forall + \dot{\iint}_{c.s} \mathbf{V} \rho \mathbf{V} \cdot \mathbf{dA} \qquad \textbf{(2.22)}$$

which gives the momentum equation. For obtaining Saint-Venant momentum equation fisrt of all forces should be deifend.

$$\Sigma F = F_g + F_f + F_e + F_w + F_p \tag{2.23}$$

in which F_g is the *gravitiy force*, F_f is the *friction force*, F_e is the *contraction/expansion force*, F_w is the *wind shear force* and F_p is the *unbalanced pressure force*. Formulatin all thos in details will lead to

$$\Sigma F = \rho g A S_0 dx - \rho g A S_f dx - \rho g A S_e dx - W_f B \rho dx - \rho g A \frac{\partial y}{\partial x} dx \tag{2.24}$$

When momentum inflow and outflow of the control volume formulated separately

$$\iint_{inlet} \mathbf{V}\rho\mathbf{V} \cdot \mathbf{dA} = -\rho(\beta V Q + \beta v_x q dx) \tag{2.25}$$

$$\iint_{outlet} \mathbf{V}\rho\mathbf{V} \cdot \mathbf{dA} = \rho\left[\beta V Q + \frac{\partial(\beta V Q)}{\partial x} dx\right] \tag{2.26}$$

The time rate of change in momentum storage is

$$\Sigma F = F_g + F_f + F_e + F_w + F_p \tag{2.23}$$

Finally the putting all together the calculations in **2.17**, **2.18** and **2.19**

$$\frac{\partial Q}{\partial t} + \frac{\partial(\beta\, Q^2/A)}{\partial x} + gA\left(\frac{\partial h}{\partial x} + S_f + S_e\right) - \beta q v_x + W_f B = 0 \tag{2.28}$$

Neglecting lateral inflow, wind shear, and eddy loses and assuming β=1, **2.28** and **2.29** will be respectively continuity eqauation and momentum equatinon of Saint-Venant.

$$\frac{\partial Q}{\partial x} + \frac{\partial A}{\partial t} - q = 0 \tag{2.28}$$

$$\underbrace{\frac{1}{A}\frac{\partial Q}{\partial t}}_{\substack{Local \\ Accelaration}} + \underbrace{\frac{1}{A}\frac{\partial}{\partial x}\left(\frac{Q^2}{A}\right)}_{\substack{Convective \\ Accelaration}} + \underbrace{g\frac{\partial y}{\partial x}}_{Pressure} - g\left(\underbrace{S_0}_{Gravity} - \underbrace{S_f}_{Friction}\right) = 0 \tag{2.29}$$

2.2.2 Hydrologic model for flood routing

In flood routing in chanelds for handling a variable discharge-storage relationship most widely used method is *Muskingam Method*. This method is called by this name beacuse is is firstly used by U.S Corps of Engineers in Ohio,USA Muskingum River at 1871. This method divides the storage in a channel to two, namely *wedge storage* and *prism storage*. *K* being proportionality ceofficent, the volums of storage as prsim equals to *KQ*, and *X* being weightning factor, the volume of storage as wedge equals to $KX(I-Q)$.

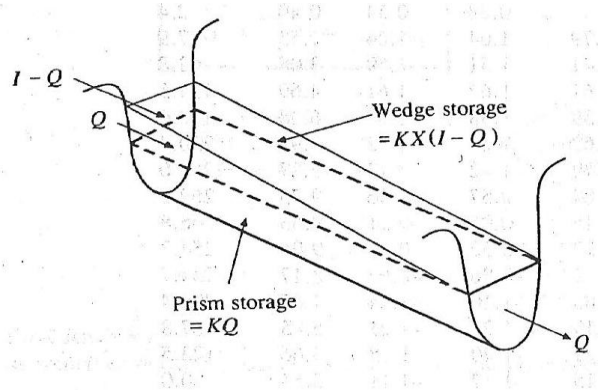

Figure 2.3 : Prism and Wedge Storage in a channel reach (Chow,1959).

The reason behind wedge and prism storage formation in channels is, during the advance of a flood wave, inflow exceeds outflow, hence wedge is producted. On the other hand during the recession, outflow exceeds inflow, hence negative wedge is produced. According to Musking Method the volume will be stored as wedge and prism in a channel is

$$V = K[Q + X(I - Q)] \tag{2.30}$$

As it can be seen form 2.30, the assumption of the amount of storage is a function of outflow alone is no longer valid. Storage is function of both inflow and outflow.

$$I - Q = \frac{dV}{dt} \tag{2.31}$$

When the formulas rearranged with the coefficients of Muskingum method

$$\frac{1}{k_1} = K(1-X) \quad \frac{1}{k_2} = KX \;\rightarrow\rightarrow\; \frac{dQ}{dt} + k_1 Q = k_1 I - \frac{k_1}{k_2}\frac{dV}{dt} \tag{2.32}$$

equations are obtained. Mutliplying both sides of the **2.33** with $e^{k_1 t}$ ant integrating both sides lead to

$$Qe^{k_1 t} = \int \left(k_1 I - \frac{k_1}{k_2}\frac{dV}{dt}\right) e^{k_1 t} dt \qquad \textbf{(2.34)}$$

Huge amount of resources in literature for solving the integral in **2.34**.

Even tough muskingam method is a widely used method, it can't be said it is logically complete (Henderson,1966). Calculation of I and Q does not alwas give the corrects answers for storage. According to Chezy equation

$$Q = CA\sqrt{RS_f} \qquad \textbf{(2.35)}$$

gives the flow. Subsutution of S_f value for an unsteady flow leads to

$$Q = CA\sqrt{R(S_0 - \frac{\partial y}{\partial x} - \frac{u}{g}\frac{\partial u}{\partial x} - \frac{1}{g}\frac{\partial u}{\partial t})} \qquad \textbf{(2.36)}$$

In 2.36, because of the reason that S_0 much too bigger than other terms, the other terms can be neglected. In this case *Q* will be the function of *h* only and Muskingum Method will be justified. Even tough most of the time this conditions ocur, *Q* is only related to *h* asssumption is not valid. A diagram like Figure is observed.

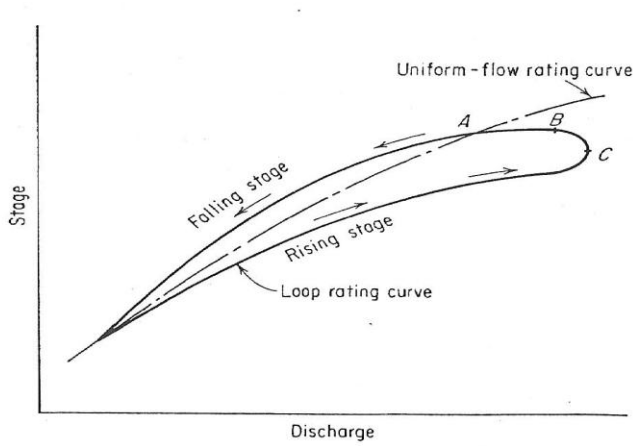

Figure 2.4 : Stage-Discharge Relationship During a Flood (Henderson,1966).

2.3 The Role of Unsteadiness on Bedload Transport and Armoring Processes

Bed forms are a very common in alluvial channels, and they are the main driever of river morphology. While understanding and modelling bedload formations having such significance for most types hydraulics engineering endeavours, and also for ecologist and fluvial geormorphologists, it is a very challenging especially for filed measurements.

The unsteadines plays an improtant role in sedimet trasport processes. Most of the sediment formuluzations come from flume experiments. But flume experiments ussuliay carried out under steady conditions which does not approximate field conditions (Mao,2012).

In an unsteady nature of flow, losts of sediment transport properties show different characterisitcs in rising and falling stages whicih is called hysteris. In gravel beds sediment trasnprot shows and hysteric nature due to differences in sediment availability between rising and falling stages. For different types of unsteady flow contions created in labartory, results show that in all types of them sediment transport during the falling stage is less than during risisng stage. Even it is valid for all types of hydrographs, for low magnitude hydrgraphs this hysterisi is more evident.

The grain size of bed on the other hand, shows a diiferent pattern. Laboroty study shows that even under different types of hydrographs, the grain size of the bed remains essentially constant (Wilcock et al., 2001). Despite of the fact the grain size remains constant, the grain size of transported sediment exhibit counter-clockwise hysterisis (Mao, 2012).

Due to temporal lags flow and sediment transport, hysteric effects are observed in sediment transport for flood events. If the peak of the sediment transport occurs before the peak of flow discharge, the hysteric pattern is called clockwise. Lots of reasons can be behind this incident, such as early rupture of static armor, time lags in sediment supply or loose materials left form an earlier flood(Mao, 2012). If the peak of the sediment transport occurs after the peak of the flow discharge, the hysteric pattern is called counter clockwise. The counter clockcwise sediment transport hysterisis may be realted to bed form development lagging changes in flow, well

established armor layers and consodilation of grains during intraflood periods (Mao,2012).

Because of different sediment availablity in rising and falling stages of and fallins stages bed load hysterisis obsevred. Even for different variations of sediment availability conditions, bed load exhibits a clockwise pattern.And all types of hydrogrphs and sediment recirculations bed sediment size appears relatively invarient.

Another hysteresis pattern is observed for mobility. During the falling stage mobility reduces. Percantage of active grains shows difference between rising and falling stages. In rising stage percentage of active grains is larger then falling stage, hence the grains are easily mobilized before the peak of the hydrograph which means clockwise hysteresis.

The Figure 2.5 shows different patterns of hysteresis circles for different properties such as, grain size of transported sediment(D_t), grain size of bed surface(D_s), correlation length scale(L_x), scaling region(H_x), the standard deviation of bed surface elevation(σ), percentage of active grains of each size entraind from the bed(Y_i), refenrence shear stress (τ_r).

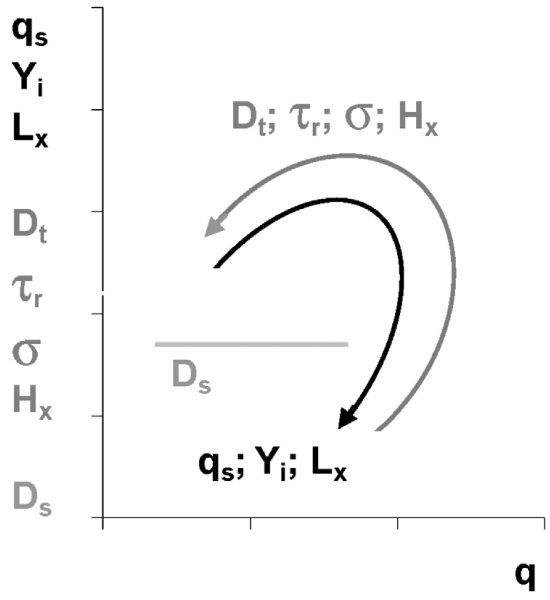

Figure 2.5 : Conceptual Scheme of Hysteris Cycles (Mao,2012).

Analysis of the flow sediment hysteresis shape may assist in determining the sediment source area in a small basin. A clockwise hysteresis occurs when sediment is derived from the bed and banks of the channel or areas adjacent to the channel, whereas an anti-clockwise hysteresis occurs when the upper part of the slopes is the sediment source area (Klein, 1984).

In an other study (Alexandrov et al., 1996) relations between suspended sediment concentration and water discharge during flash floods in an ephemeral stream of the northern Negev are analysed. Only 50% of the variance in suspended sediment concentration is explained by variations in discharge. This indicates that changes in sediment supply and variations in the importance of source areas are also significant in this semi-arid water catchment. Hysteresis between rising and falling limbs of the flood hydrograph is shown to contribute a considerable amount of indeterminacy at individual flood level. However, any attempt at partitioning the entire database in order to derive separate rating relations for rising and falling limbs has been confounded by the fact that the hysteresis can be clockwise and counterclockwise in successive floods for reasons that are not yet fully understood.

For two decades, research on gravel-bed rivers has focused on the important role that an armour layer plays in initiation of motion and how its disruption at times of flood releases considerable amounts of fine bed material from the subsurface. However, fine bed material is mobilized from patches prior to that being released from beneath an armour layer; it is therefore the initial source of bedload under conditions of initial motion.

According to another sytudy (Picouet et al., 2000) the relationship between suspended sediment concentration and water discharge by using the data collected at two monitoring stations of the African tropical Upper Niger river is investigated. At each gauging station on the Niger river, a clockwise hysteresis was observed in the relationship between water discharge and suspended sediment concentration during the annual flood (Ahanger et al., 2008).

2.4 The Effect of Unsteadiness on Hydraulic Parameters

Tu and Graf (1993) used friction velocity as a key parameter to describe the impact of rising and falling satges of different hydrographs on friction. They computed two

different friction velolcity: one from St. Venant Eq. and one from steady uniform flow formula. Also, in order to characterize the unsteadiness of the flow they employed the parameter β which is the ration of the forces due to longitidunal pressure and the ones due to friction (positive values of beta indicates decelerating and negative ones indicates accelerating). Their experimental findings indicated that for an equal water in a hydrograph the true value of friction velocity and thus the bottom shear stress is larger in the rising branch than the one in falling branch. They also revealed that the true value of friction velocity reaches its maximum always before the maximum water depth.

Song and Graf (1996) experimentally studied unsteady flow properties in an open channel with a rough bed. Unsteady flow can be characterized by the overall unsteadiness parameter, , and by the longitudinal pressure-gradient parameter. Using the equation of Reynolds, they obtained a theoretical expression for the Reynolds-stress which compares reasonably well with the measured data. Additionally they drawn the following major conclusions from their experimental data:

- For an equal water depth, the horizontal point velocities in the rising branch are generally larger than the ones in the falling branch. The larger the unsteadiness-values, the more is this difference.

- During the passage of a hydrograph, the turbulence intensities (root-mean-square values) and the Reynolds stress in the rising branch are larger than in the falling branch.

Acrording to the study of Nezu et al. (1997) in the rising stage, the concentration of suspended sediment increases due to the kolk-boil vortex because the rising stage corresponds to the growing period of dunes; separated vortices from a dune crest collide intermittently at the next dune and wash out bed materials around there. It is therefore very important to investigate unsteadiness effects on both the time-mean flow and the coherent structure in unsteady openchannel flows to improve an understanding of the growth process of dunes and the associated transport of suspended sediment.

Hayashi et al. (1988) have for the first time conducted some turbulence measurements in unsteady open-channel flows by making use of the hot-film

anemometer and have suggested that turbulence becomes stronger in the rising stage than in the falling stage.

The wall shear stress attains its maximum before the flow depth. This strongly suggests that various sediment transports in unsteady flood flows become stronger in the rising stage than in the falling stage (Nezu et al., 1997).

Nezu and Sanjou (2006) studied turbulence structure in depth-varying unsteady open-channel flows. Their numerical tests indicated that in low unsteadiness category, turbulence characteristics remain almost unchanged during the floods. In contrast, in high unsteadiness category, the turbulence structure is influenced significantly by the unsteadiness near the wall, especially in the rising stage.

Shimizi et al. (2009) studied stage-discharge relationship with hysteresis effect. Numerical experiments reveal that stage-discharge relationships significantly depend on the pattern of discharge variation with time, though most of the behavior can be characterized in terms of Froude number variation. For symmetrically shaped unit hydrographs, the hysteresis loop appeared to be more pronounced in case of temporally varying flows with higher intensity (finer particles). For the scenario with lower peak discharge, transitional bed forms (standing waves or/and flat bed) do not appear; consequently a hysteresis loop is absent. However, a lag in stage-discharge relation can be observed between rising and falling limb in the lower part. For the scenarios with different flow duration, the same peak unit discharge and symmetric shape of rising and falling limbs, results show different characteristics of stage discharge relationship and hysteresis loop. Consequently, it can be inferred that the duration of flood flow is also a significant factor in determining nature of bed form evolution and, in turn, the stage-discharge relationship.

3. EXPERIMENTAL SETUP AND PROCEDURE

3.1 Experimental Setup

The experiments were performed in a flume in Hydraulics Laboratory of Istanbul Technical University (**Figure 3.1**). The flume was 26 m in length, 0.98 m in width and 0.85 m in depth and was able to supply unsteady flow by an external re-circulating system. The flume was composed of Plexiglas sidewalls and smooth concrete bottom (with a representative surface roughness height smaller than 1mm). During the experiments, symmetrical (i.e. with equal rising and falling durations) and asymmetrical hydrographs were generated in the flume. The test matrix along with the properties of the applied hydrographs is summarized in **Table 3.1** based on the definition sketch given in **Figure 3.2**. Throughout the experiments, the base flow discharge (discharge before the rising stage and after falling stage) of the applied hydrographs was set to a constant value of 15 lt/s.

At the inlet of the flume, a flow straightener was placed to mitigate the fluctuation on the water surface and to eliminate the swirl within the cross-section. At the outlet of the flume, a sharp crested rectangular weir was present. The water surface profile was adjusted by this downstream tailgate weir. The flow passing over this weir free falls into the steel stilling basin which has a V-notch sharp crested weir at the final section. In the preliminary experiments, under the steady flow conditions, the v-notch sharp crested weir was utilized to verify the discharge measured electronically by the magnetic flow meter located on the pipe that supplies the water into the flume. The water which leaves the steel stilling basin was discharged into concrete-lining internal canals located under the base level of hydraulics laboratory.

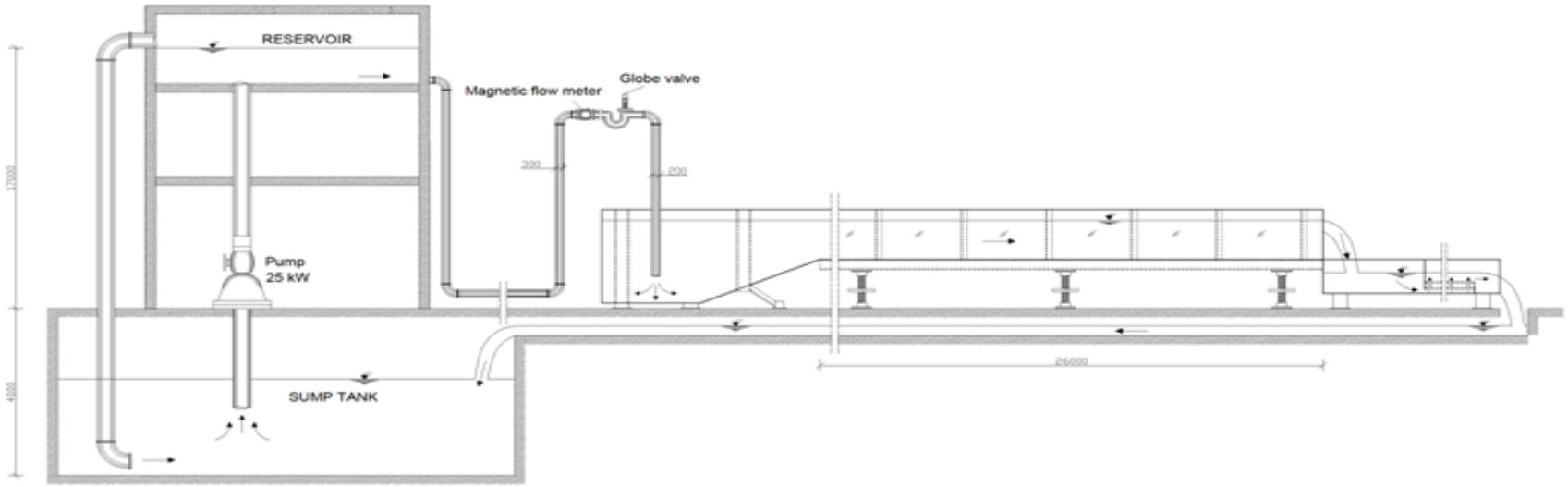

Figure 3.1 : The sketch of the circulating flume.

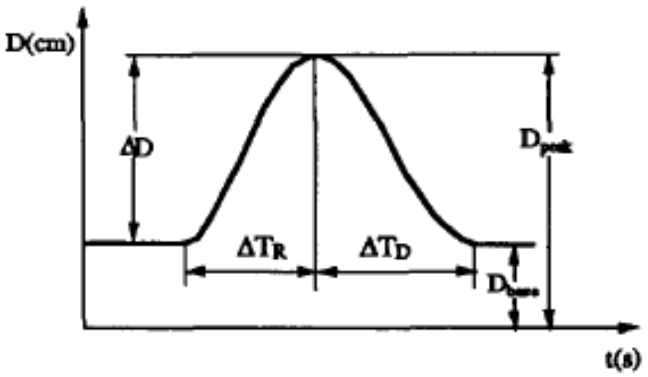

Figure 3.2 : Conceptual Figure of a Typical Hydrograph (Song and Graf, 1996).

The canal transmits the water back into large sump tank. The water which returned into the sump tank was pumped up to the reservoir to maintain gravitational flow for the experiments. The water released from the reservoir transmitted to the flume by a steel pipe with a diameter of 200mm.

The unsteady flow conditions are produced by the combination of a set of devices: a magnetic flow meter, a proportional control (globe) valve, an electronic PID control unit. The target discharge was set by an operator via PID control panel unit. The seat of the globe valve was chosen as “linear” to make the variation between “discharge” and “openness ratio” linear. The instantaneous discharge passing through the pipe was measured by the magnetic flow-meter simultaneously. Depending on the measured instantaneous value, for the fine tuning of the discharge, the openness of the proportional globe-valve is updated with a real-time correction by the control unit.

3.2 Measurement Devices

In technical speaking, the major goal of the measurements was to directly record the variation of instantaneous vertical velocity profile, turbulence, water surface profiles and indirectly to obtain the instantaneous unit discharge. In the experiments, the variations of the instantaneous velocity and water surface profile were recorded with high temporal resolution in a synchronized way during the passage of the unsteady flow. This allowed overlapping of the collected data in the time domain. Recently released Vectrino II (i.e. NORTEK Vectrino profiler, flexible headed version) which is capable of measuring instantaneous 3D velocity profile was used for the velocity

measurements near the rigid bottom. Vectrino profiler measured flow characteristics at 18 vertically consecutive points with 2 mm distance intervals by. Since this instrument very recently released, preliminary tests were carried out before the major experiments under steady flow conditions to understand the impact of measurement method on the collected data. In addition to Vectrino profiler, a previous generation of Vectrino velocimeter was employed for the point measurements. The combined utilization of these two velocimeters enable to attain the variation of instantaneous velocity profile and unit discharge.

During the measurements, the velocimeters are located to identical position within the measurement cross-section. One of the velocimeters was on the left and at 15 cm distant to centerline of the flume, and the other one was on the right and at 15 cm distant to centerline. These two positions are identical to each other in terms of having the same side effect. Sampling volume of the Vectrino profiler was focused on the bottom based. Vectrino 1 point gage is located to the 15 cm distance from the bottom. The measurement cross-section was located in the middle of flume which has a length of 26m.

Sampling frequency should be sufficiently dense in the turbulence measurements so as to capture the real fluctuating (turbulence) peaks of the instantaneous velocity. Nezu and Nakagawa (1993) introduced a criterion as a function of mean flow characteristics, i.e water depth and mean velocity to determine the required sampling frequency for taccurate urbulence measurements. The required sampling frequency for the turbulence measurements was preliminarily calculated before the major experiments. In order to satisfy this criterion proposed by Nezu and Nakagawa (1993), sampling frequency of the velocimeters were set to 100 Hz throughout the experiments. In addition to velocimeters, two non-intrusive two acoustic sensors were utilized to record the variation of instantaneous water surface profile. Sampling frequency of these sensors were 100 Hz. The distance between acoustic sensors were 1 m. All of the measurement devices were connected to the data logger and these measurement devices were started to data recording with the same reference signal.

It is a commonly practiced fact that in the measurements, the higher the particle ratio in water, higher the data quality obtained by ADV. Hence to collect more reliable data in the experiments, special attention was given to offer particle rich environment in water. Nortek (2000) describes criterion regarding quantification of data quality.

According to Nortek (2000) “the correlation parameter should have the values between 70 and 100”. The same document also recommends that SNR values to be consistently above 15 dB during a measurement to obtain good quality of data. Throughout the tests these values were checked and satisfied. The capability of the flume in terms of generating logarithmic velocity profile has already been tested by Yagci et al. (2010).

3.3 The Procedure for the Experiment

To attain an insight about the effects of unsteadiness, different unsteady flow conditions were generated. The experiments were conducted for 2 Sets, which means for Set-1 the still water level is 20 cm and for Set-2 the still water level is 14 cm.

By the usage of the PID control unit first all of the experiments are started with 15 *l/s* baseflow. Then to create a spiky hydrograph in the flume, the discharge is changed with time. In order to create different types of unsteadiness degrees, different types of hydrogpraphs were generated. The rising and falling durations of hydrograhs were changed for each number of experiment, and both symmetrical and asymmetrical hydrogrph shapes were observed.

Starting from 15 *l/s* baseflow value, for all experiments the discharges is brought to a peak value which is between 50-55 *l/s*. The difference in unsteadiness degrees were originated from changing the rising and falling durations. For all rising and falling duration and all peak discharge values are presented in **Table 3.1**.

For each experiment, velocity and turbulence measurement were taken with ADV. By the help of two ADVs velocity profile and discharge values were also collected, which gave satisfactorly same results with PID control unit. This uniformity between ADVs and PID control unit proves the well being of conducted data.

With the help of Acoustic Sensors water depth was calculated for two points which one is located in downstream and the other is upstream of the ADVs. This collected data showed the difference of water depth between baseflow and peak discharge conditions which was used to create water depth- discharge diagrams for the major experiments.

All of the measuring instruments were connected to a one computer throughout the experiments. Vectrıno I and two acoustic sensors are set as slave to Vectrino profiler (i.e Venctrino II). All the experiments were performed by two staff. One person regulated the flow conditions and the other one collected the data on computer. When the flow was started to increase, at the exact time measuring process is started. With starting the Vectrino Profiler which is the master of Acoustic Sensors and Vectrino I, all measuring devices started at the exact same time and collected data with same 100 HZ frequency throughout all experiments.

Table 3.1 : The properties of the applied hydrographs.

Experiment	T(s)	T_r(s)	T_f(s)	D(cm)	U(cm/s)	q(L/s/m)	Fr	Re(x10^5)	Γ_{rise}(x10^-2)	Γ_{fall}(x10^-2)	Γ (x10^-2)
Set1FW11	247	150	97	23.4 - 28.5	5.2 - 17.9	12.0 - 50.7	0.04 - 0.11	0.6 - 2.0	10.86	10.21	5.26
Set1FW12	350	130	220	23.5 - 28.5	5.2 - 18.1	12.2 - 51.5	0.03 - 0.11	0.5 - 2.0	12.29	5.95	4.01
Set1FW14	580	150	430	23.5 - 28.5	5.5 - 18.5	13.0 - 53.1	0.04 - 0.11	0.5 - 2.1	10.65	3.26	2.50
Set1FW44	580	460	120	23.8 - 28.8	5.7 - 18.2	13.6 - 52.6	0.04 - 0.11	0.5 - 2.1	3.52	9.46	2.56
Set2FW11	195	120	75	17.3 - 21.5	8.0 - 23.4	13.8 - 50.3	0.06 - 0.16	0.5 - 2.0	8.47	9.36	4.45
Set2FW12	259	148	111	17.2 - 22.0	6.8 - 24.4	12.0 - 53.8	0.05 - 0.17	0.5 - 2.1	7.85	7.20	3.76
Set2FW14	500	158	342	17.0 - 22.1	6.5 - 24.3	11.8 - 53.4	0.05 - 0.16	0.5 - 2.1	7.74	2.37	1.82
Set2FW41	664	535	129	17.1 - 22.1	8.0 - 24.0	13.6 - 53.1	0.06 - 0.16	0.5 - 2.1	2.26	7.51	1.74
Set2FW22	549	283	266	17.2 - 22.0	7.7 - 24.1	13.4 - 52.7	0.06- 0.17	0.5 - 2.1	4.13	3.90	2.01

4. ANALYSIS METHOD

4.1 Despiking of Data

In experimental studies, spikes in the data (i.e. velocity time series) might cause undesirable problems. . In other words, the contaminated data (i.e. that includes oulier velocity values) can lead to misleading outcomes In the light of this fact, a despking method is applied before starting the velocity data analysis.

ADVs are commonly used velocity measurement devices both in controlled laboratory conditions and in field studies. However it has some disadvantages. Since the tool is measuring the data with widely known phenomenan called Doppler Effect, the tool is vulnerable to distraction of noise and signals, namely, Doppler noise floor and aliasing of Doppler signals.

In the presented study, data filtered with a software code modified by Nobuhito Mori (2005) which uses phase-space method created by Goring and Nikora (2002). This method consists of two steps. First step is detecting the spike and the second step is replacing it.

The spike detection was carried out by the method called Phase-Space Tresholding Method. In this method first and second derivaties are calculated at the beginning. Then standart devaitons were calculated for all variables which are velocity data itself and its first and scond derivaties. For each pair of variables, an elipse is calculated that has maxima and minima from 3 above (Nikora and Goring, 2002). The points which lie outside of the calculated ellipsoid considerd as spike.

For replacing the data there are several way that works sufficiently good. Nevertheless the most satisfactory method is to use third order polynomial fit for ADV data (Nikora and Goring, 2002). For extra spike cubic allow enough curvature on both side of the spike.

To make a clear and undisturbed data set all velocity and water depth measurements were filtered by this method and it showed a real efficiency for all data.

4.2 Time Averaging of The Data and Reynolds Decomposition

For a hydrodynamic quantity such as velocity, *u*, the mean value with respect to time is defined by

$$\bar{u} = \frac{1}{T}\int_{t_o}^{t_o+T} u\, dt \qquad \textbf{(4.1)}$$

in which t_o is an arbitrary time and *T* is the time over where the velocity averaged. For this formula the *T* should be sufficiently large (Sumer, 2007).

A time series of velocity can be separated to two parts with Reynolds Decomposition method. This is a method defines a time series of velocity with two parts, namely, mean and fluctuating part. The fluctuating part of the velocity, u', is defined by

$$u - \bar{u} = u' \qquad \textbf{(4.2)}$$

In the present study, first of all, the collected data is time averaged for making the decomposition. Due to Taylor's frozen turbulence approximation, the time scale (Eularian time scale) can be defined by

$$T_E = \frac{\Lambda_f}{V} = u' \qquad \textbf{(4.2)}$$

in which, Λ_f is the size of a coherent structure and *V* is the depth averaged velocity. The significance of T_E is that it gives the time of a coherent structure or an eddy will reamain unchanged. So, it can be said that if *T* is taken larger than T_E than it would be a sufficiently large time to represent the data.

Considering Λ_f is equal to 3 times of the water depth, than for our experiments the T_E will vary between 10-15 seconds. For averaging *T* is chosen as 10% of total time for each experiment which makes *T* at least 20 seconds. It shows that for all experiments chosen *T* satisfies the condition that being larger than T_E , so the analysis method for time averaging is justified.

4.3 Velocity and Water Depth Calculations

As stated in previous section, velocity measurements were carried out by ADVs. Vectrino Profiler which was located at the bottom collects data from 18 points which starts from to bottom and having 2mm distances between every adjacent points. The other ADV, Vectrino I, which collets data for a single point, is located above to collect velocity measurements close to free stream.

Water depth measurements were taken with two non-intrusive acoustic sensors. One of the acoustic sensors was located upsteram side and the other was at the downstream side of ADVs. The acoustic sensors collectd data with same sampling frequency with ADVs. So as to define the water depth for the location where velocity measurements taken, two values were taken from the acoustic sensors were averaged.

For the analysis, first of all every data set was filtered with the methods mention above. Subsequent to filtering procedure, each point of velocity measurements time averaged and decomposed to *mean* and *fluctuating parts*.

With time averaged velocity data, velocity profiles were calculated with for each experiment with 100 Hz frequency. By the help of Velocity profiles and Water Depth calculations both were taken for every 0.01 seconds, flowrate is calculated by taking the integral of velocity profile. Since the flowrate, *q*, is found, the depth averaged velocity, V, calculated throughtout experiments by dividing flowrate to water depth.

$$V = \frac{q}{h} \tag{4.3}$$

After calculating velocity and water depth values, hydraulic parameters ,namely, Reynolds Number and Froude Number is calculated for identifiying the hydraulic conditions. Reynolds Number, *Re*, and Froude Number, *Fr*, is defined by

$$Re = \frac{4hV}{\nu} \tag{4.4}$$

$$Fr = \frac{V}{\sqrt{gh}} \tag{4.5}$$

4.4 Turbulence Calculations

Turbulence components and their hysterisis play an important role for flow behavior. To gain a beter understanding, velocity measurements were decomposed and turbulence fluctions of the three dimensions of flow calculated. The notations u, v, and w are the velocities in the direction of x, y, and z respectively.

$$v - \bar{v} = v' \tag{4.6}$$

$$w - \bar{w} = w' \tag{4.7}$$

Turbulence hysterisis patterns are drawn for *Turbulence Kinetic Ener*gy of the flow which is the kinetic energy per unit volume of fluid for the fluctuating flow (Sumer, 2007). *Turbulence Kinetic Energy* is defined by

$$TKE = \frac{1}{2}\rho(\overline{u'^2} + \overline{v'^2} + \overline{w'^2}) \tag{4.8}$$

To draw a hysterisis pattern for variation of *TKE* with respect to *h*, first of all both *TKE* and *h* are recalculated in dimensionless form, which are TKE/TKE_B and h/h_{max}, where TKE_B is turbulence kinetic energy for baseflow. Since TKE is composed of averaging windows, both *h* and *TKE* avareged with same time Windows systematically.

4.5 Unsteadiness Degree

For each experiment having different durations for rising and falling limbs, differenet unsteadiness degrees appear. The changes in water depth level and time durations of hydrographs, created different usteadiness degrees for different experiments.

For a hydrograph of a flow which can be characterized like **Figure.3.2**, the unsteadiness degree is defined by

$$\Gamma = \frac{1}{u_b^*}\frac{\Delta D}{\Delta t} \tag{4.8}$$

in which u_b^* is the friction of the baseflow, ΔD is the difference between water depth for minimum and maximum values, Δt is the total time duration of the hydrograph (Song and Graf, 1996).

5. RESULTS AND DISCUSSION

5.1 The Variation of Velocity During The Passage of an Unsteady Flow

The velocity measurements taken, showed a very small amount of spikes. This indicated for a well conducted experiment. To achieve a better quality of velocity data, the spikes were eliminated from the velocity time series as explained above in detail.

After despiking procedure, point velocity measurements were time averaged and mean and fluctuation parts were decomposed for every point from the bottom to the top of the stream.

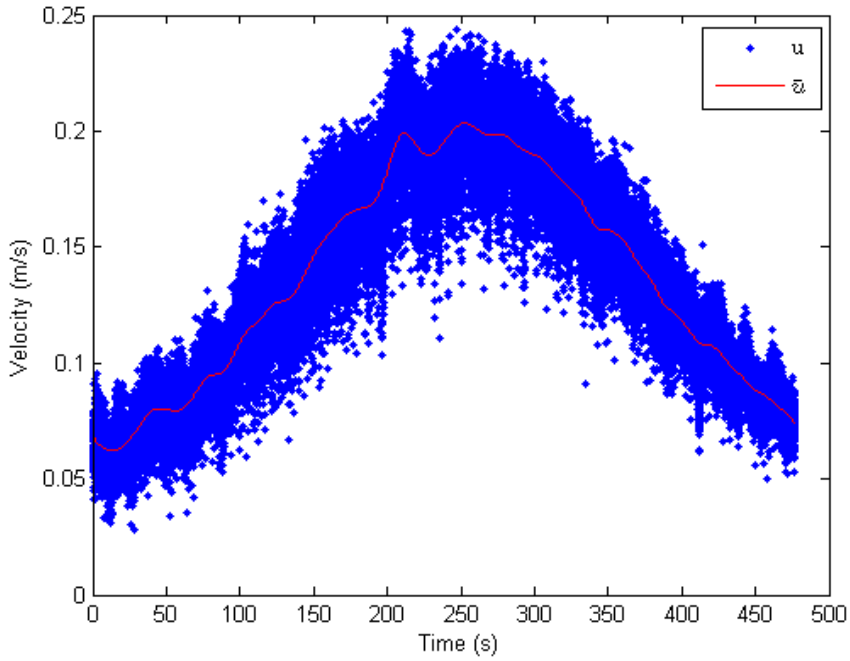

Figure 5.1 : The variation of velocity with respect to time for Set-1 (d=20 cm).

The Figure 5.1 shows measured instantaneous velocity, u, and time averaged velocity, $\bar{u}$, in the same graph. Since the total duration of the experiment is 470 seconds, the time averaging window chosen as 47 seconds which is %10 of the total

duration and sufficiently larger than eularian time scale ,T_E, therefore and enoguh time to understand and describe turbulence behaviors.

The first hysterical pattern was observed in time averaged velocity. In all experiments same pattern of hysterisis was observed for time averaged velocity, that for the same water depth larger velocity values occured for rising limb (APPENDIX B).

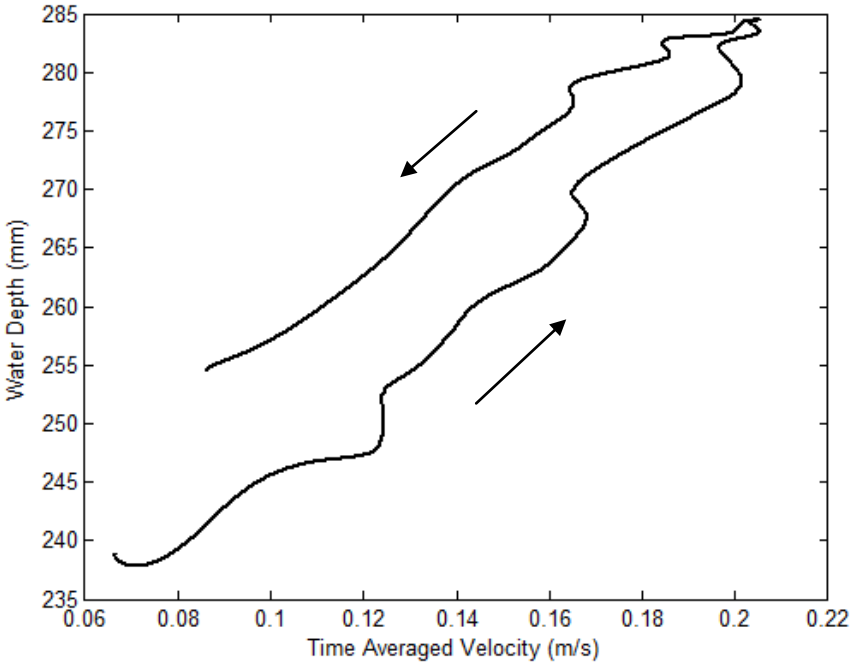

Figure 5.2 : The variation of time avergaed velocity with respect to time for Set-1 (d=20 cm), Γ=0.0526.

The **Figure 5.2** is a clear representation for the evidence and significance of hystrisis for unsteady flow. It can be seen from Figure 5.2 that for the same water depth, velocity differnce between rising and falling limb of the hydrograph can be up to 4 cm/s. This clearly shows for unsteady flows hysteric effects are not to be ignored and single value approach is no longer valid.

Besides time averaged velocity, flowrate and depth averaged velocity are also key indicators to describe flow characteristics. After every point of vertically distributed data from bottom to free surface level is timely averaged to describe mean flow charateristics, this timely averaged data connected from bottom to surface for creating a velocity profile in every 0.01 seconds.

The obtained velocity profiles were integrated along the depth and flowrate ,*q*, was found. By diving this values to their respective water depth values frequency, depth averaged velocity, *V*, calculated during the passage of hydrograph (APPENDIX G).

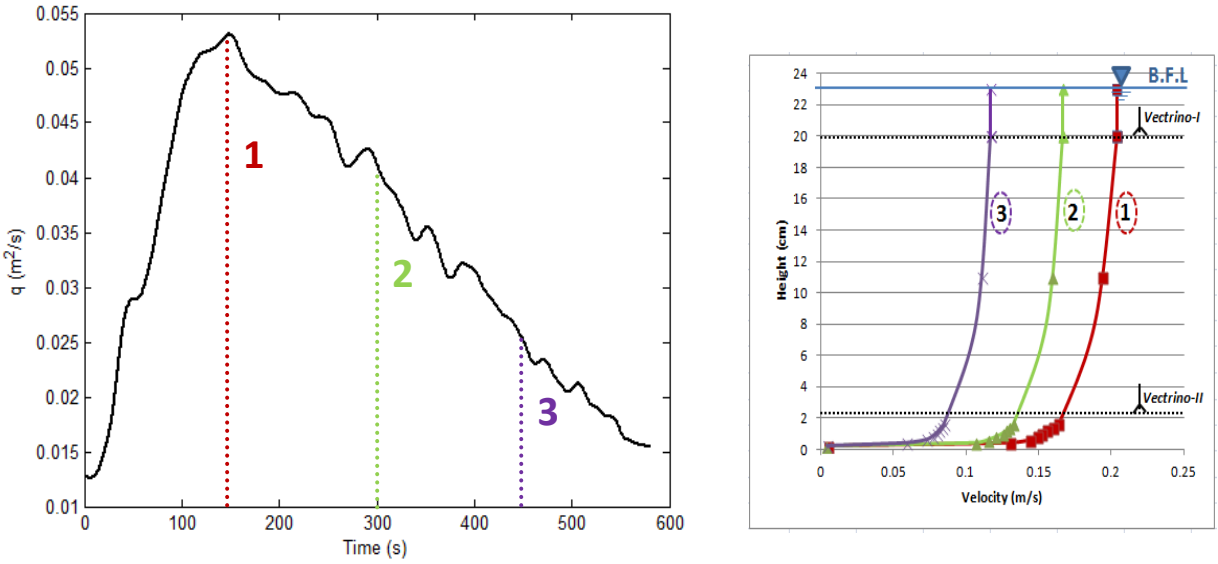

(a) **(b)**

Figure 5.3 : For Set-1 d=20 cm Γ=0.0250 (a) Flowrate (b) Velocity profiles for three arbirtrarily chosen times(B.F.L denotes base flow level).

The single value approch clearly suggests that for the same water depth value, same discharge should occur for flow. However, in our all experiments, which have all differrent degrees of unsteadiness, hystressis patterns observed for every experiment (APPENDIX F). The Figure 5.4 shows that for unsteady flows single value approach is not valid, becuse the water depth-discharge diagram presents a loop not a line/curve as it was supposed to be if the single value approach was true.

All results clearly showed that unstadiness plays a vital role on hyrdaulic properties and it should be taken into consideration for engineering calculations. Since many commonly utilized formulas are used for hydraulic desing are based on single value approach, the results of the study shows that for unsteady conditions this formulas should be adjusted.

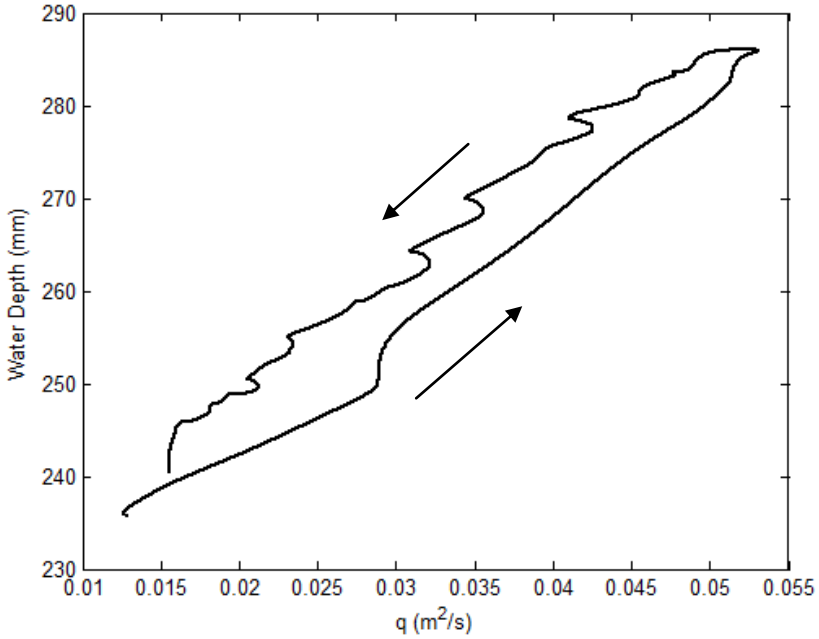

Figure 5.4 : The variation of q(m^2/s) with respect to water depth for Set-1 (d=20 cm), Γ=0.0250.

5.2 Depth Averaged Veloctiy, Reynolds Number and Froude Number

The depth averaged velocity, *V*, calculations were carried out as it explained above, and dimesionless flow numbers such as Reynolds Number and Froude Number calculated based on the depth averaged velocity values.

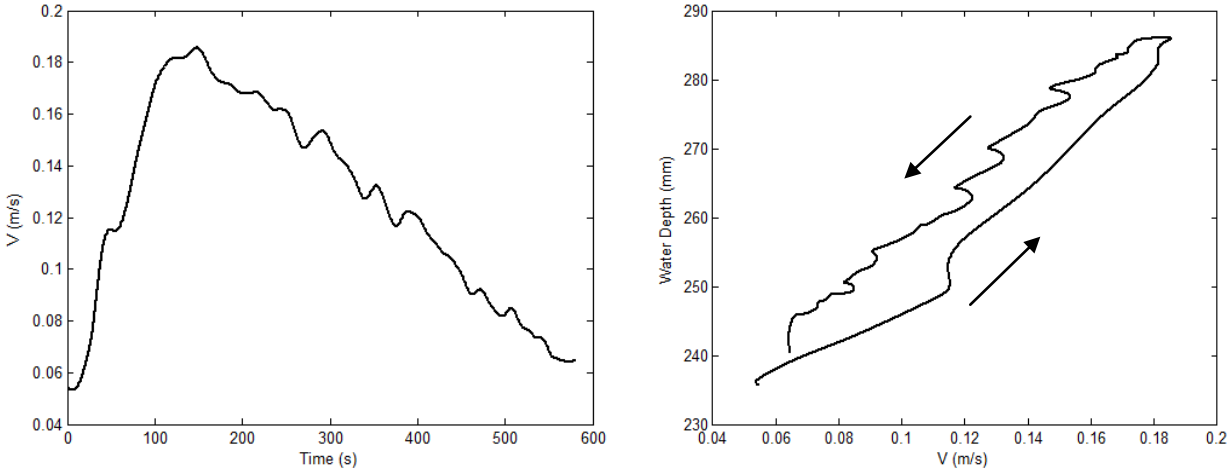

(a) **(b)**

Figure 5.5 : For Set-1 (d=20 cm), Γ=0.0250 The variation of *V* with respect to (a) Time (b) Water depth.

The Reynolds Numbers calculations were made by equation **4.4**. Since the flow is unsteady, naturally Reynolds Numbers varied troughout the passage of the unsteady hydrograph for each experiment. Resembling the shape of the depth averaged velocity, Reynolds Number rised and falled paralel to the increasing flow velocity for all experiments and all times it was always sufficiently large that shows turbulent flow conditions (APPENDIX D). Figure 5.6 shows a sample for the variation of Reynolds Number with respect to both time and water depth troughout an experiment. The Reynolds Number also showed a hysterisis pattern like other flow parameters. All the maxima and minima values of Reynolds Number for the entire experiments are presented in Table 3.1.

Froude Number calculations are made by Equ. (4.5) characteristic length is chosen as water depth for calculations which changes simultaneously with velocity of the mean flow. The results show that, Froude Number is less than 1 for each and all of the experiments which signifies a subcritical regime for a flow. Froude Number also showed a hysterisis pattern(APPENDIX C). This substantial effect observed in all flow parameters once again proves the role of unsteadiness on hydraulic characteristics. Figure 5.7 shows a sample for the variation of Froude Number with respect to both time and water depth troughout an experiment. For all The maximum and minimum of Froude Number values are presented in Table 3.1.

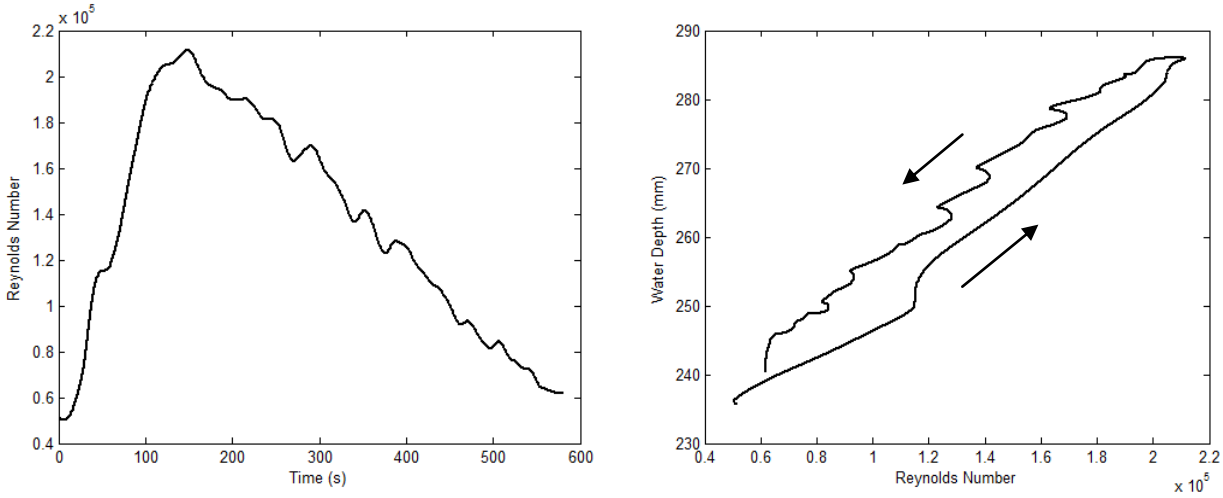

Figure 5.6 : For Set-1 (d=20 cm), Γ=0.0250 The variation of ReynoldsNumber with respect to (a) Time (b) Water depth.

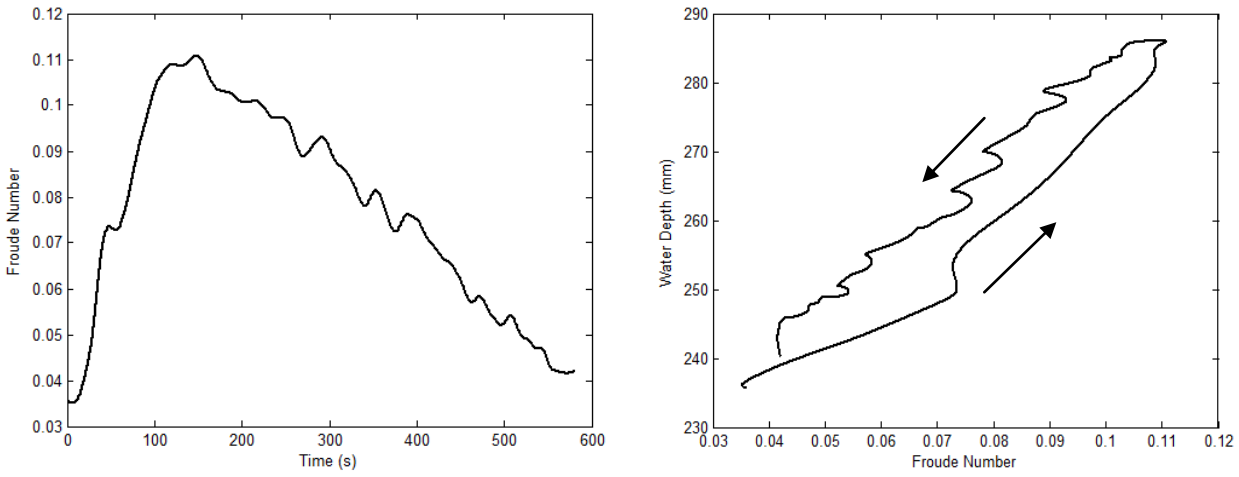

Figure 5.7 : For Set-1 (d=20 cm), Γ=0.0250 The variation of Froude Number with respect to (a) Time (b) Water depth.

5.3 Turbulence Chracteristics and Turbulence Kinetic Energy

Turbulence is a key parameter that controls flow characteristics and behaviors in a very influential way. Because of this reason, effects of unsteadines on turbulence hystersis pattern is a crucial point to investigate.

Figure 5.1 clearly shows the difference in the fluctions from the time averaged velocity between rising and falling limbs of the hydrograph. In the rising stage the instantaneous velocity measurements spreads more widely than falling stage. This larger fluctuation indicates turbulence in the rising stage is larger than the falling stage.

The variation of dimensionless turbulence kinetic energy, TKE/TKE_B, with respect to dimensionless water depth, h/h_{max}, is represented for three different experiments having three different unsteadiness degrees in Figure 5.8 a), b), c) respectively**.** Even though the size of the hysteresis changes, for the three experiments hysteresis patterns are clearly observed. The relationship between the changes in unsteadiness degree and hysteresis magnitude is investigated in next chapters.

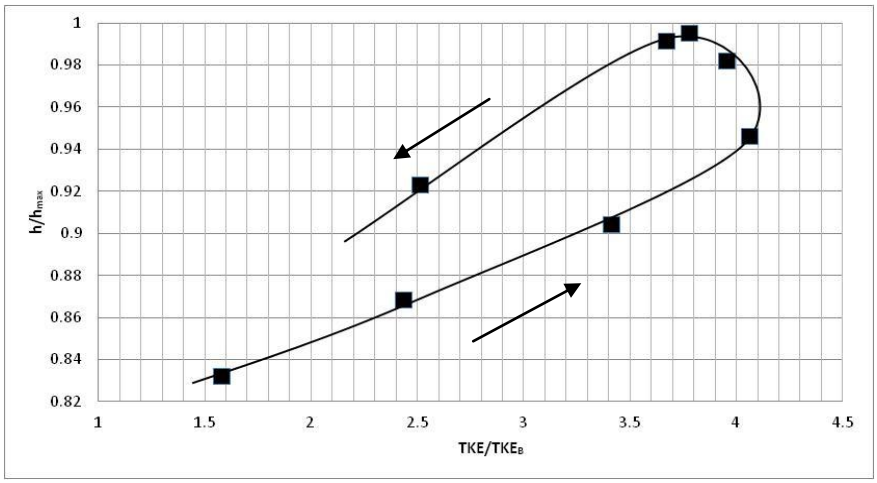

(a)

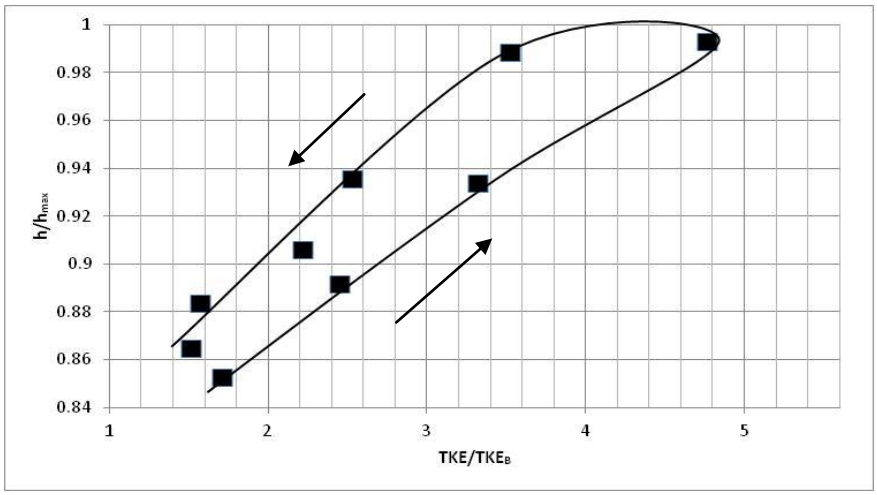

(c)

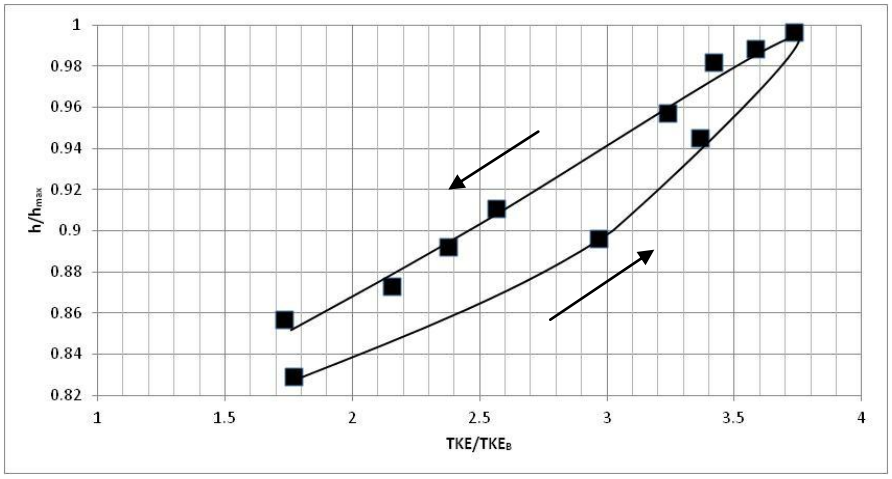

(e)

Figure 5.8 : The Variaton of TKE/TKE_B with respect to h/h_{max} for Set-1 (d=20 cm), and (a) Γ=0.0526. (b) Γ=0.0401. (c) Γ=0.0250.

5.4 Unsteadiness Degree and Water Depth

The experiments were conducted for different rising and falling durations (i.e. unsteadiness degrees). These changes in the rising and falling durations caused different unsteadiness degrees. Figure 5.9 shows the variation of water depth with respect to time for Set-1(d=20 cm), Γ=0.0250. This experiment has four times larger falling duration than the rising duration. This ratios of rising and falling durations are changed trough all experiments to create different unsteadiness degrees.

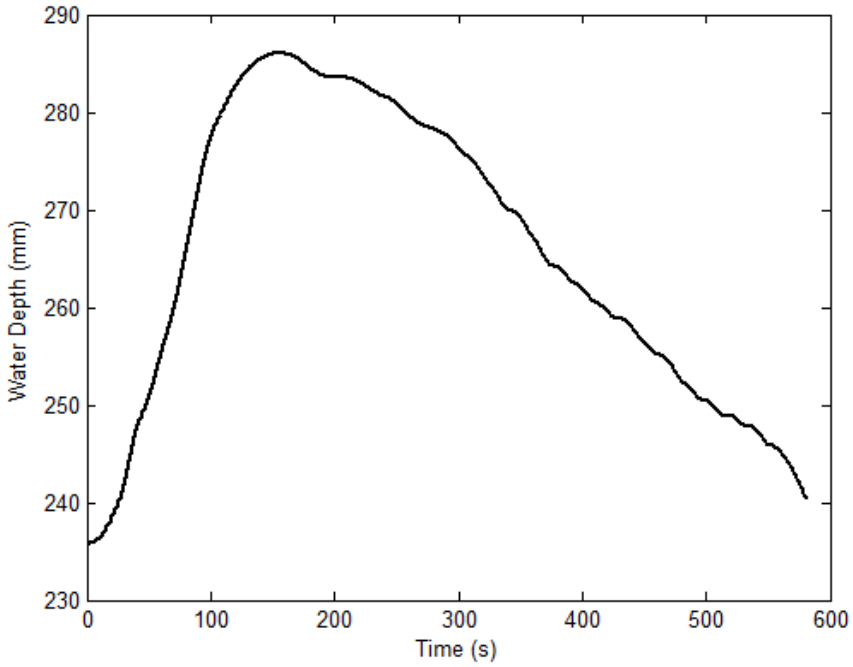

Figure 5.9 : The variation of water depth with respect to time for Set-1(d=20 cm), Γ=0.0250.

Unsteadiness degrees for all experiments are calculated by the equation **4.8.** All different values of unsteadines degress are represented in Table 3.1.

5.5 The Influence of Unsteadiness Degree on Hysteresis Patterns

The unsteadiness changes the flow properties in a substantial way. All of the results clearly shows for unsteady flow, hysteresis patterns are highly evident in almost every hydraulic characteristics. The existence of this pattern unjustify all single value approximations.

A crucial question arise at this stage. When a flow is truly unsteady? When it is truly influential on hysteresis patterns? When single value approach formulas are has to be adjusted?

To answer this questions, the hysteresis pattern of each experiments with different unsteadiness degress were observed. The relation between unsteadiness degree and hysteresis pattern was investigated. To achive that goal, first of all the hysteretic effect was needed to be quantified. This objective is completed by a schemetic representation of the hysteresis patterns (Figure 5.10).

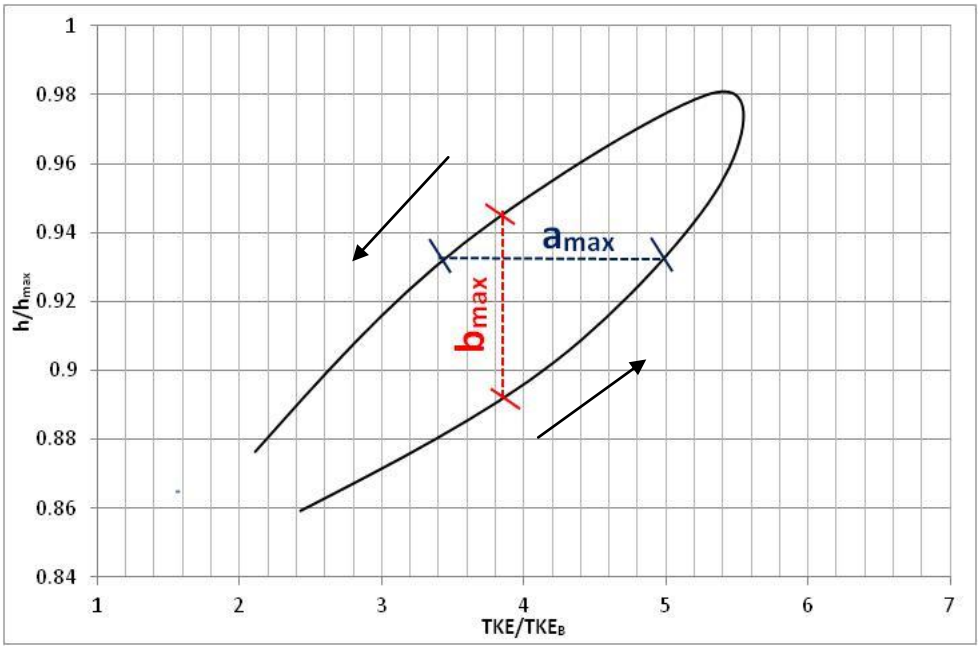

Figure 5.10 : The Schemtic Represantation of Hysteresis Pattern.

The above figure represent an example for an hysteresis loop which is very similar to presented results earlier in this study. To make a quatification on hysteria, two numbers ***a*** and ***b*** were placed. As it can be seen from the figure, ***a*** represent the horizontal span of the loop, which indicates for the hysteresis between turbulence kinetic energy with for the same water depth. And ***b*** represents the vertical span of the loop, which indicates the hysteresis between water depth for the same turbulence kinetic energy value.

One can easily say that, if the loop expands, ***a*** and ***b*** will have larger values which indicates larger hysteria. And if the loop shrinks, ***a*** and ***b*** will have smaller values which means the hysteria is small maybe even negligible. When ***a*** and ***b*** are too large, severe hysterical effects will influence the flow properties, and when ***a*** and ***b***

are too small the loop will shrink and can even approach to become a single line/curve which indicates no hysteresis and single value approach will be valid.

To make a quatification, the dimensionless number ***a***x***b*** is used. By this multiplication, an estimate for the area of hysteresis loop is obtained. Larger this number, larger the area and hysteris, smaller this number, smaller the area and hysteresis. By the this simple quantification, the relationship between hysteresis and unsteadiness degree can be found.

The variation of hysteresis with respect to unsteadiness degree plots are calculated for dimesionless kinetic energy and depth averaged velocity. The Figure 5.12 and 5.13 are calculated for dimesionless kinetic energy. The Figure 5.13 is calculated for depth averaged velocity.

For Set-1 and Set-2, all experiments are plotted in a graph according to their own hysteresis values and unsteadines degrees. The Figure 5.11, Figure 5.12 and Figure 5.13 shows the relationship between unsteadiness degree and hyteresis. This three figures show that, there is hysteresis is related to unsteadiness degree. As the unsteadiness degree increases, hysteresis increase for all experiments.

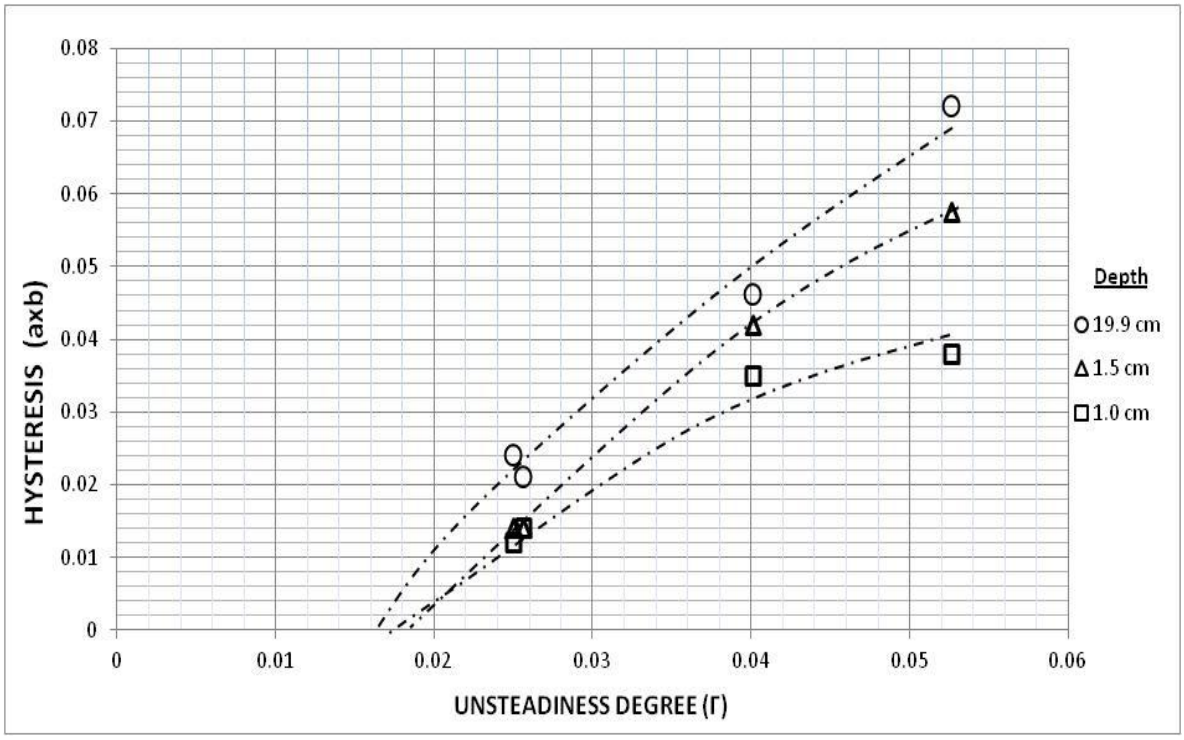

Figure 5.11 : The variation of hysteresis of TKE with respect to unsteadiness degree for Set-1 (d=20 cm).

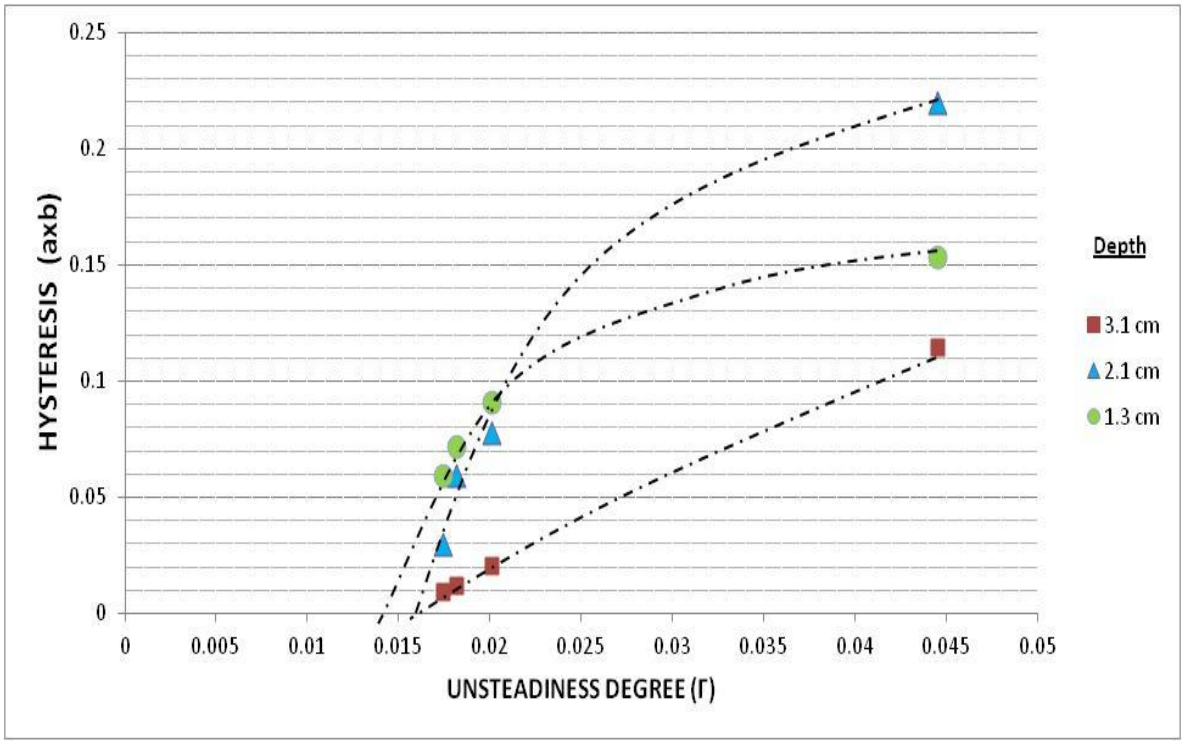

Figure 5.12 : The variation of hysteresis of TKE with respect to unsteadiness degree for Set-2 (d=14 cm).

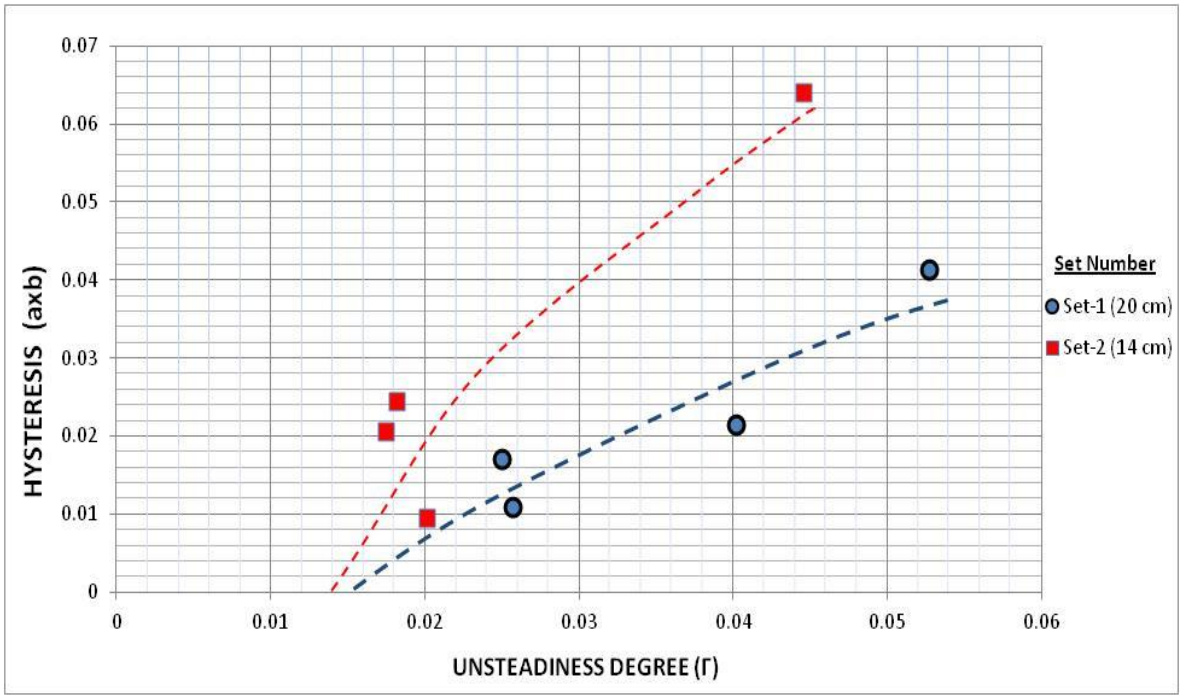

Figure 5.13 : The variation of hysteresis of V with respect to unsteadiness degree for Set-1(20 cm) and Set-2(14 cm).

By the light of the three figures above, this is clear that increasing unsteadines degree values also increases hysteresis for both turbulence kinetic energy and depth averaged velocity. This first result is quite significant to see the influence of unsteadiness degree on hydraulic parameters.

Another sigficant result can be drawn by observing the trendlines plotted on each experiment's unsteadiness degree and hysteria points in Figure 5.11, Figure 5.12 and Figure 5.13. All this trendlines drawn by following the increasing path of hysteresis and unsteadniess.

The intersection of trendlines to unsteadniess degree axis shows zero hysteria level. This is a very singficant point for trendlines. It means that, this point is where unsteadiness starts to influence the flow characteristics. For the unsteadines degrees below that point, the flow can be treated as steady. But for any unsteadiness degrees above that point the flow definitely should be treated as unsteady.

This minimum unsteadiness degree that starting the unsteady influences is seem to be occur in an interval. For both turbulence kinetic energy and depth averaged velocity this dimensionless number of unsteadiness degree found in between 0.01 and 0.02. This is the maximum value of unsteadiness that can be treated as steady. Above this point steady assumptions will not be valid. The single value approach can be below this point. This significant results defines the types of flow which can be treated as steady or not.

5.6 Comprasion of The Peak Timings of Different Hydraulic Characteristics During The Passage of Unsteady Flow

The peak timing of hydraulic characteristics, namely, Reynolds Stress, flowrate, water depth and depth averaged velocity was compared during the passage of unsteady flow for each experiment. The experiments showed (APPENDIX I) that during the passage of unsteady flow, Reynolds stress reaches it peak before all other parameters. This effect can cause early raptures of armor layer and clock wise hysteresis for sediment transport also which will lead for the same discharge value sediment transport will less for the falling limb than the rising limb. By the light of this result, it is seen that the effect of unsteadiness on sediment transport calculations, can be a key indicator .

6. CONCLUSIONS

Unsteady flow conditions are observed extensively in nature. The cilamte changes effect the types of hydrgogrphs dramatically to flood. The increasing rainfall intensity causes rapid changes in flow discharges. In this condtions unsteady flows and its influence on hydraulic characteristics becomes an important topic to investigate and study.

The influence of unsteadiness is investigated in this study. In two Sets labarotory experiments different types of hydrographs generated. It is aimed to create different unsteady conditions to observe its effects on hydraulics characteristics and also investigate the differences of this influence for different types of unsteadiness degrees.

The most important influence of unsteadiness on hydraulic characteristics is observed as hysteresis patterns. The hysteresis indicates for the difference in the flow characteristics for a same water depth value. In the present study, a quantification is made to describe the magnitude of hysteresis. This quantification of the hysteresis is made by a dimensionless number $\boldsymbol{a}$x$\boldsymbol{b}$.

The experiments showed significant results. For all hydraulic characteristics, namely, time averaged velocity, depth averaged velocity, flowrate, Reynolds Number, Froude Number, the hysteresis pattern is observed. This clearly injustified the single value approach for unsteady flows. The results pointed that, for unsteady flow conditions single value approach formulas must be adjusted to unsteady contions.

To gain an understanding on the effect of unstediness on hydraulic characteristics, experiments having different unsteady degrees are compared. The results clearly showed that increasing unsteadiness degrees causes larger hysteresis for both turbulence kinetic energy and depth averaged velocity. This important result signified that the influence of unsteadiness on hysteresis is higly effective and must be considered for engineering calculations.

Another significant result of this study is the definition of a criteria for specifying the flow conditions as either steady or unsteady. For this purpose the relationship between unsteadiness degree and hysteresis is pictured with a diagram for both turbulence kinetic energy and depth averaged velocity. Introducing trendlines, which follows the unstediness degree-hysterisis data, to this diagram the point where unsteadiness becomes no longer influential is found. The founding showed an interval between unsteadiness degrees 0.01-0.02. This worthy result used as an key indicator to define flow conditions. The flows having larger unsteadiness degree values than this interval are said to be considered as unsteady. The single value approach is no longer valid. If the flow has a smaller unsteadiness degree flow can be treated as steady.

The peak times of hydraulic characteristics were compared and it was observed that Reynolds Stress reaches it peak before all other hydraulic characteristics. The result emphasize the effects of unsteadiness also on sediment transport.

REFERENCES

Ahanger M. A., Asawa G. L., Lone, M. A. (2008). Experimental study of sediment transport hsyteresis, *Journal of Hydraulic Research*., Vol. *46*, No. 5, pp. 628-635.

Alexandrov, Y., Laronne, J. B., Reid, I. (1996). Suspended sediment concentration and its variation with water discharge in a dryland ephemeral channel, northern Negev, Israel. *Journal of Arid Enviroments*. Vol. *5*, pp. 73-84.

Bayazit, M. (2003). Hidroloji, Birsen Yayınevi, Istanbul.

Chow, V. T., Maidment, D. R., Mays, L. W. (1988). Applied Hydrology, McGraw-Hill., Singapore.

Graf, W. H. and Song, T. (1996). Bed shear stress in non-uniform and unsteady open-channel flow. *Journal of Hydraulic Research*. Vol. *33*, No. 5, pp. 699-704.

Goring, D. G. and Nikora, V. I. (1998). ADV Measurements of Turbulence: Can We Improve Their Interpretation. *Journal of Hydraulic Engineering*. Vol. *124*, No. 6, pp. 630-634.

Goring, D. G. and Nikora, V. I. (2002). Despiking Acoustic Doppler Velocimeter Data. *Journal of Hydraulic Engineering*. Vol. *128*, No. 1, pp. 117-126.

Gordon, N. D., McMahon, T. A., Finlayson. B. L., Gippel. C. J., Nathan, R. J., (2004). Stream Hydrology An Introduction for Ecologists, Wiley&Sons, New York.

Hayashi, T., Ohashi, M, Oshima, M. (1988) Unsteadiness and Turbulence Structure of Flood Wave. *Proc., 20th Symp on Turbulence*, 154-159

Henderson, F. M. (1966). Applied Hydrology, Macmillian Publishing, New York.

Holtan, H. N. and Overton, D. E. (1996). Storage-flow hysteresis in hydrograph synthesis. *Journal of Hydrolgy*. Vol. *2*, Issue 4, pp. 309-323.

Klein, M. (1984). Anti clockwise hysteresis in suspended sediment concentration during individual storms. *Catena*,11,251-257.

Mao, L. (2012). The effect of hydrographs on bed load transport and bed sediment spatial arrangement. *Journal of Geophysical Research*, 117, F03024, doi:10.1029/2012JF002428.

Nezu, I., Kadota, A., Nakagawa, H. (1997). Turbulent structure in unsteady depth-varying open-channel flows. *Journal of Hydraulic Engineering*. Vol. *123*, No. 9, pp. 752-763.

Nezu, I., Nakagawa, H. (1993). Turbulence in open-channel flows, IAHR-Monograph, Balkema, Rotterdam, The Netherlands.

Nezu, I. Sanjou, M. (2006) Numerical Calculation of Turbulence Structure in depth-varying unsteady open-channel flows. *Journal of Hydraulic Engineering*. Vol *123*, No. 7, pp. 681-695

Nortek.(2000) Nortek 10 MHz Velocimeter; Nortek AS, Norway; 30pp

Picouet, C., Hingrey, B., Olivery, J. C. (2000) Lumped conceptual modeling of suspended sediment transport in african tropical rivers: the upper niger and bani river basins. *Rev*ue *Sci. Eau.*. Vol *13*, No. 4, pp. 463-481.

Shimizi, Y., Giri, S., Yamaguchi, S., Nelson, J., (2009) Numerical simulation of dune–flat bed transition and stage-discharge relationship with hysteresis effect. *Water Resources Research*, 45, W04429.

Song, T. and Graf, W. H. (1996). Veloocity and turbulence distribution in unsteady open-channel flows. *Journal of Hydraulic Engineering*. Vol. *122*, No. 3, pp. 141-154.

Sumer, B. M., Ünsal, I., Bayazıt. M., (2007). Hidrolik, Birsen Yayınevi, İstanbul.

Sumer, B. M. (2007). Lecture Notes on Turbulence, Lyngby, Denmark.

Tu, H. Z. and Graf, W. H. (1993). Friction in unsteady open channel flow over gravel beds. *Journal of Hydraulic Research*. I.A.H.R. 31(1), pp. 141-154.

Yagci. O., Tschiesche U. and Kabdasli, M. S., (2010). The role of differente forms of natural riparions vegetation on turbulence and kinetic energy characteristics. *Advance in Water Resources*. Vol. *33*, No. 5, pp. 601-614.

Wilcock T. R., Kentworthy S. T., Crowe, J. C. (2001). Experimental study of the transport of mixed sand and gravel . *Water Resources Research*. 37, 3349-3358, doi:10.1029/2001WR000683.

APPENDICES

APPENDIX A: The Variation of Depth Averaged Velocity (V) with respect to Water Depth (h) During The Passage of Unsteady Flow
APPENDIX B: The Variation of Time Avaraged Velocity ($\bar{u}$) with respect to Water Depth (h) During The Passage of Unsteady Flow
APPENDIX C: The Variation of Froude Number (Fr) with respect to Water Depth (h) During The Passage of Unsteady Flow
APPENDIX D: The Variation of Reynolds Number (Re) with respect to Water Depth (h) During The Passage of Unsteady Flow
APPENDIX E: The Variation of Turbulence Kinetic Enegy/Base Turbulence Kinetic Energy (TKE/TKE_B) with respect to Water Depth (h) During The Passage of Unsteady Flow
APPENDIX F: The Variation of Flowrate (q) with respect to Water Depth (h) During The Passage of Unsteady Flow
APPENDIX G: The Time Series of Depth Averaged Velocity (V) During The Passage of Unsteady Flow
APPENDIX H: The Time Series of Water Depth (h) During The Passage of Unsteady Flow
APPENDIX I: Time Variation of Hydraulic Parameters During The Passage of Unsteady Flow

APPENDIX A

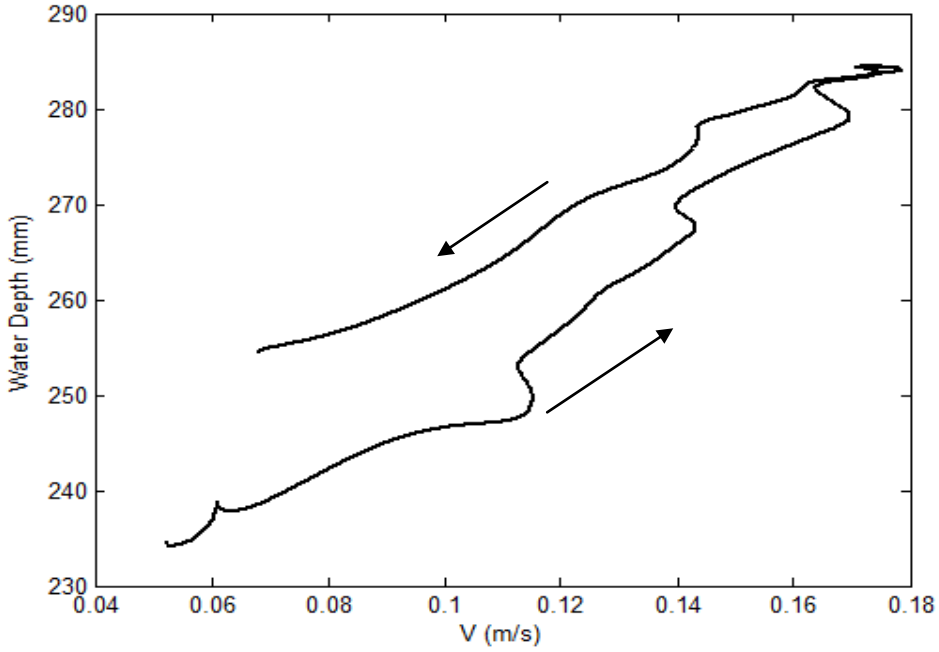

Figure A.1 : The Variation of Depth Avaraged Velocity (*V*) with respect to Water Depth (*h*) During The Passage of Unsteady Flow for Set-1 (d=20 cm), Γ=0.0526.

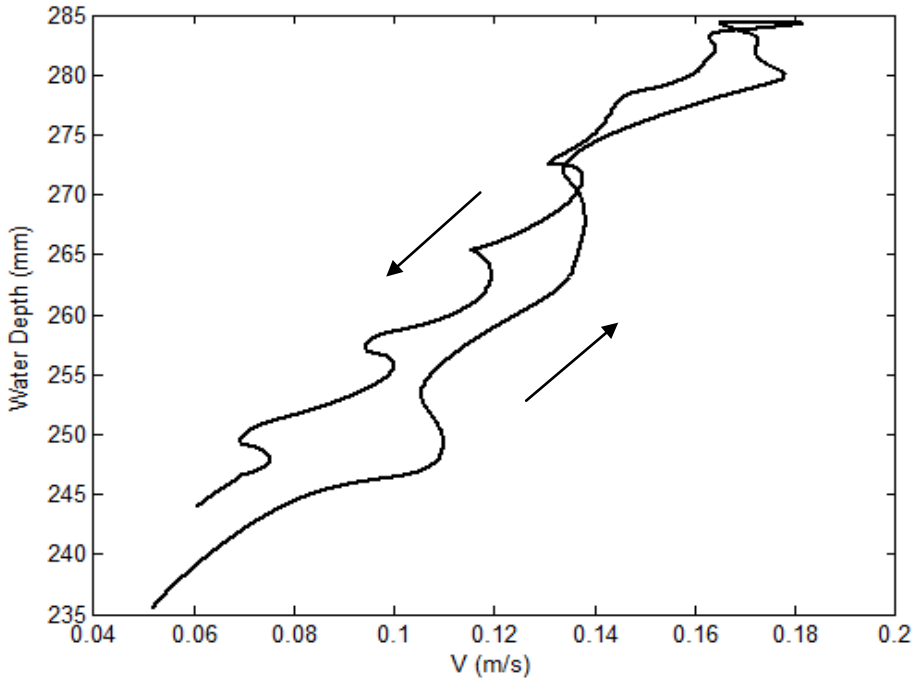

Figure A.2 : The Variation of Depth Avaraged Velocity (*V*) with respect to Water Depth (*h*) During The Passage of Unsteady Flow for Set-1 (d=20 cm), Γ=0.0401.

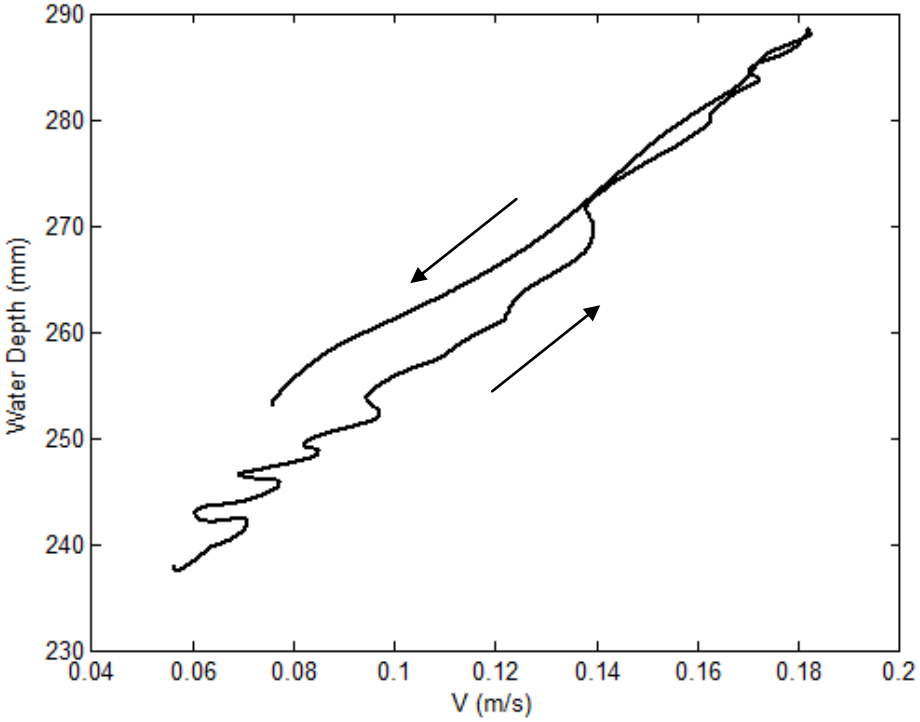

Figure A.3 : The Variation of Depth Avaraged Velocity (*V*) with respect to Water Depth (*h*) During The Passage of Unsteady Flow for Set-1 (d=20 cm), Γ=0.0256.

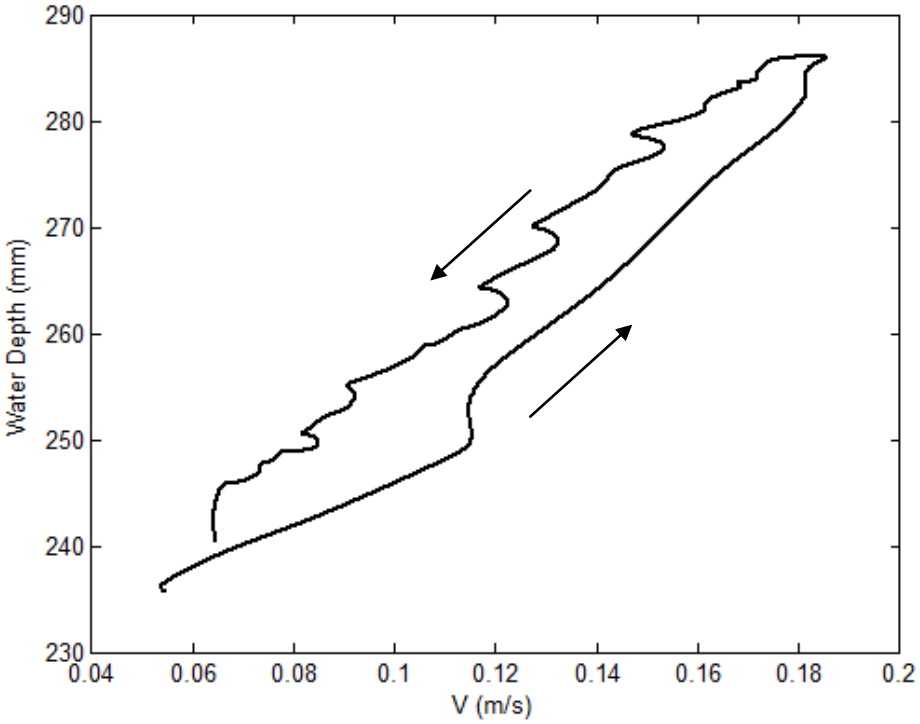

Figure A.4 : The Variation of Depth Avaraged Velocity (*V*) with respect to Water Depth (*h*) During The Passage of Unsteady Flow for Set-1 (d=20 cm), Γ=0.0250.

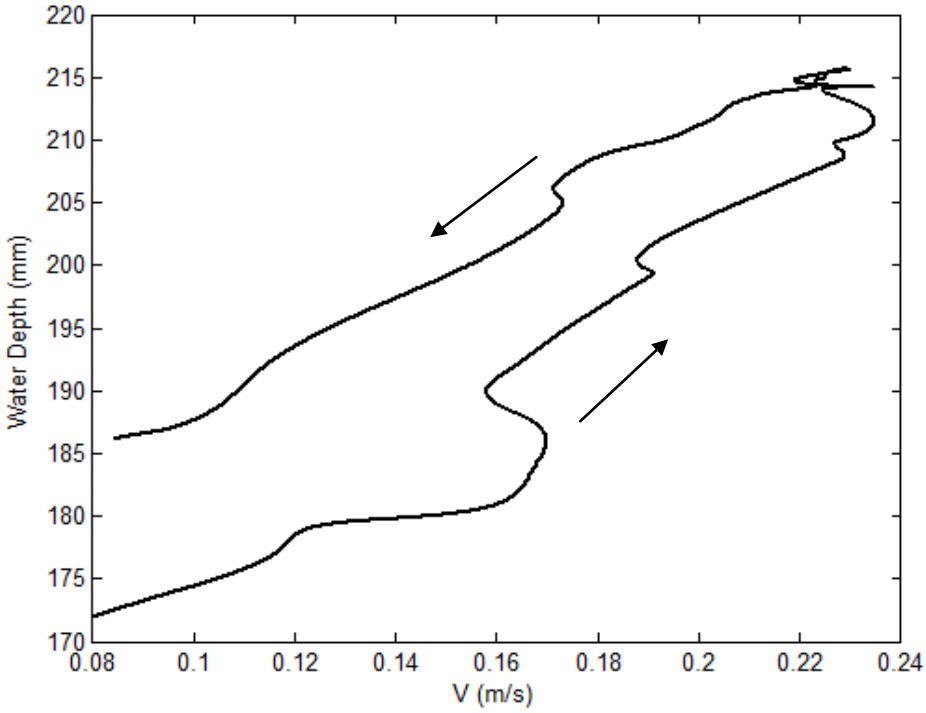

Figure A.5 : The Variation of Depth Avaraged Velocity (*V*) with respect to Water Depth (*h*) During The Passage of Unsteady Flow for Set-2 (d=14 cm), Γ=0.0445.

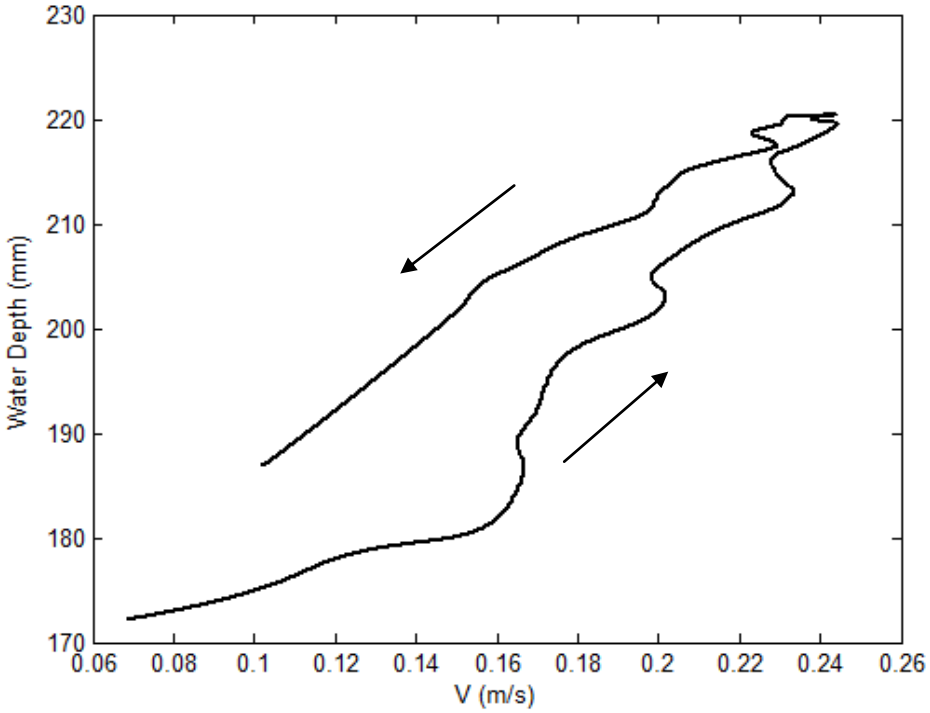

Figure A.6 : The Variation of Depth Avaraged Velocity (*V*) with respect to Water Depth (*h*) During The Passage of Unsteady Flow for Set-2 (d=14 cm), Γ=0.0376.

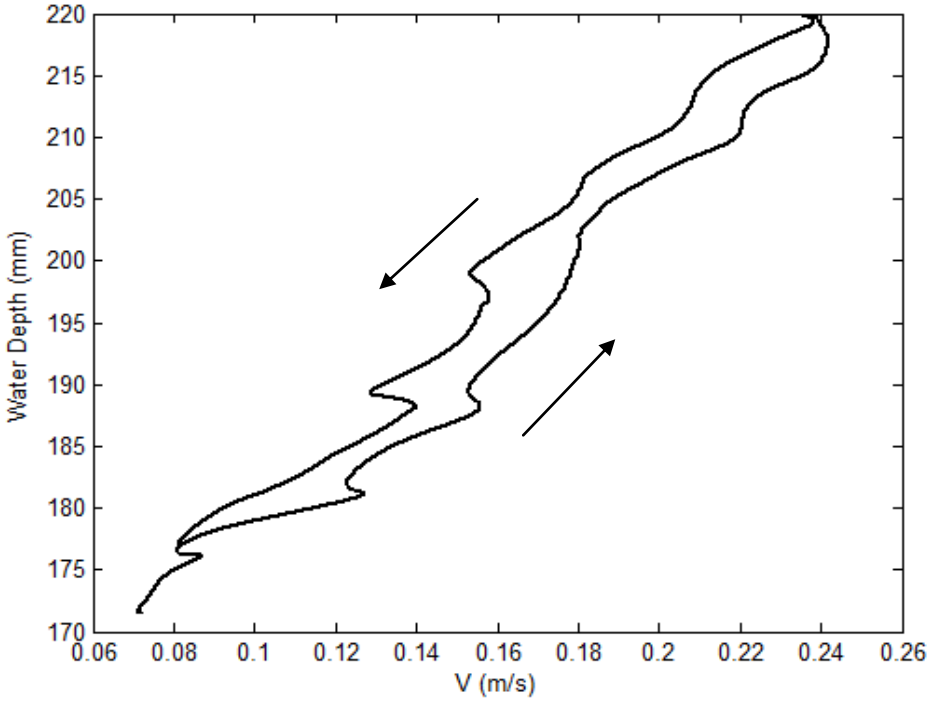

Figure A.7 : The Variation of Depth Avaraged Velocity (*V*) with respect to Water Depth (*h*) During The Passage of Unsteady Flow for Set-2 (d=14 cm), Γ=0.0201.

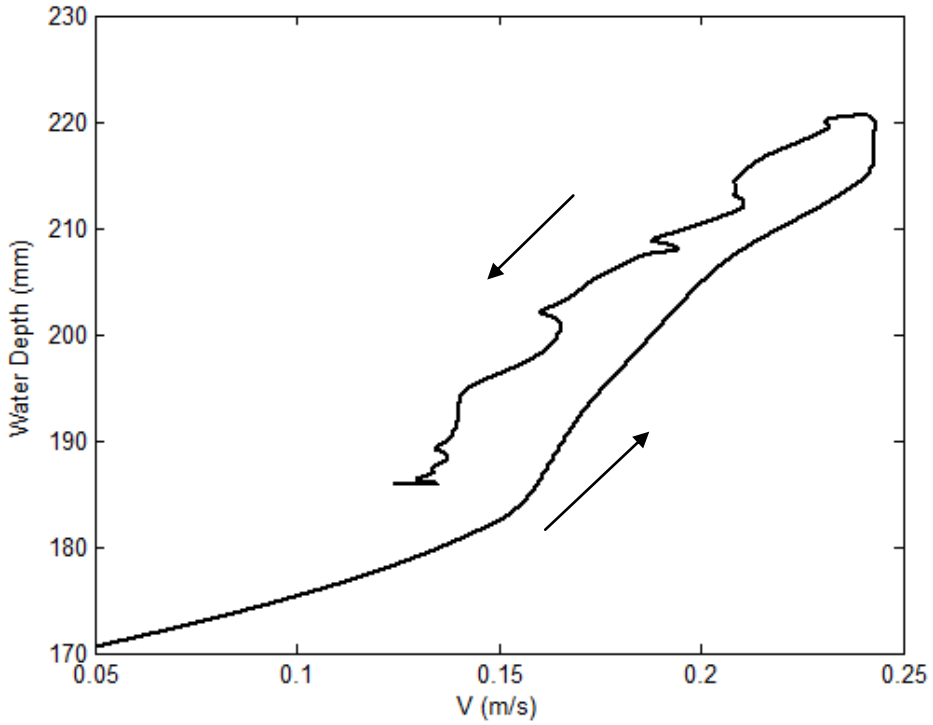

Figure A.8 : The Variation of Depth Avaraged Velocity (*V*) with respect to Water Depth (*h*) During The Passage of Unsteady Flow for Set-2 (d=14 cm), Γ=0.0182.

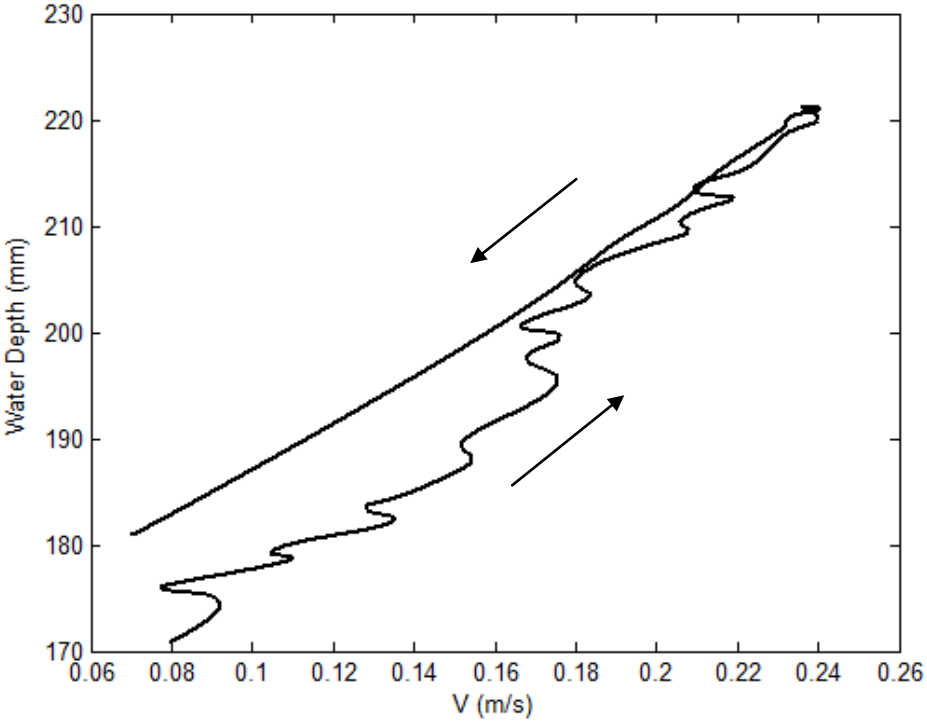

Figure A.9 : The Variation of Depth Avaraged Velocity (*V*) with respect to Water Depth (*h*) During The Passage of Unsteady Flow for Set-2 (d=14 cm), Γ=0.0174.

APPENDIX B

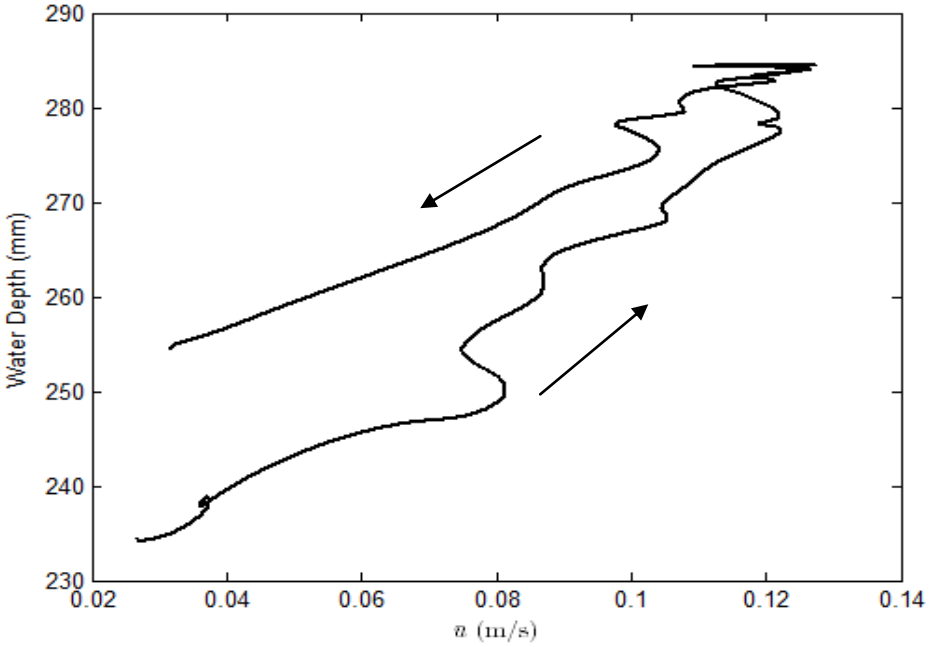

Figure B.1 : The Variaton of Time Avaraged Velocity ($\bar{u}$) at a selected point with respect to Water Depth (h) During The Passage of an Unsteady Flow for Set-1 (d=20 cm), h_1=0.64 cm, Γ=0.0526. .

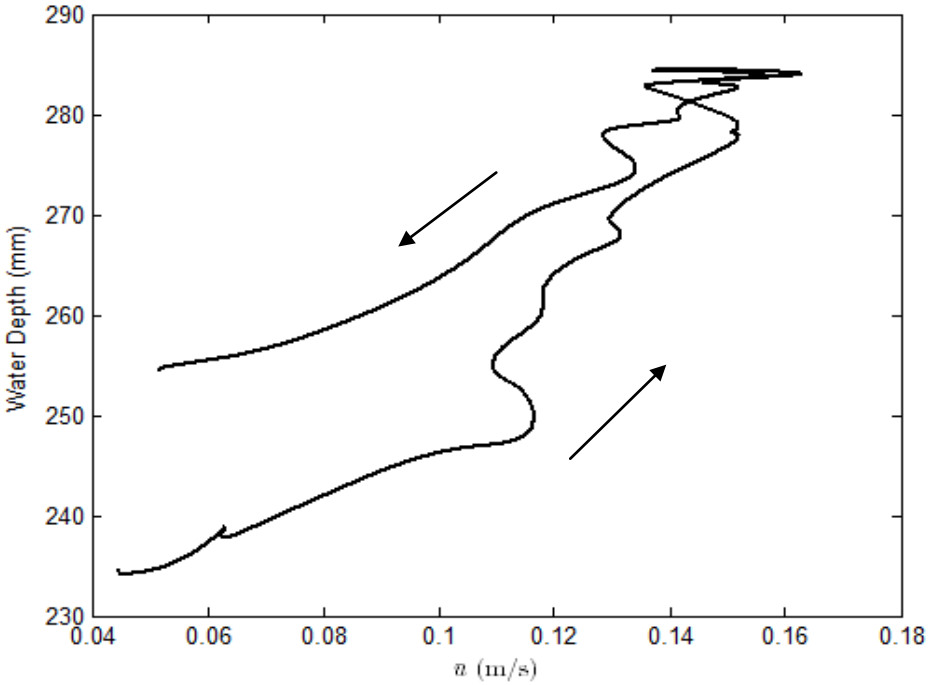

Figure B.2 : The Variaton of Time Avaraged Velocity ($\bar{u}$) at a selected point with respect to Water Depth (h) During The Passage of an Unsteady Flow for Set-1 (d=20 cm), h_1=2.60 cm, Γ=0.0526.

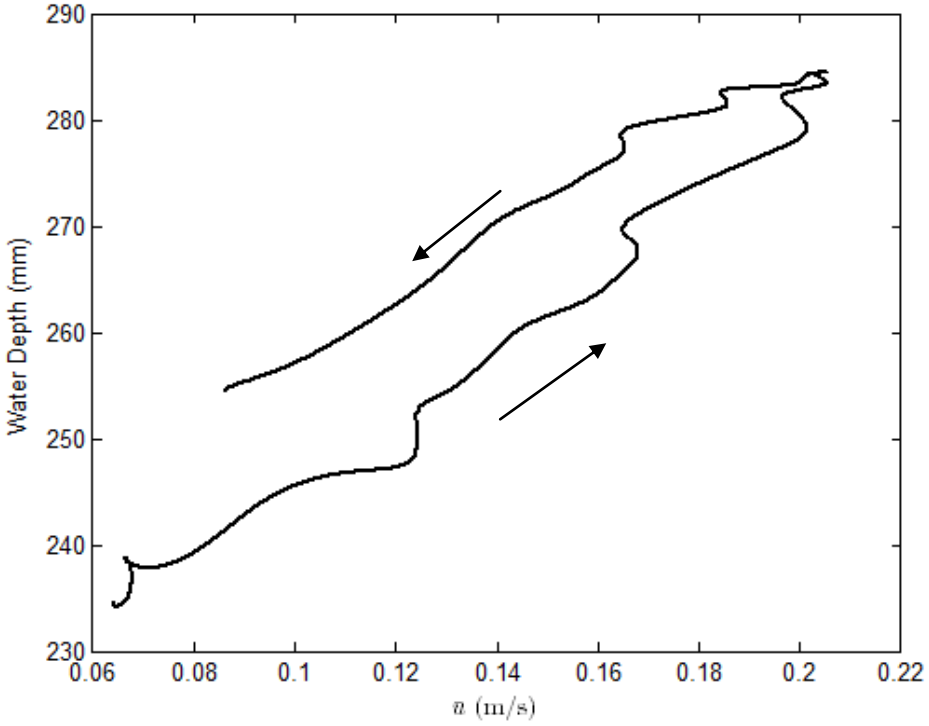

Figure B.3 : The Variaton of Time Avaraged Velocity ($\bar{u}$) at a selected point with respect to Water Depth (h) During The Passage of an Unsteady Flow for Set-1 (d=20 cm), h_1=19.90 cm, Γ=0.0526.

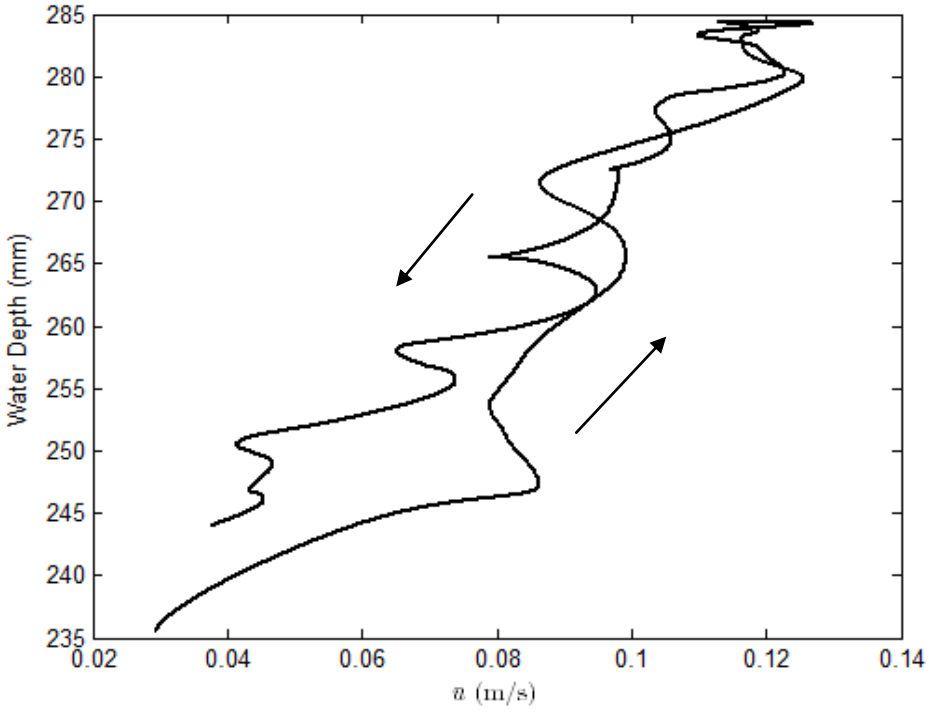

Figure B.4 : The Variaton of Time Avaraged Velocity ($\bar{u}$) at a selected point with respect to Water Depth (h) During The Passage of an Unsteady Flow for Set-1 (d=20 cm), h_1=0.64 cm, Γ=0.0401.

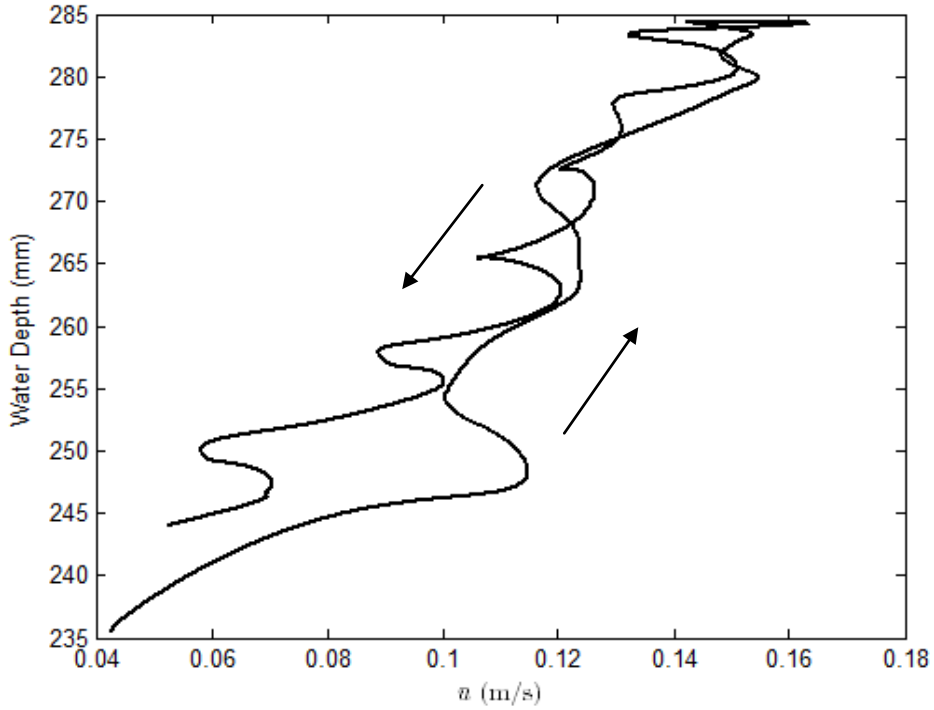

Figure B.5 : The Variaton of Time Avaraged Velocity ($\bar{u}$) at a selected point with respect to Water Depth (h) During The Passage of an Unsteady Flow for Set-1 (d=20 cm), h_1=2.60 cm, Γ=0.0401.

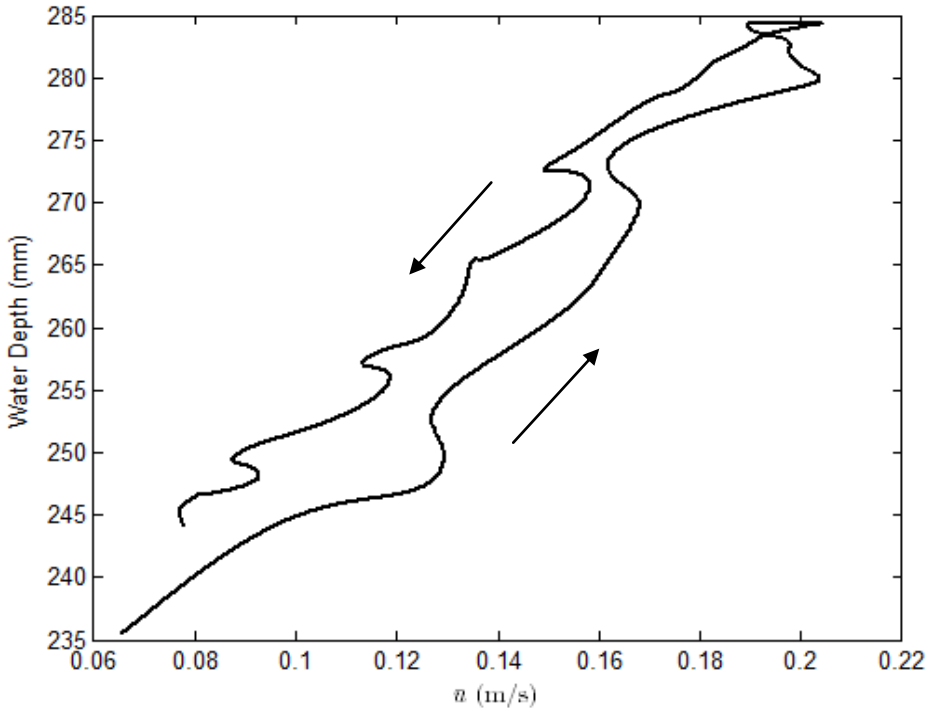

Figure B.6 : The Variaton of Time Avaraged Velocity ($\bar{u}$) at a selected point with respect to Water Depth (h) During The Passage of an Unsteady Flow for Set-1 (d=20 cm), h_1=19.90 cm, Γ=0.0401.

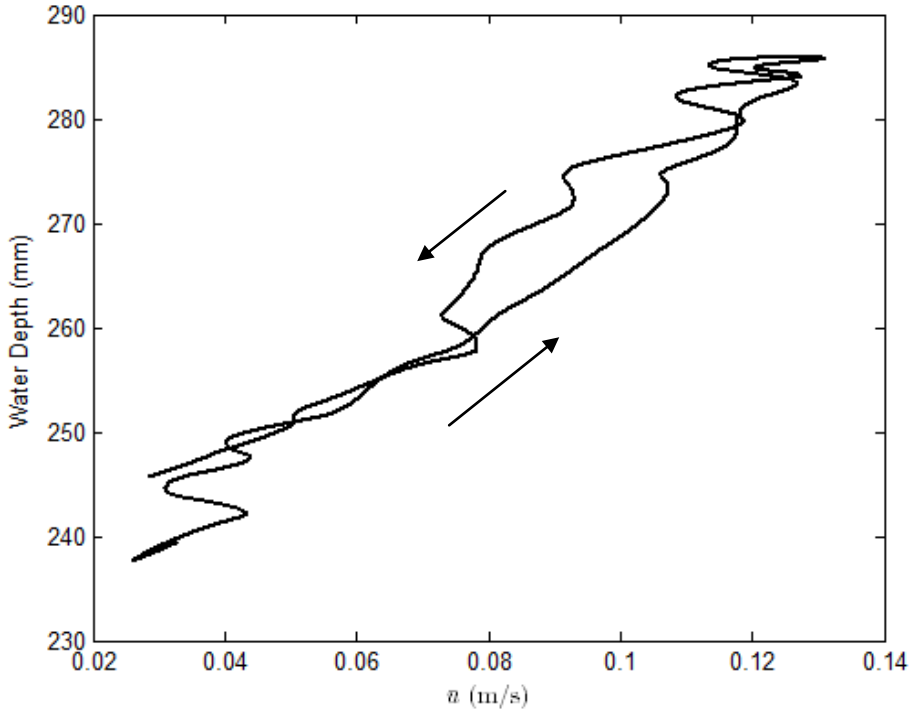

Figure B.7 : The Variaton of Time Avaraged Velocity ($\bar{u}$) at a selected point with respect to Water Depth (h) During The Passage of an Unsteady Flow for Set-1 (d=20 cm), h_1=0.64 cm, Γ=0.0291.

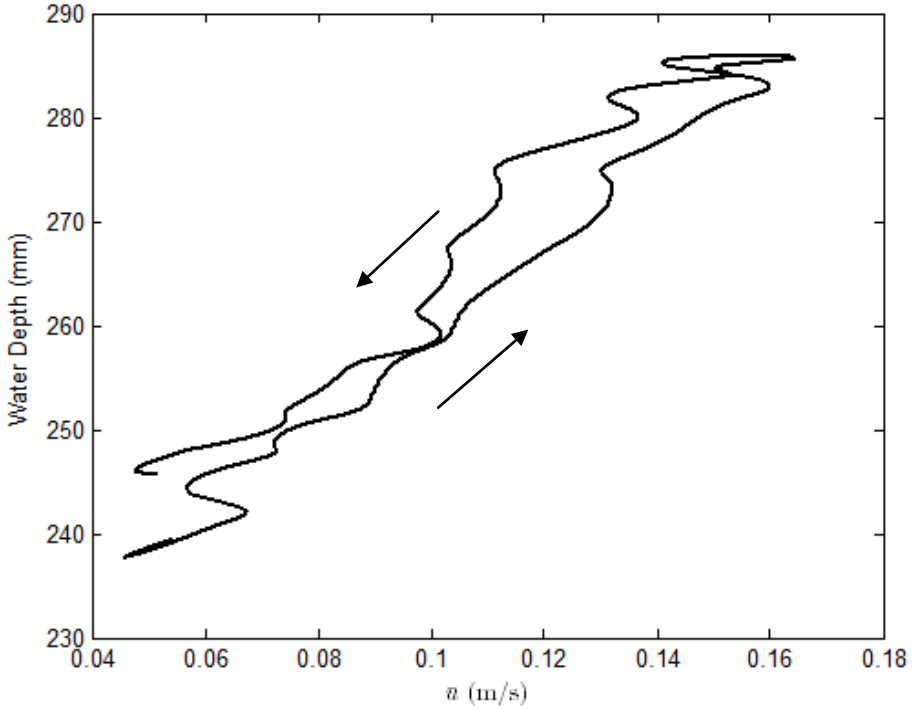

Figure B.8 : The Variaton of Time Avaraged Velocity ($\bar{u}$) at a selected point with respect to Water Depth (h) During The Passage of an Unsteady Flow for Set-1 (d=20 cm), h_1=2.60 cm, Γ=0.0291.

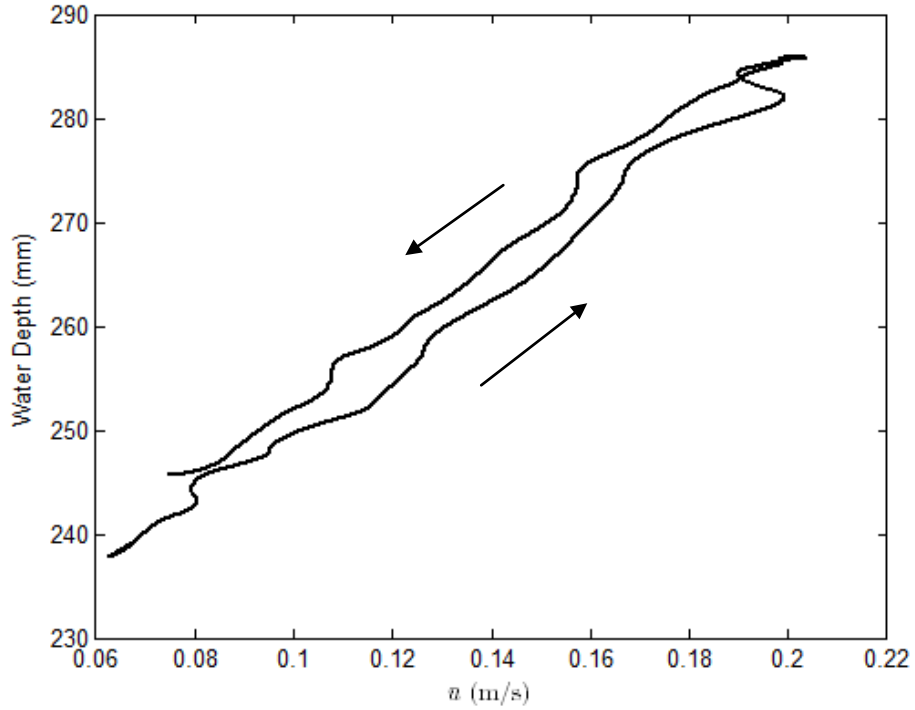

Figure B.9 : The Variaton of Time Avaraged Velocity ($\bar{u}$) at a selected point with respect to Water Depth (h) During The Passage of an Unsteady Flow for Set-1 (d=20 cm), h_1=19.90 cm, Γ=0.0291.

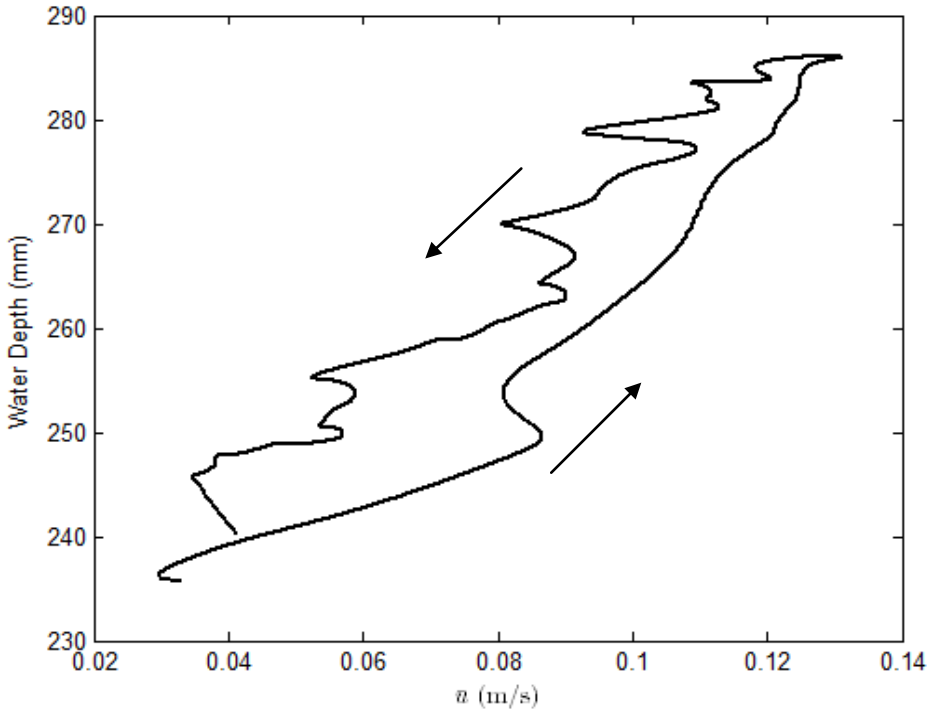

Figure B.10 : The Variaton of Time Avaraged Velocity ($\bar{u}$) at a selected point with respect to Water Depth (h) During The Passage of an Unsteady Flow for Set-1 (d=20 cm), h_1=0.64 cm, Γ=0.0250.

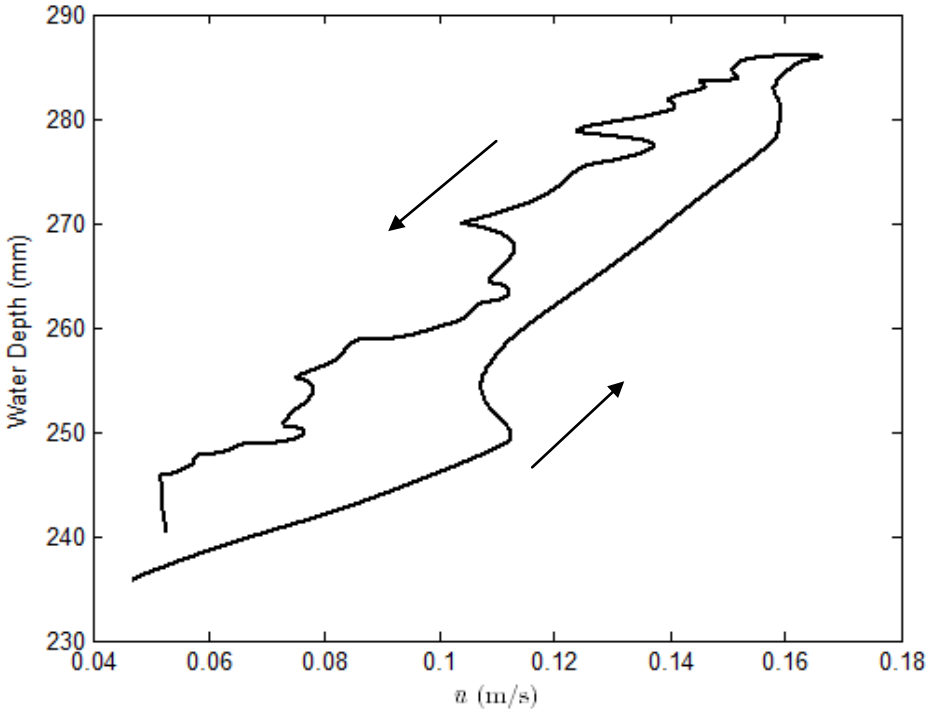

Figure B.11 : The Variaton of Time Avaraged Velocity ($\bar{u}$) at a selected point with respect to Water Depth (h) During The Passage of an Unsteady Flow for Set-1 (d=20 cm), h_1=2.60 cm, Γ=0.0250.

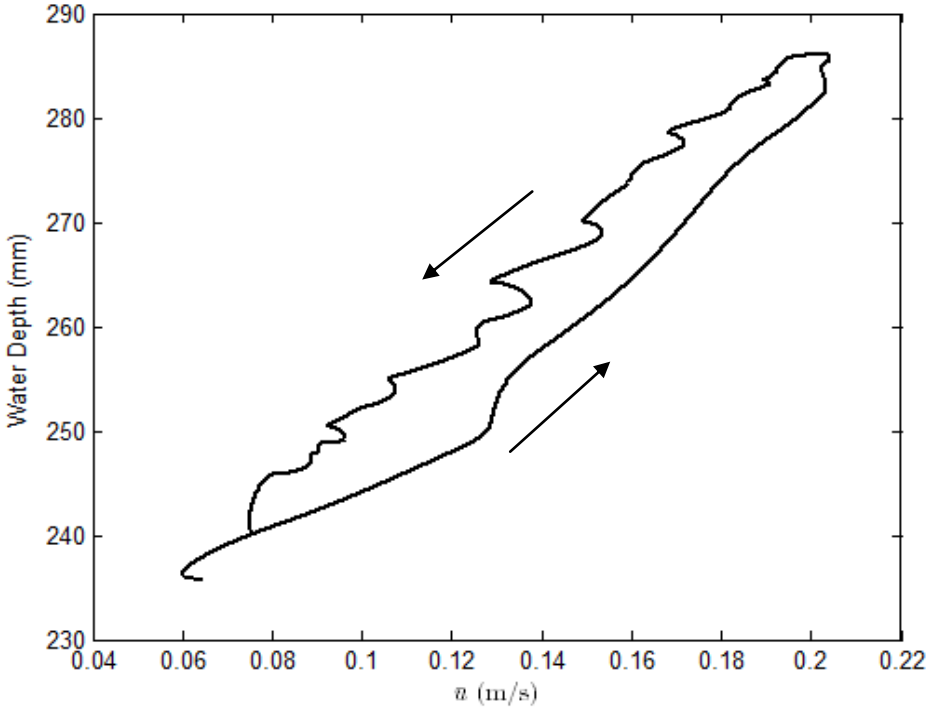

Figure B.12 : The Variaton of Time Avaraged Velocity ($\bar{u}$) at a selected point with respect to Water Depth (h) During The Passage of an Unsteady Flow for Set-1 (d=20 cm), h_1=19.90 cm, Γ=0.0250.

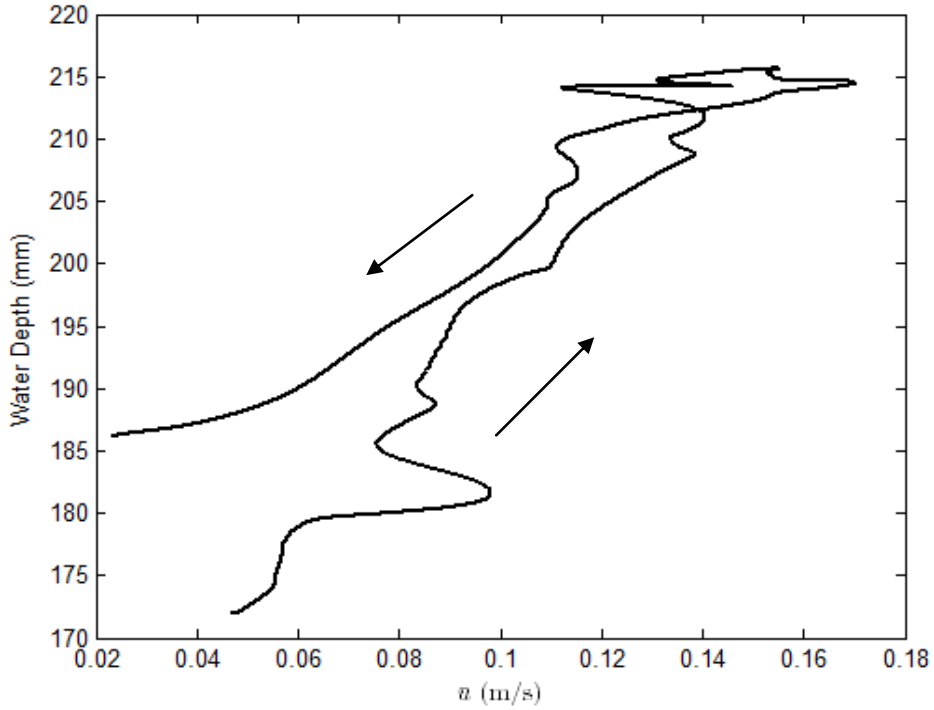

Figure B.13 : The Variaton of Time Avaraged Velocity ($\bar{u}$) at a selected point with respect to Water Depth (h) During The Passage of an Unsteady Flow for Set-2 (d=14 cm), h_1=2.24 cm, Γ=0.0445.

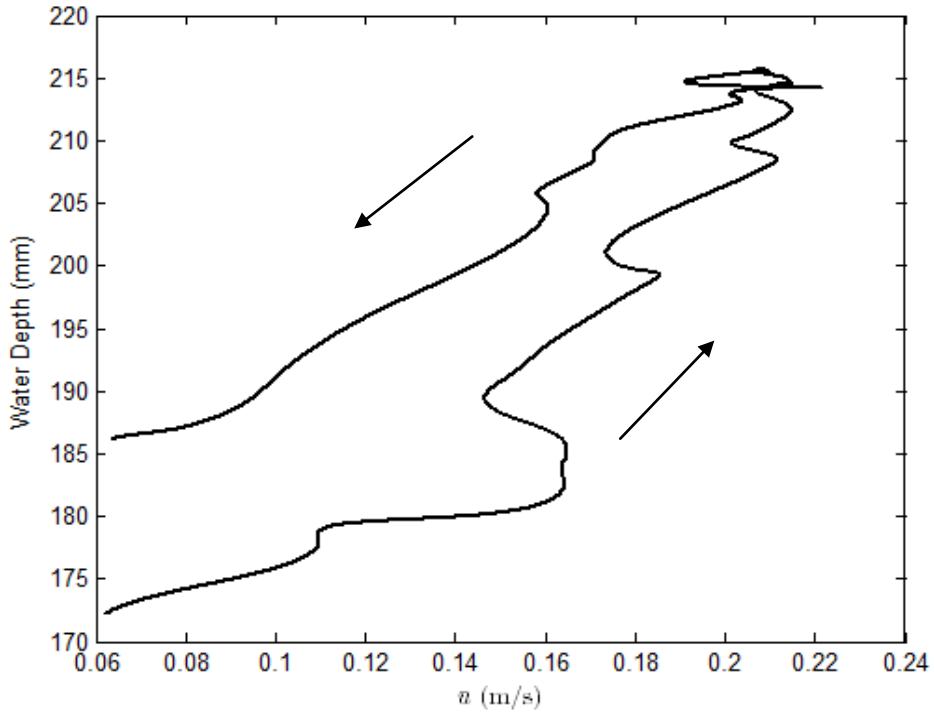

Figure B.14 : The Variaton of Time Avaraged Velocity ($\bar{u}$) at a selected point with respect to Water Depth (h) During The Passage of an Unsteady Flow for Set-2 (d=14 cm), h_1=3.67 cm, Γ=0.0445.

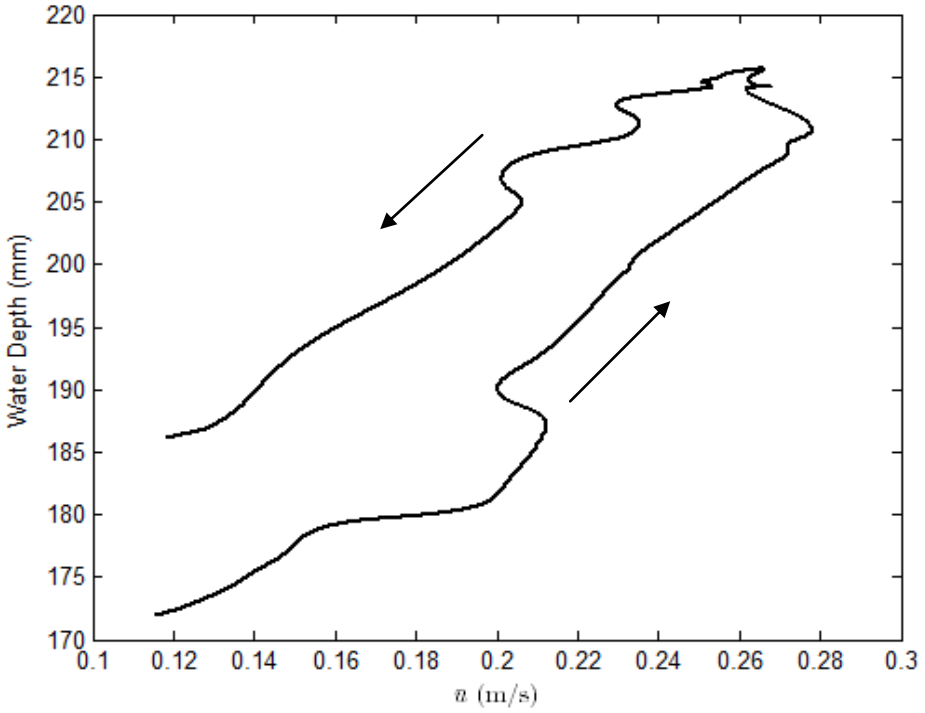

Figure B.15 : The Variaton of Time Avaraged Velocity ($\bar{u}$) at a selected point with respect to Water Depth (h) During The Passage of an Unsteady Flow for Set-2 (d=14 cm), h_1=16.34 cm, Γ=0.0445.

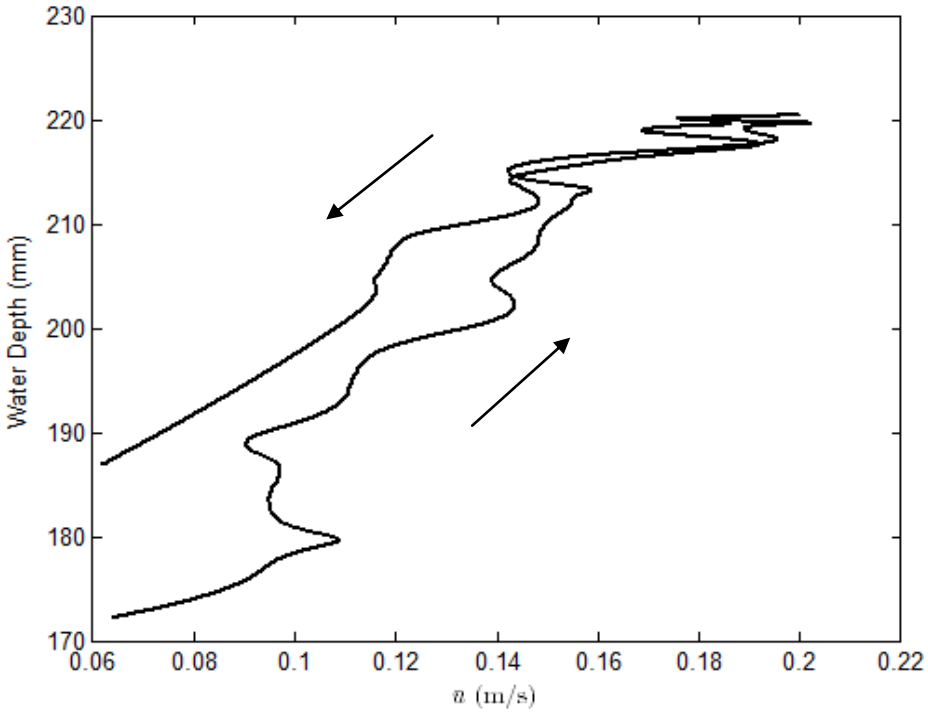

Figure B.16 : The Variaton of Time Avaraged Velocity ($\bar{u}$) at a selected point with respect to Water Depth (h) During The Passage of an Unsteady Flow for Set-2 (d=14 cm), h_1=2.44 cm, Γ=0.0376.

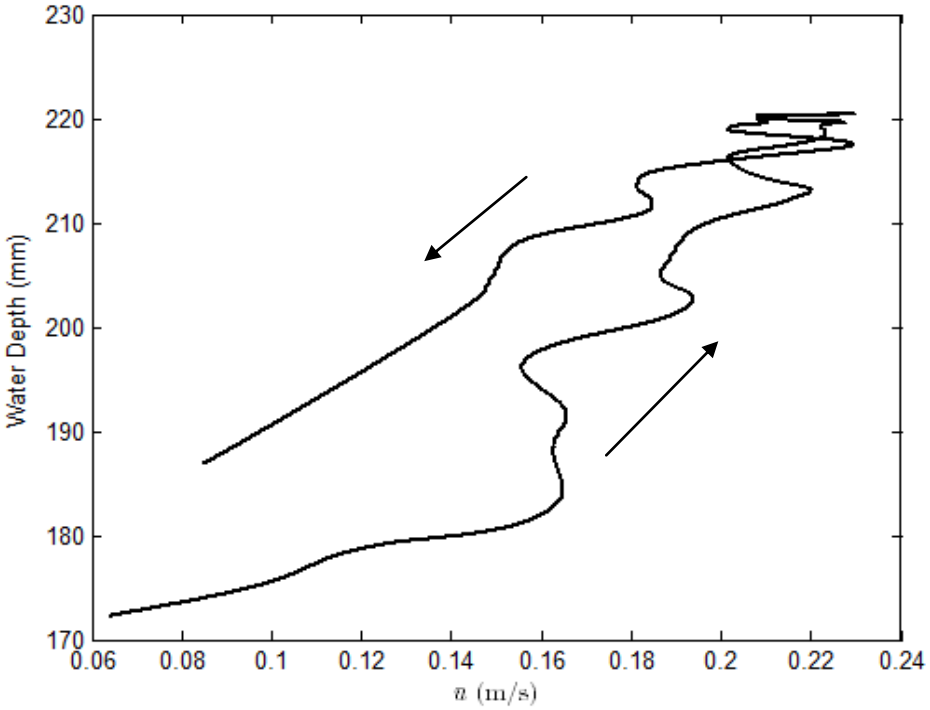

Figure B.17 : The Variaton of Time Avaraged Velocity ($\bar{u}$) at a selected point with respect to Water Depth (h) During The Passage of an Unsteady Flow for Set-2 (d=14 cm), h_1=3.67 cm, Γ=0.0376.

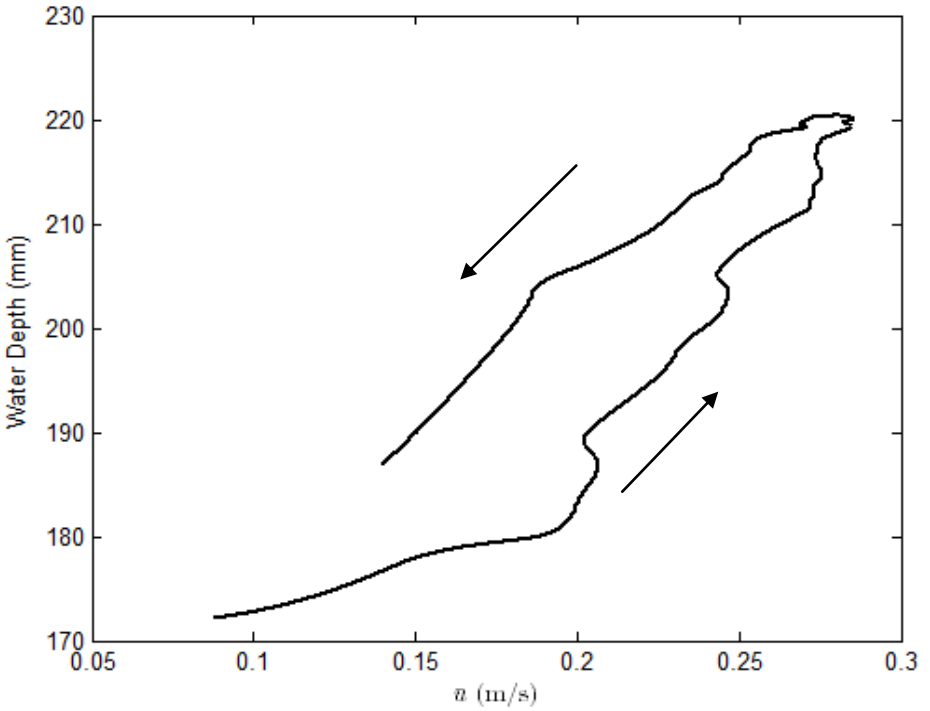

Figure B.18 : The Variaton of Time Avaraged Velocity ($\bar{u}$) at a selected point with respect to Water Depth (h) During The Passage of an Unsteady Flow for Set-2 (d=14 cm), h_1=16.34 cm, Γ=0.0376.

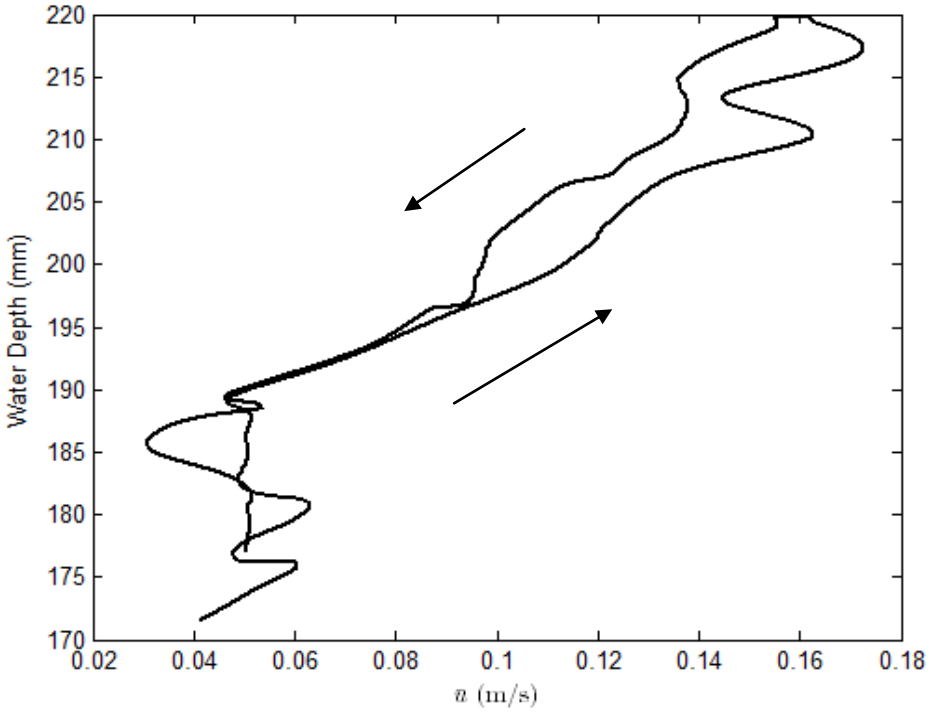

Figure B.19 : The Variaton of Time Avaraged Velocity ($\bar{u}$) at a selected point with respect to Water Depth (h) During The Passage of an Unsteady Flow for Set-2 (d=14 cm), h_1=2.24 cm, Γ=0.0201.

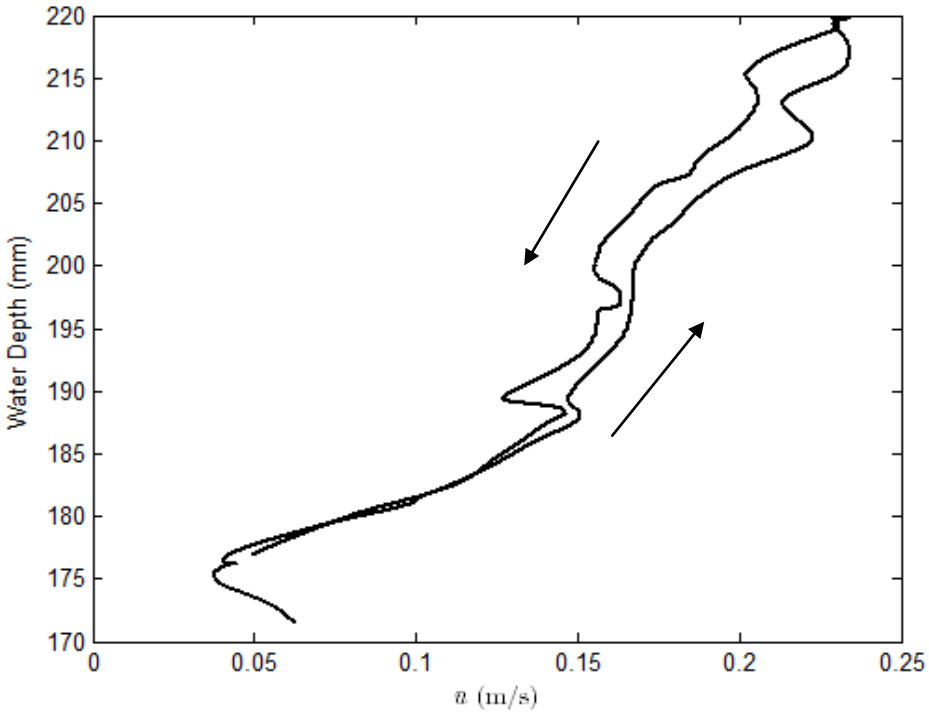

Figure B.20 : The Variaton of Time Avaraged Velocity ($\bar{u}$) at a selected point with respect to Water Depth (h) During The Passage of an Unsteady Flow for Set-2 (d=14 cm), h_1=3.67 cm, Γ=0.201.

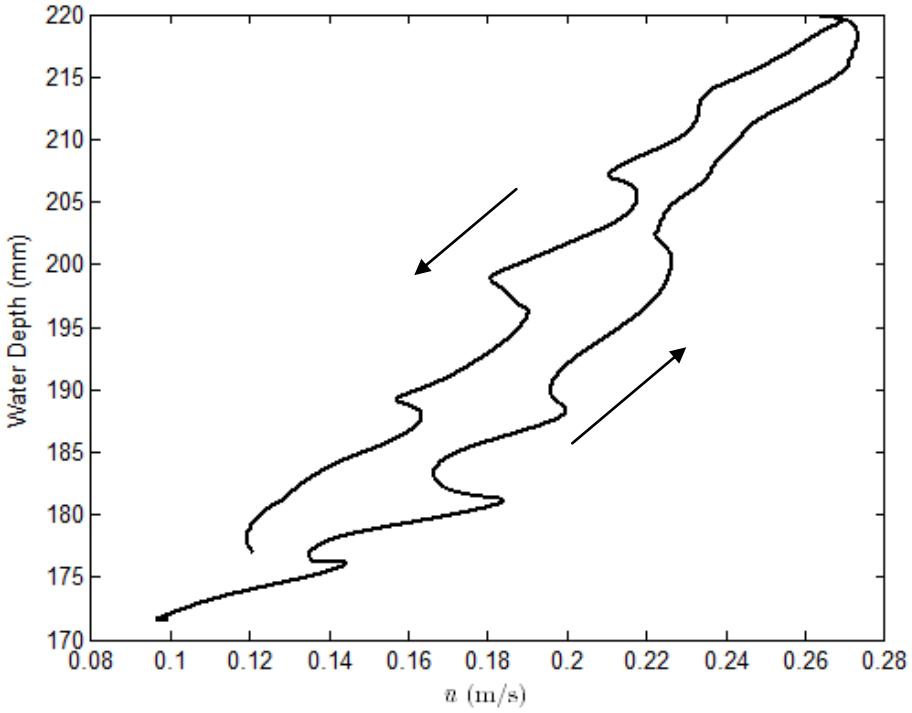

Figure B.21 : The Variaton of Time Avaraged Velocity ($\bar{u}$) at a selected point with respect to Water Depth (h) During The Passage of an Unsteady Flow for Set-2 (d=14 cm), h_1=16.34 cm, Γ=0.201.

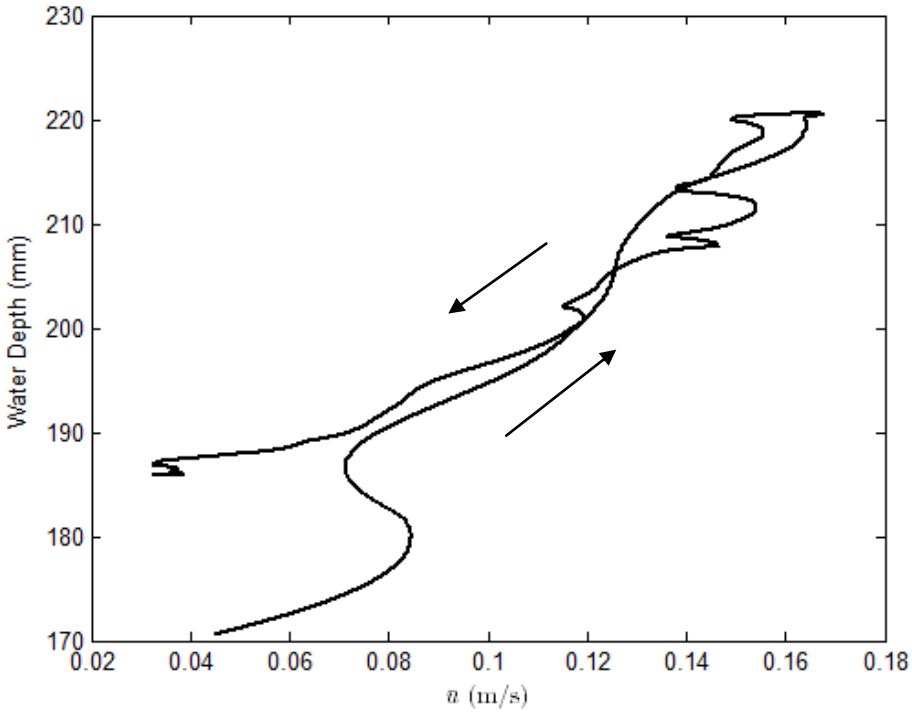

Figure B.22 : The Variaton of Time Avaraged Velocity ($\bar{u}$) at a selected point with respect to Water Depth (h) During The Passage of an Unsteady Flow for Set-2 (d=14 cm), h_1=2.24 cm, Γ=0.181.

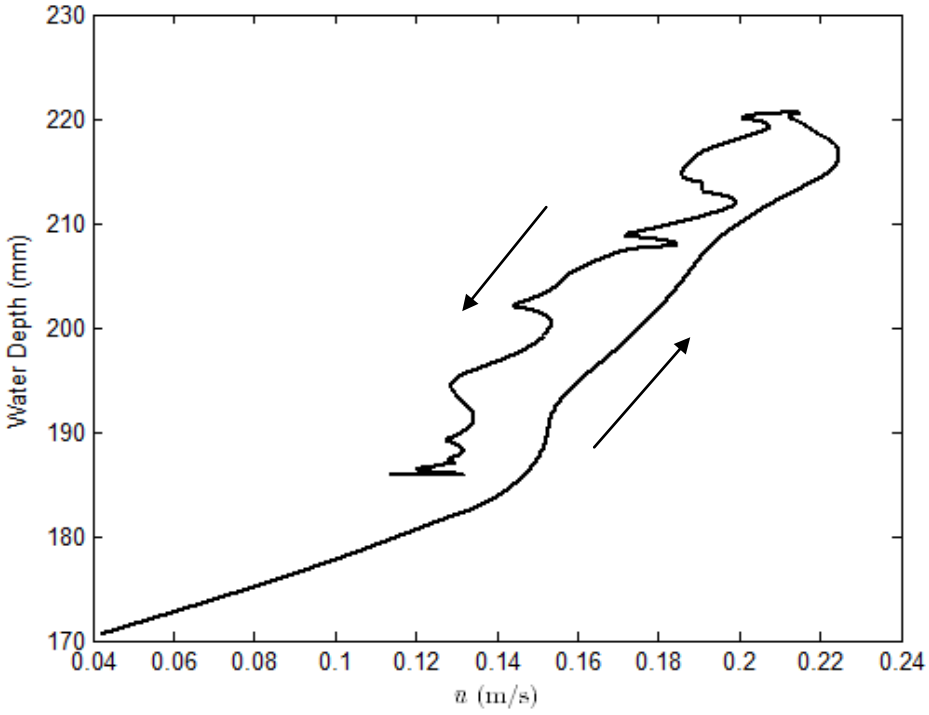

Figure B.23 : The Variaton of Time Avaraged Velocity ($\bar{u}$) at a selected point with respect to Water Depth (h) During The Passage of an Unsteady Flow for Set-2 (d=14 cm), h_1=3.67 cm, Γ=0.181.

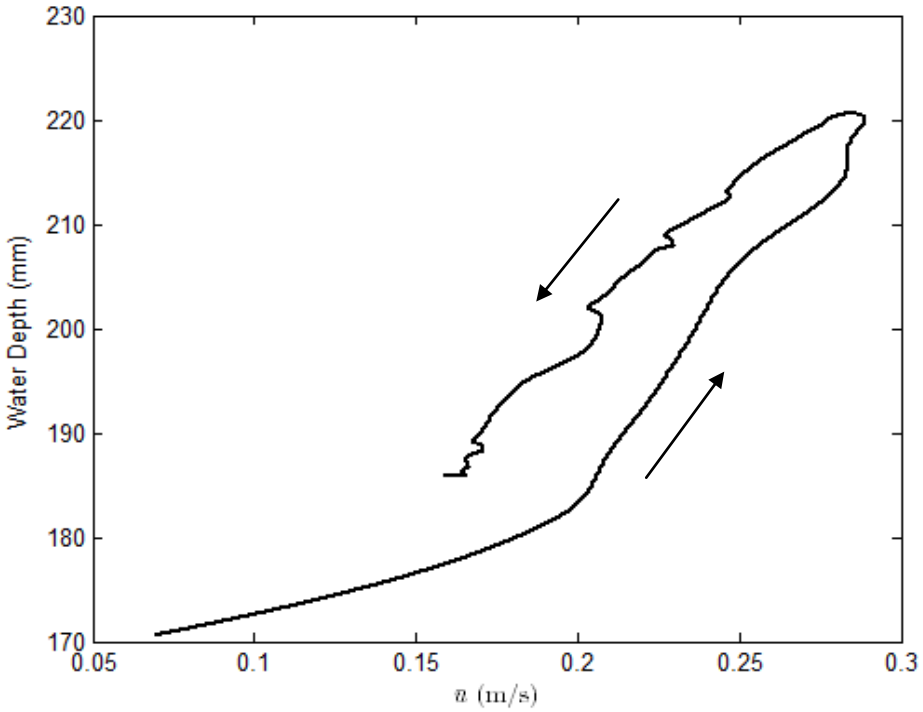

Figure B.24 : The Variaton of Time Avaraged Velocity ($\bar{u}$) at a selected point with respect to Water Depth (h) During The Passage of an Unsteady Flow for Set-2 (d=14 cm), h_1=16.34 cm, Γ=0.181.

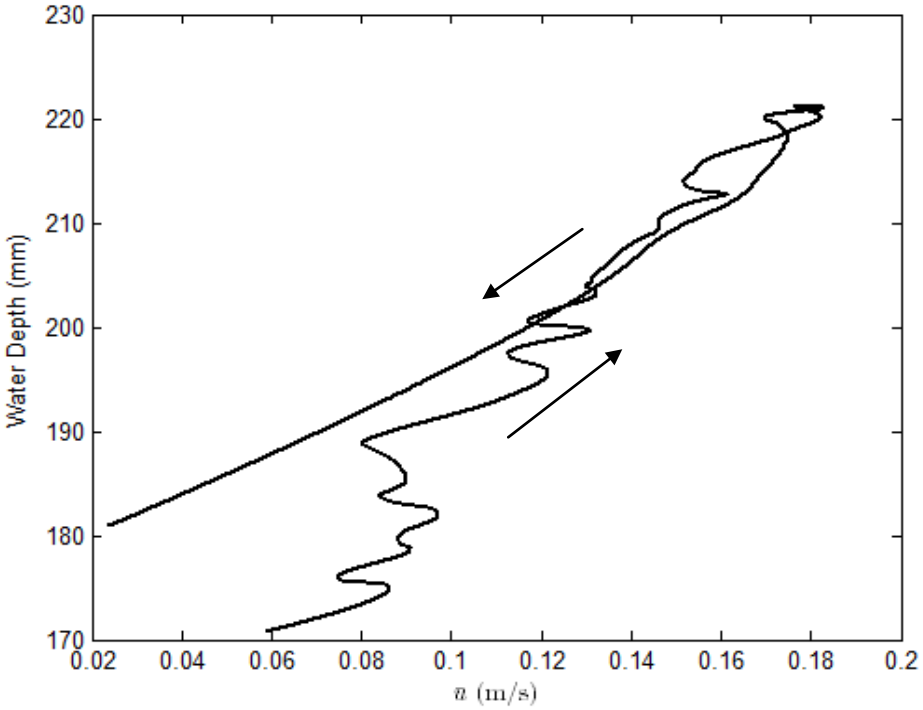

Figure B.25 : The Variaton of Time Avaraged Velocity ($\bar{u}$) at a selected point with respect to Water Depth (h) During The Passage of an Unsteady Flow for Set-2 (d=14 cm), h_1=2.24 cm, Γ=0.134.

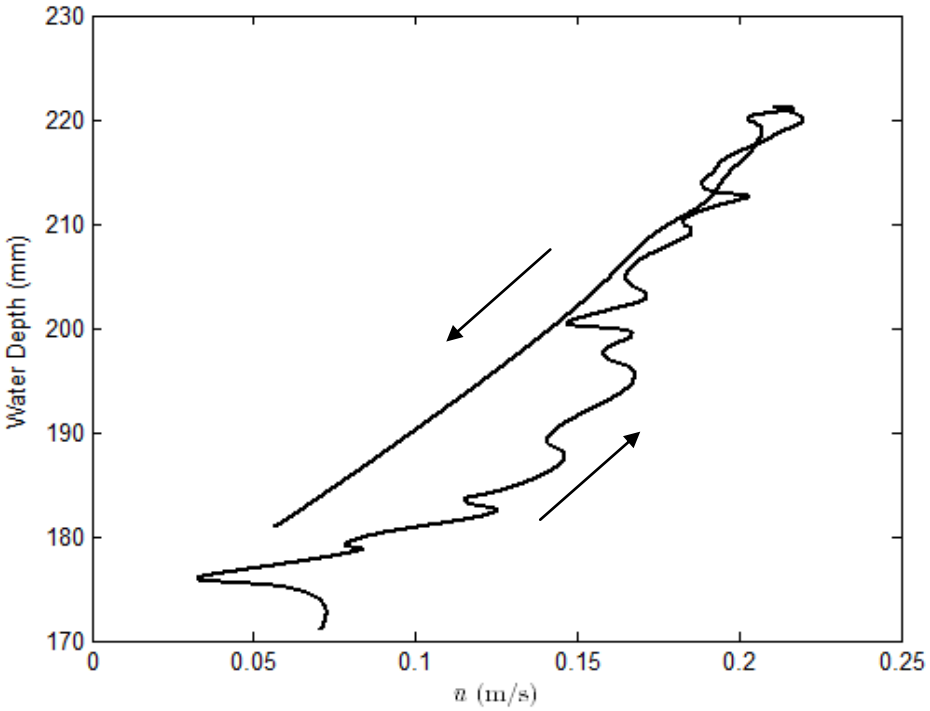

Figure B.26 : The Variaton of Time Avaraged Velocity ($\bar{u}$) at a selected point with respect to Water Depth (h) During The Passage of an Unsteady Flow for Set-2 (d=14 cm), h_1=3.67 cm, Γ=0.134.

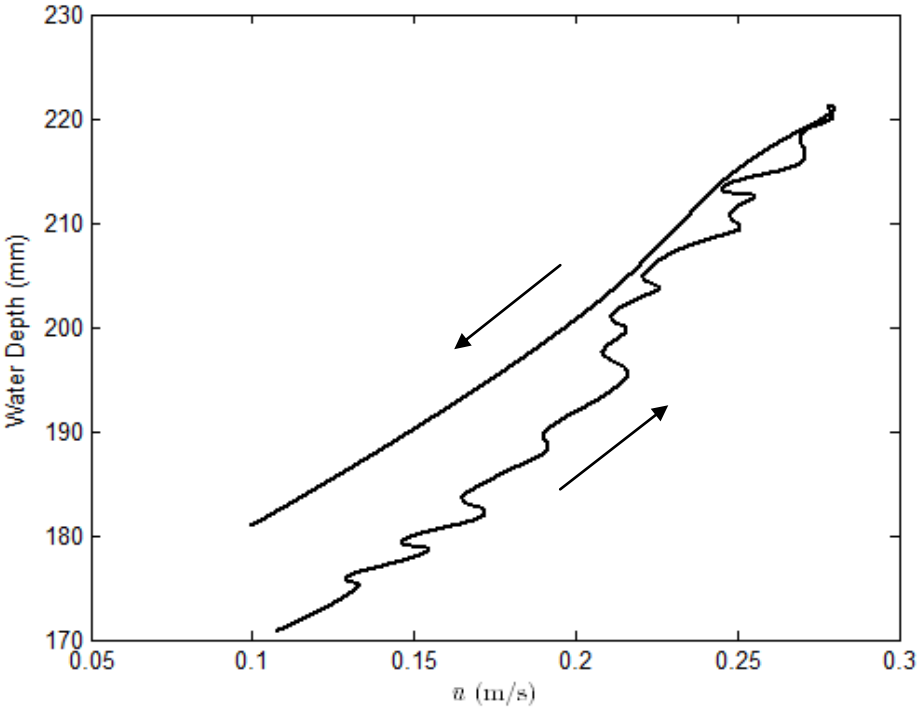

Figure B.27 : The Variaton of Time Avaraged Velocity ($\bar{u}$) at a selected point with respect to Water Depth (h) During The Passage of an Unsteady Flow for Set-2 (d=14 cm), h_1=16.34 cm, Γ=0.134.

APPENDIX C

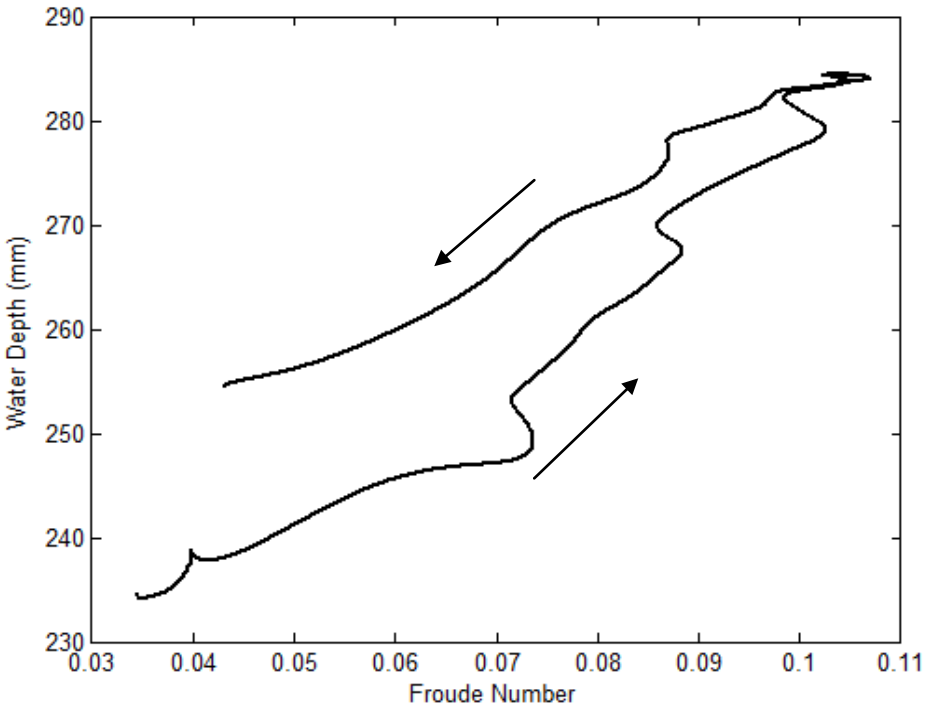

Figure C.1 : The Variation of Froude Number (*Fr*) with respect to Water Depth (*h*) During The Passage of Unsteady Flow for Set-1 (d=20 cm), Γ=0.0526.

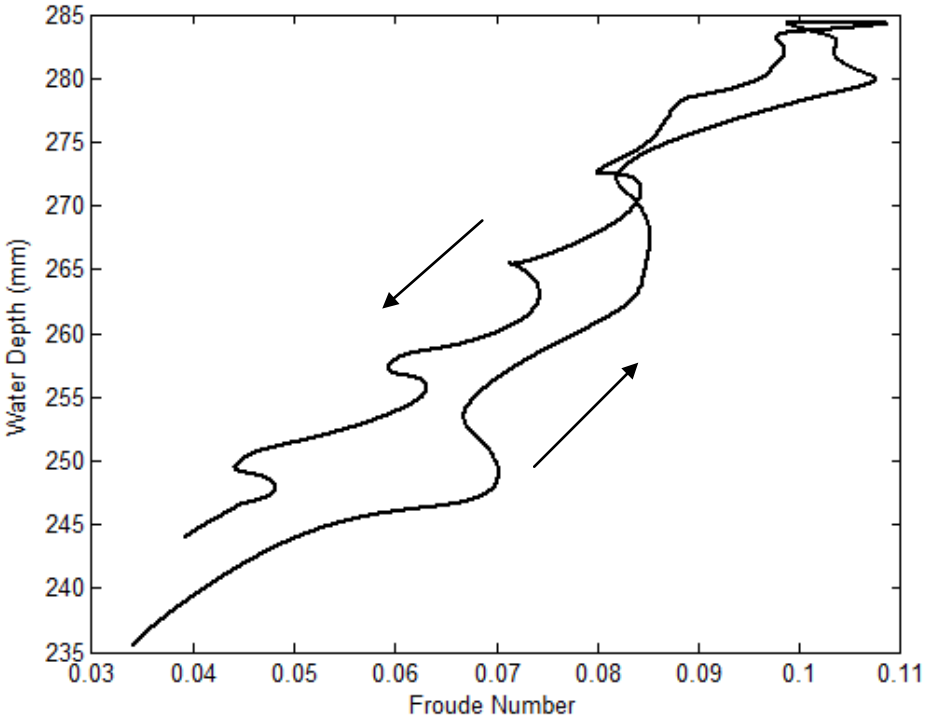

Figure C.2 : The Variation of Froude Number (*Fr*) with respect to Water Depth (*h*) During The Passage of Unsteady Flow for Set-1 (d=20 cm), Γ=0.0401.

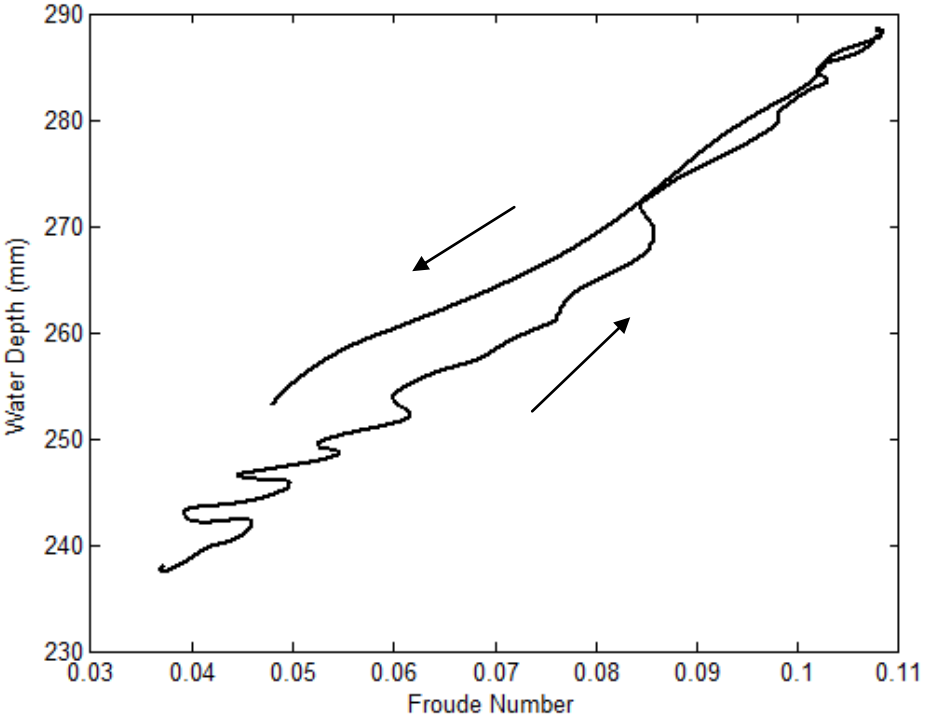

Figure C.3 : The Variation of Froude Number (*Fr*) with respect to Water Depth (*h*) During The Passage of Unsteady Flow for Set-1 (d=20 cm), Γ=0.0256.

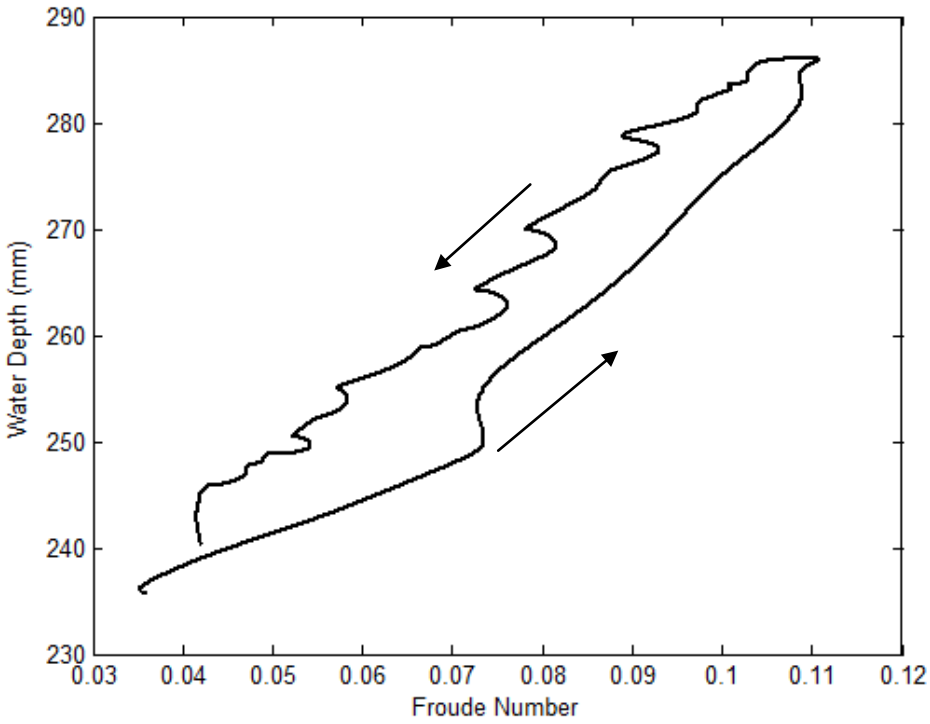

Figure C.4 : The Variation of Froude Number (*Fr*) with respect to Water Depth (*h*) During The Passage of Unsteady Flow for Set-1 (d=20 cm), Γ=0.0250.

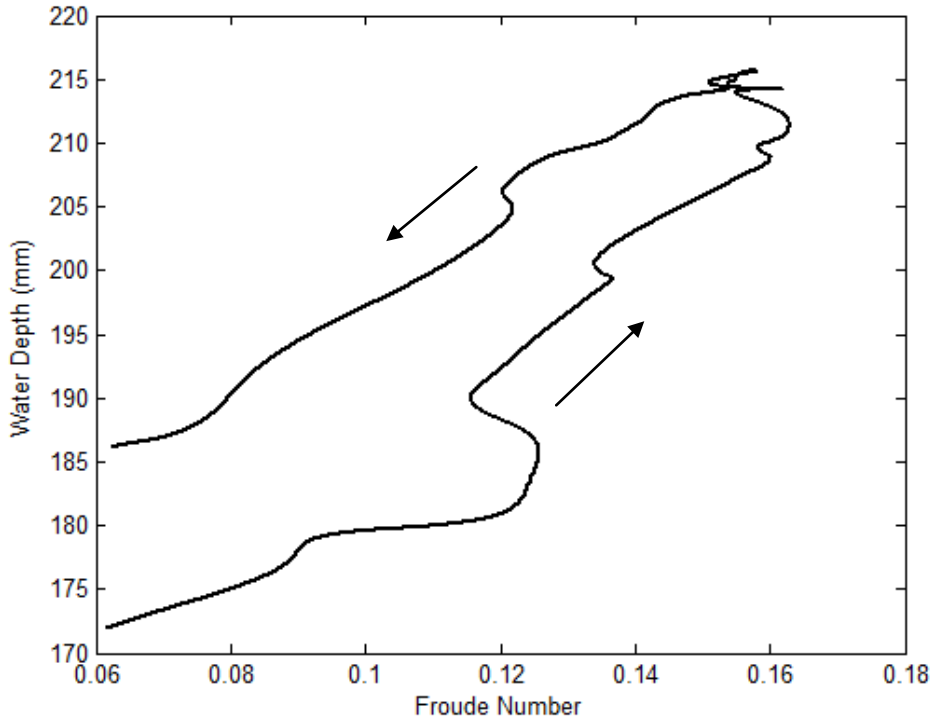

Figure C.5 : The Variation of Froude Number (*Fr*) with respect to Water Depth (*h*) During The Passage of Unsteady Flow for Set-2 (d=14 cm), Γ=0.0445.

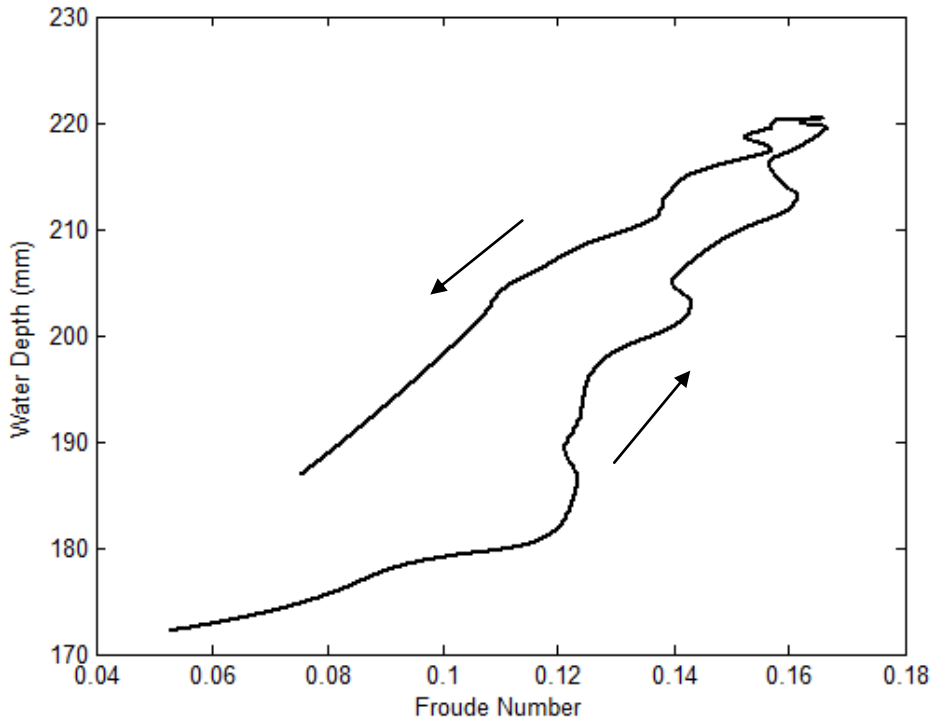

Figure C.6 : The Variation of Froude Number (*Fr*) with respect to Water Depth (*h*) During The Passage of Unsteady Flow for Set-2 (d=14 cm), Γ=0.0376.

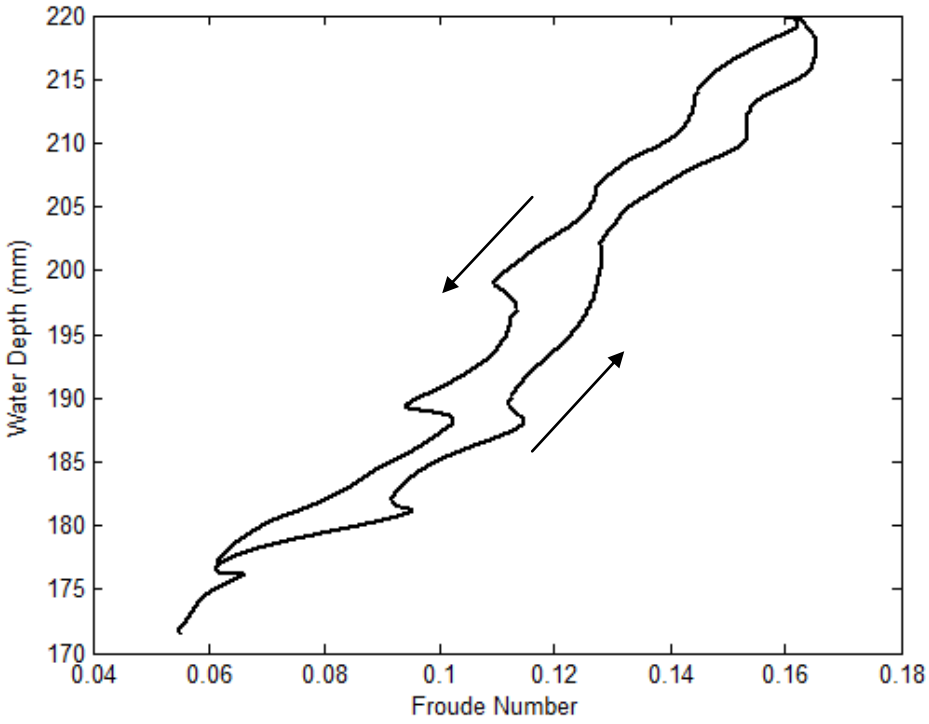

Figure C.7 : The Variation of Froude Number (*Fr*) with respect to Water Depth (*h*) During The Passage of Unsteady Flow for Set-2 (d=14 cm), Γ=0.0201.

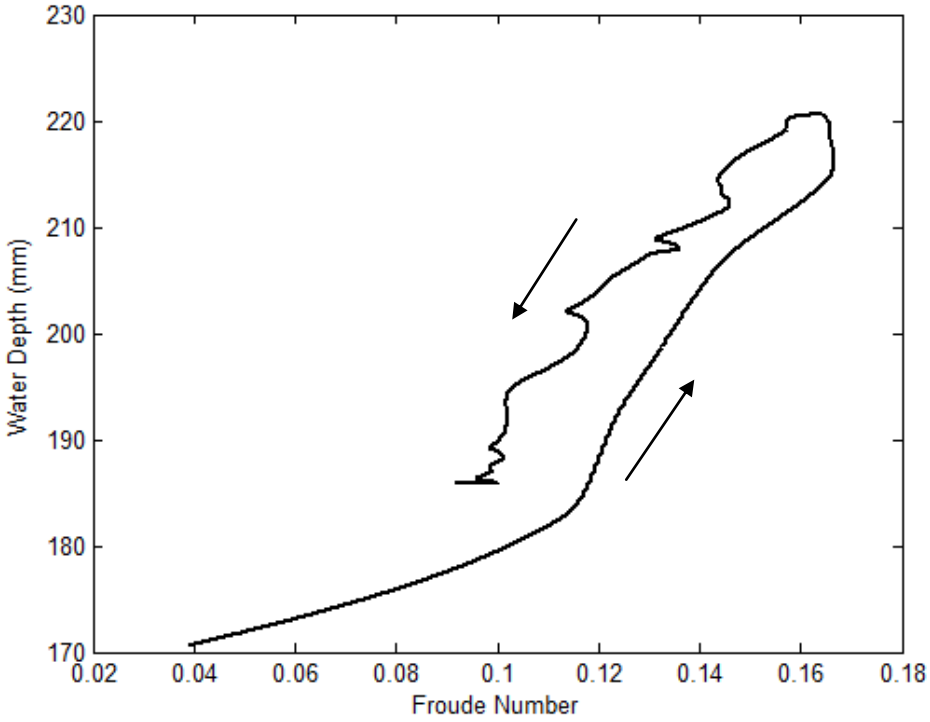

Figure C.8 : The Variation of Froude Number (*Fr*) with respect to Water Depth (*h*) During The Passage of Unsteady Flow for Set-2 (d=14 cm), Γ=0.0181.

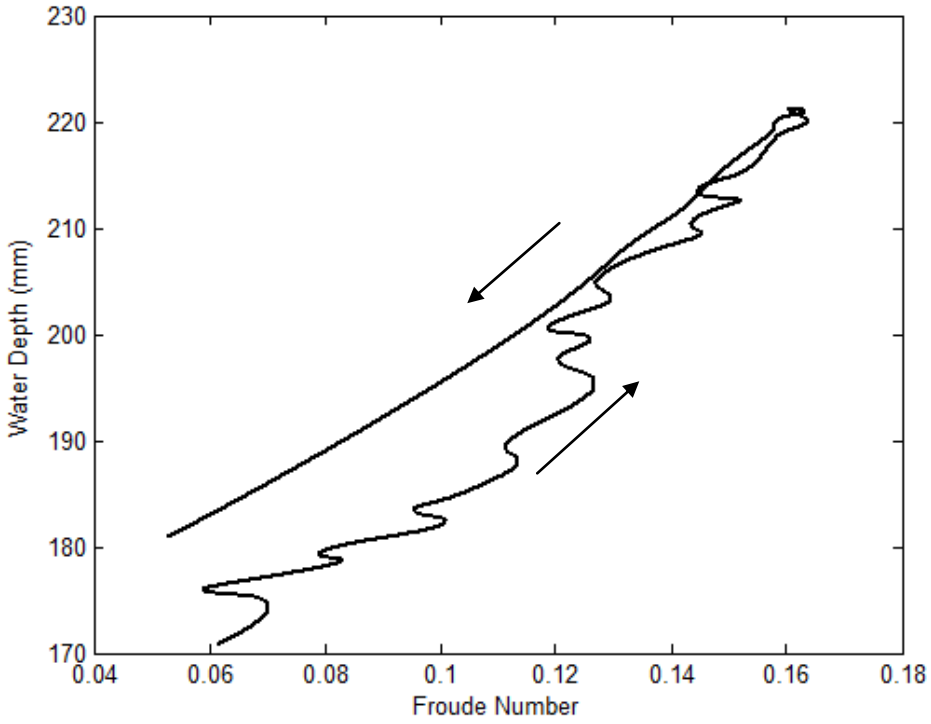

Figure C.9 : The Variation of Froude Number (*Fr*) with respect to Water Depth (*h*) During The Passage of Unsteady Flow for Set-2 (d=14 cm), Γ=0.0134.

APPENDIX D

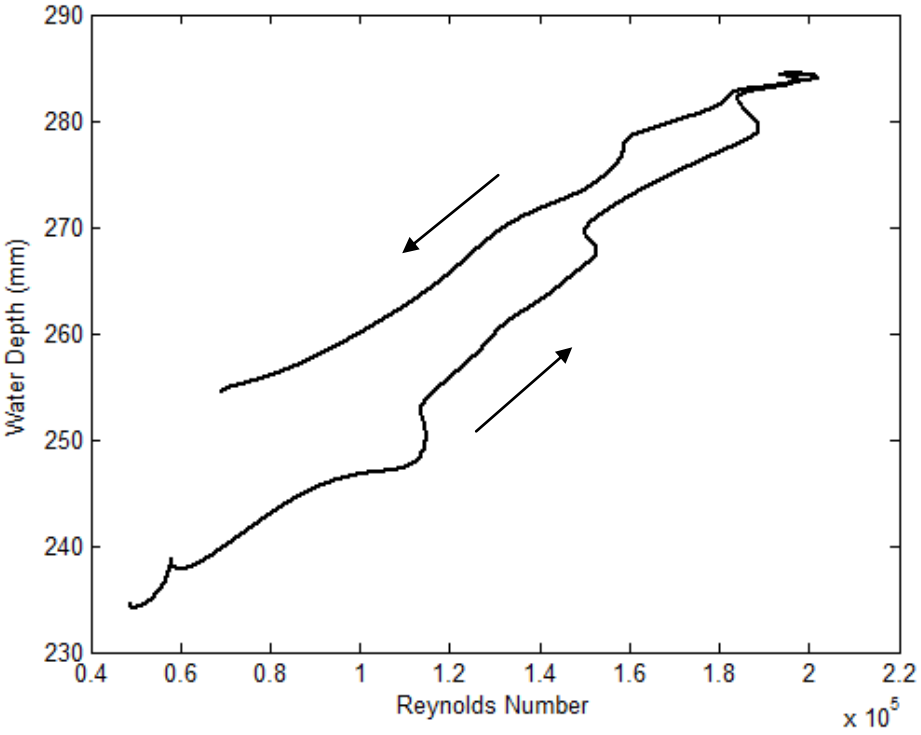

Figure D.1 : The Variation of Reynolds Number (*Re*) with respect to Water Depth (*h*) During The Passage of Unsteady Flow for Set-1 (d=20 cm), Γ=0.0526.

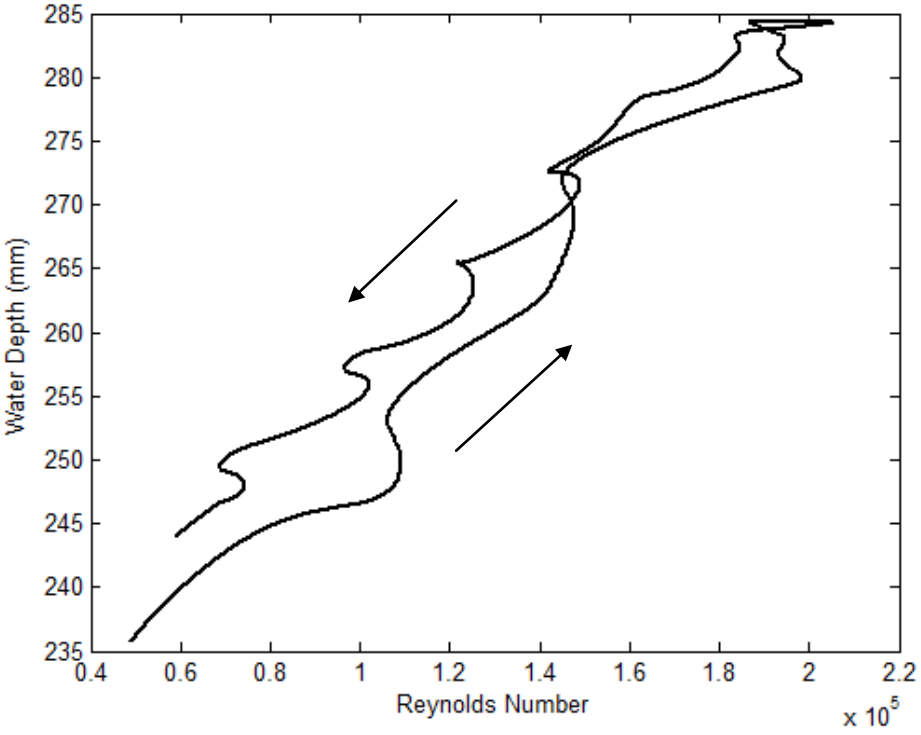

Figure D.2 : The Variation of Reynolds Number (*Re*) with respect to Water Depth (*h*) During The Passage of Unsteady Flow for Set-1 (d=20 cm), Γ=0.0401.

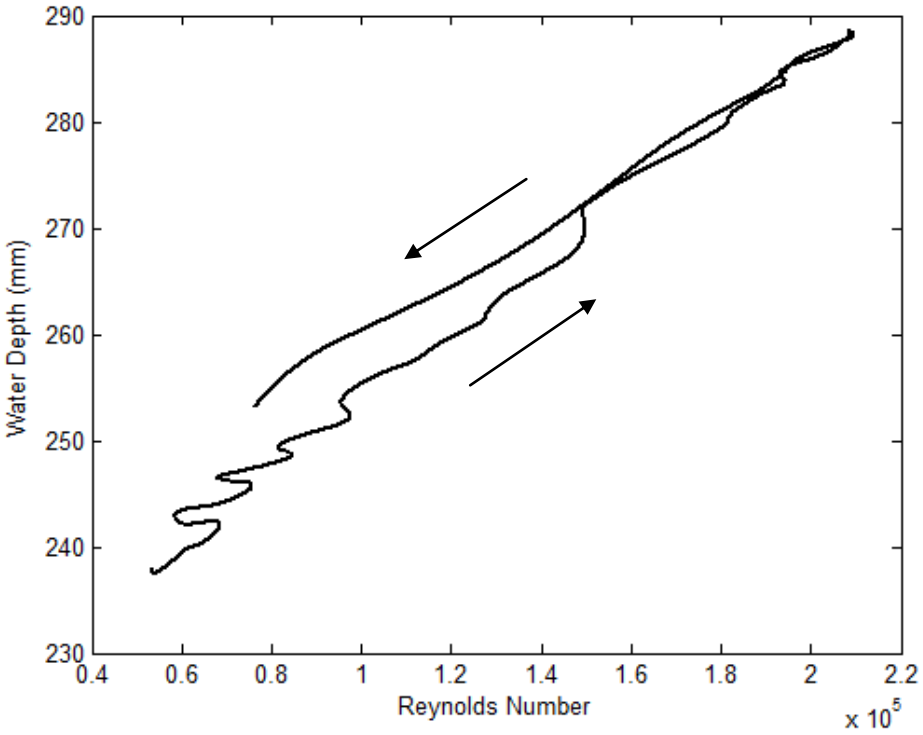

Figure D.3 : The Variation of Reynolds Number (*Re*) with respect to Water Depth (*h*) During The Passage of Unsteady Flow for Set-1 (d=20 cm), Γ=0.0256.

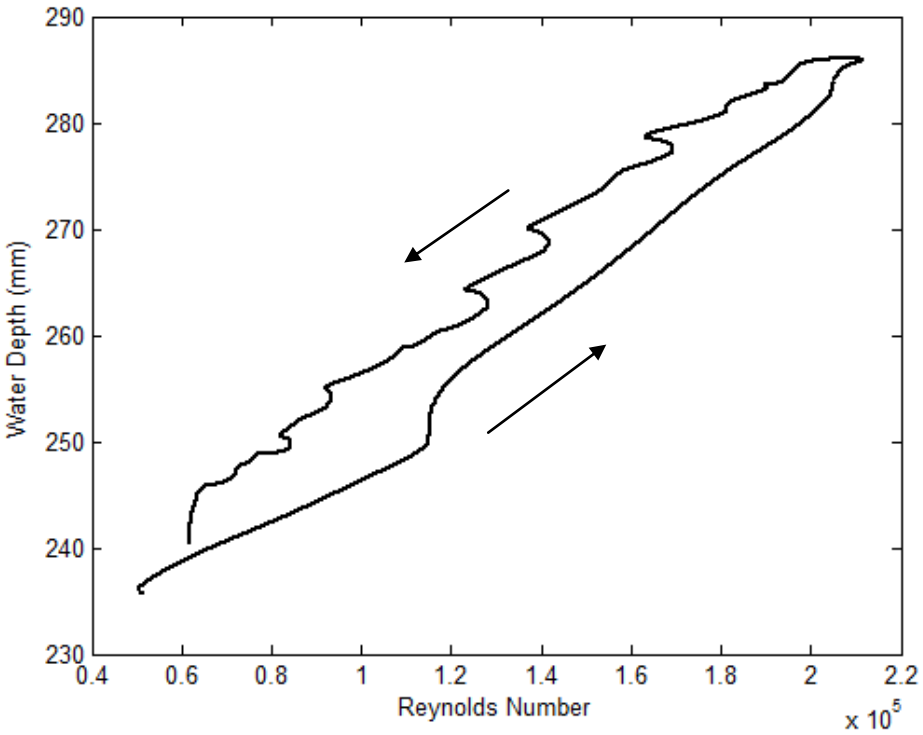

Figure D.4 : The Variation of Reynolds Number (*Re*) with respect to Water Depth (*h*) During The Passage of Unsteady Flow for Set-1 (d=20 cm), Γ=0.0250.

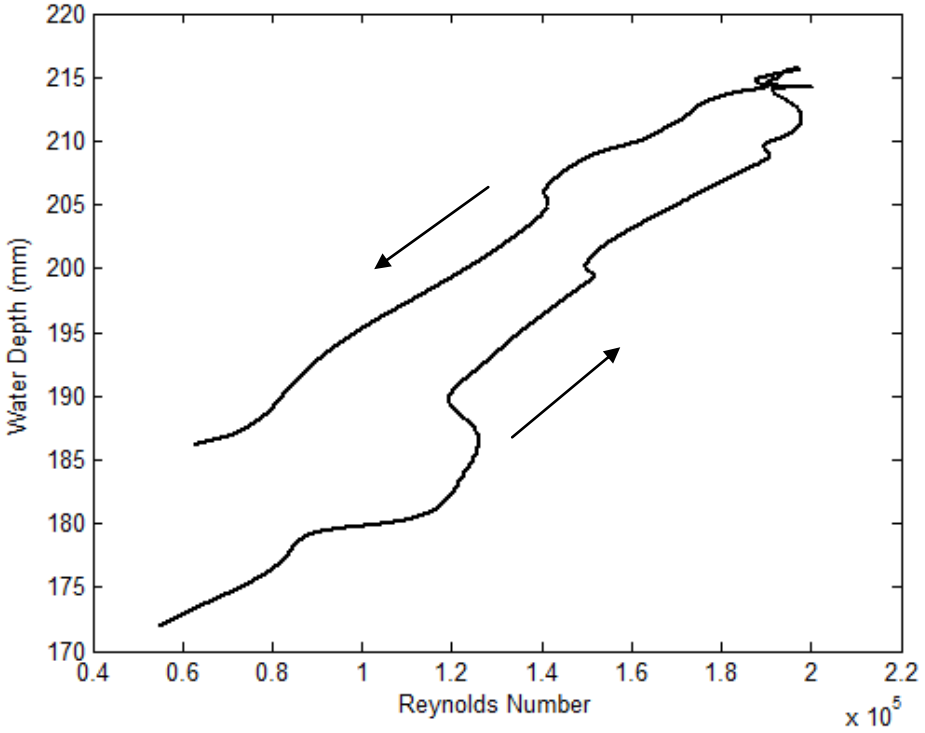

Figure D.5 : The Variation of Reynolds Number (*Re*) with respect to Water Depth (*h*) During The Passage of Unsteady Flow for Set-2 (d=14 cm), Γ=0.0376.

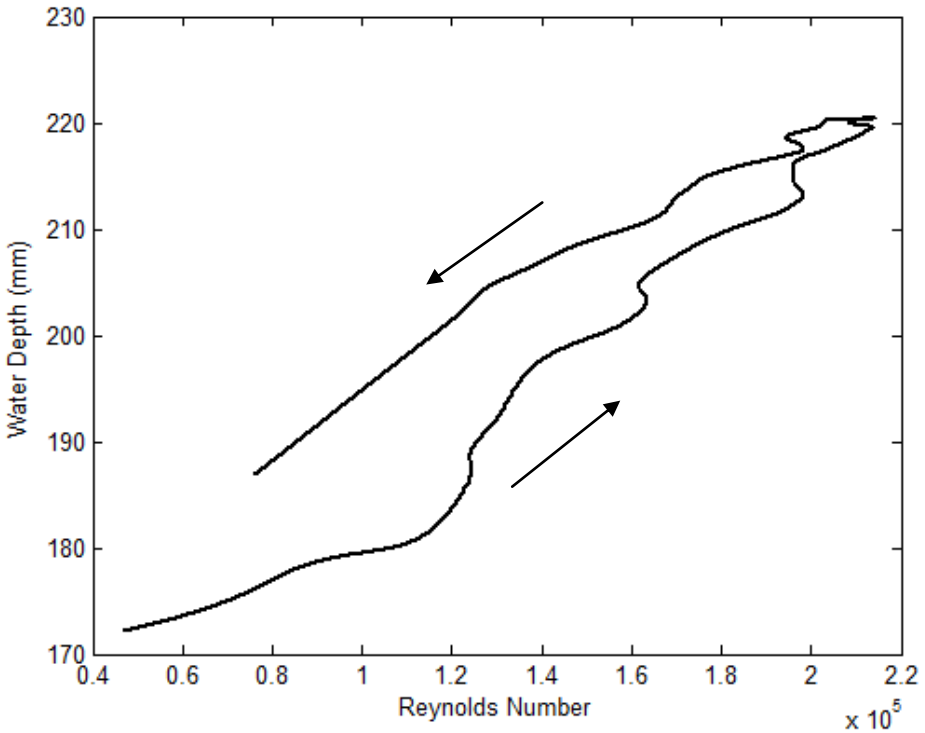

Figure D.6 : The Variation of Reynolds Number (*Re*) with respect to Water Depth (*h*) During The Passage of Unsteady Flow for Set-2 (d=14 cm), Γ=0.0376.

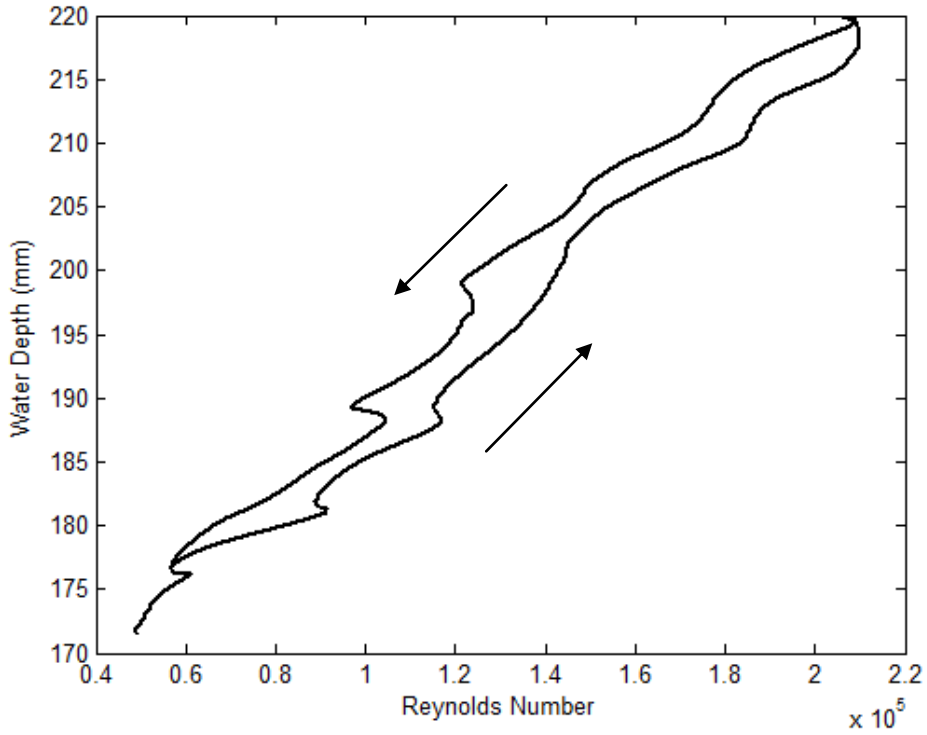

Figure D.7 : The Variation of Reynolds Number (*Re*) with respect to Water Depth (*h*) During The Passage of Unsteady Flow for Set-2 (d=14 cm), Γ=0.0201.

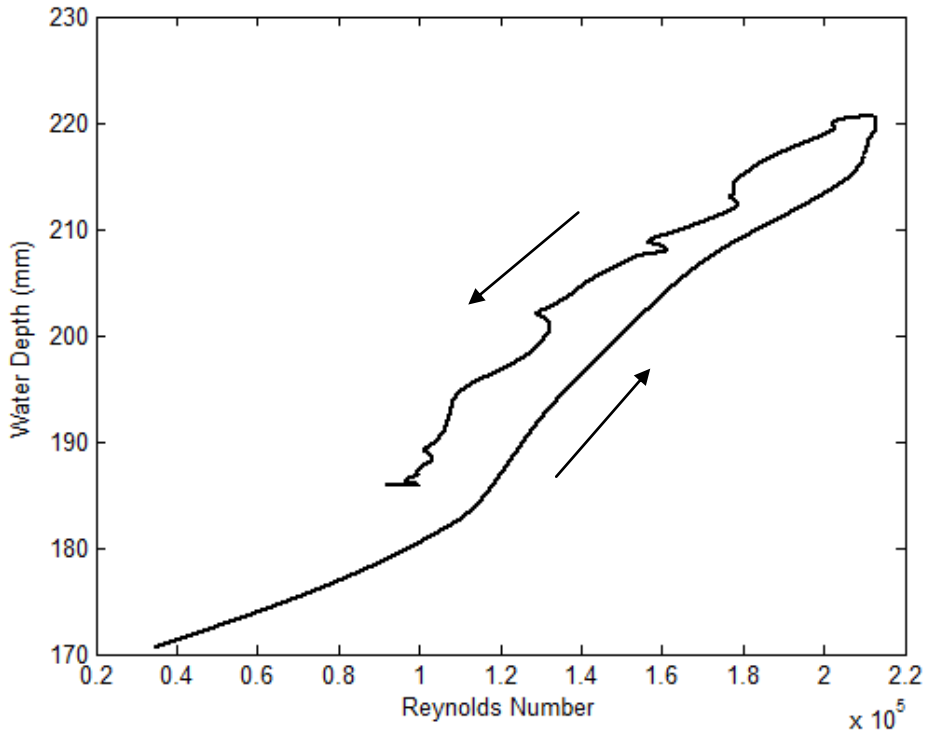

Figure D.8 : The Variation of Reynolds Number (*Re*) with respect to Water Depth (*h*) During The Passage of Unsteady Flow for Set-2 (d=14 cm), Γ=0.0181.

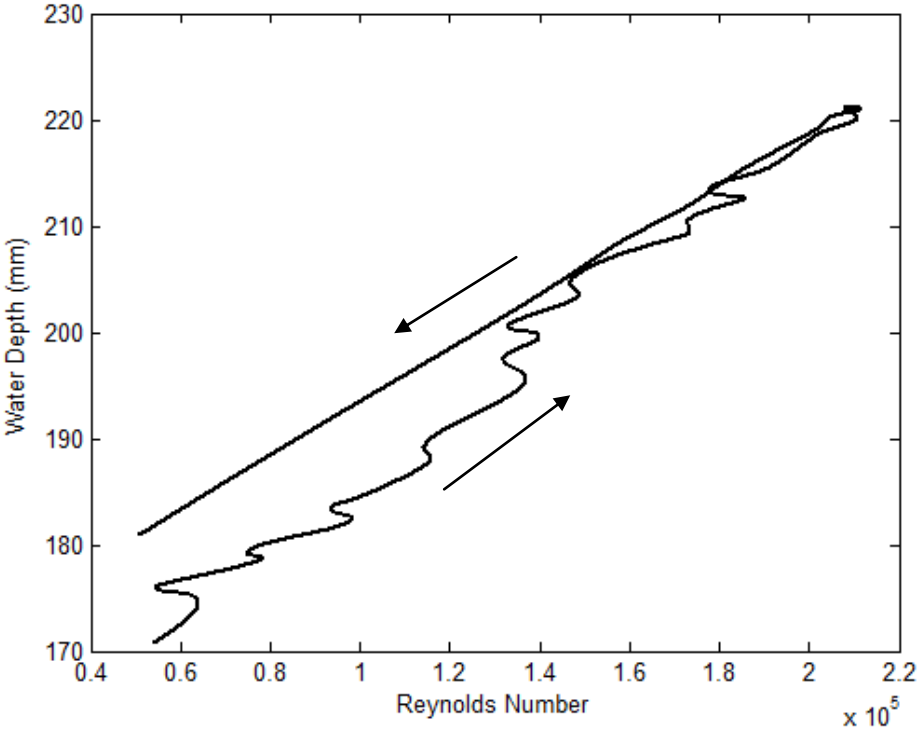

Figure D.9 : The Variation of Reynolds Number (*Re*) with respect to Water Depth (*h*) During The Passage of Unsteady Flow for Set-2 (d=14 cm), Γ=0.0134.

APPENDIX E

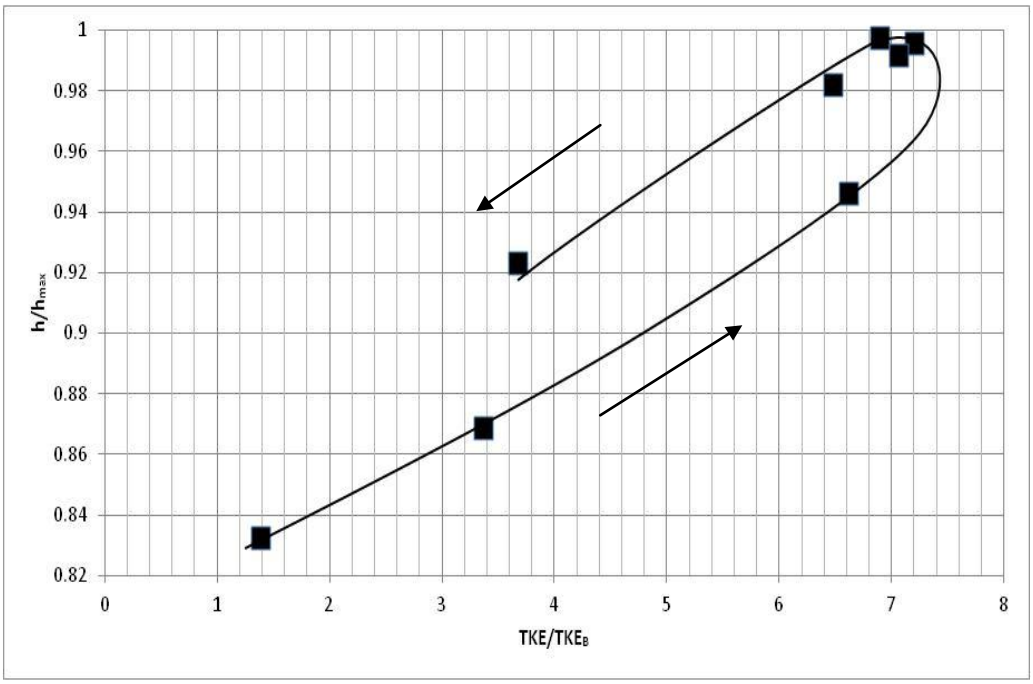

Figure E.1 : The Variation of Dimensionless Turbulence Kinetic Energy (TKE/TKE_B) with respect to Dimensionless Water Depth (h/h_{max}) During the Passage of an Unsteady Flow for Set-1 (d=20 cm) h_1=0.64 cm, Γ=0.0526.

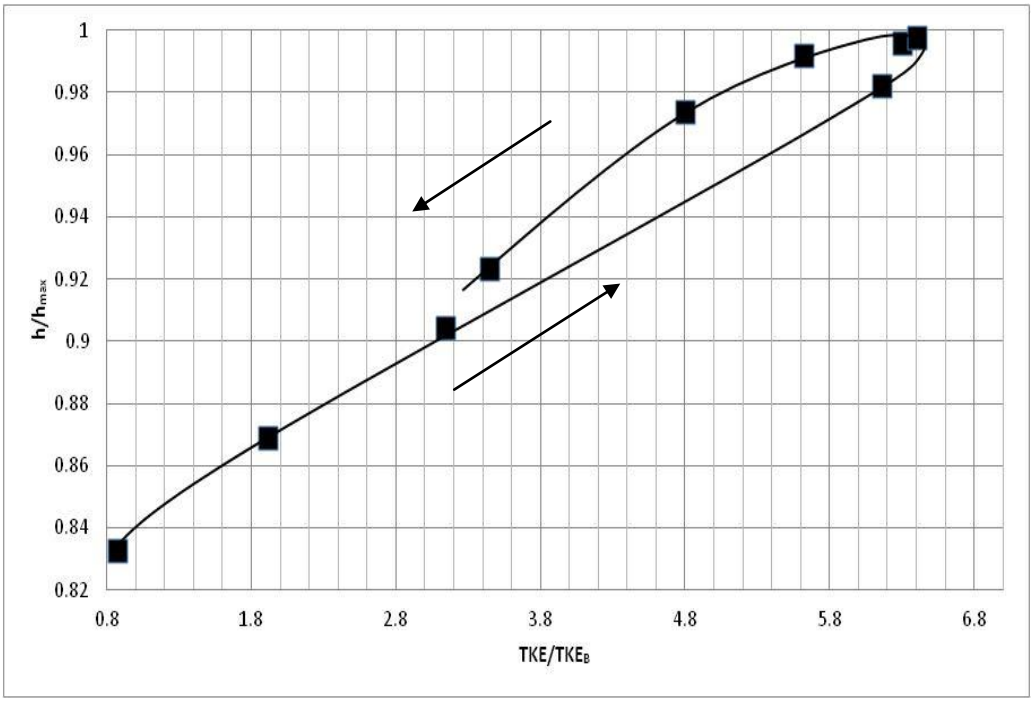

Figure E.2 : The Variation of Dimensionless Turbulence Kinetic Energy (TKE/TKE_B) with respect to Dimensionless Water Depth (h/h_{max}) During the Passage of an Unsteady Flow for Set-1 (d=20 cm) h_1=3.00 cm, Γ=0.0526.

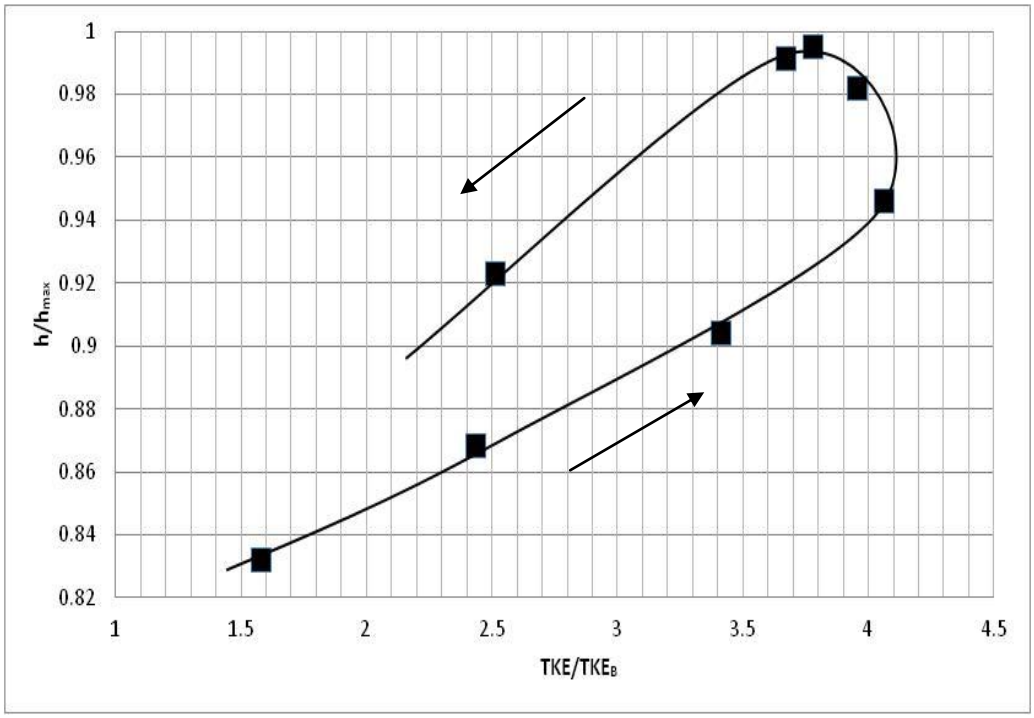

Figure E.3 : The Variation of Dimensionless Turbulence Kinetic Energy (TKE/TKE_B) with respect to Dimensionless Water Depth (h/h_{max}) During the Passage of an Unsteady Flow for Set-1 (d=20 cm) h_1=19.90 cm, Γ=0.0526.

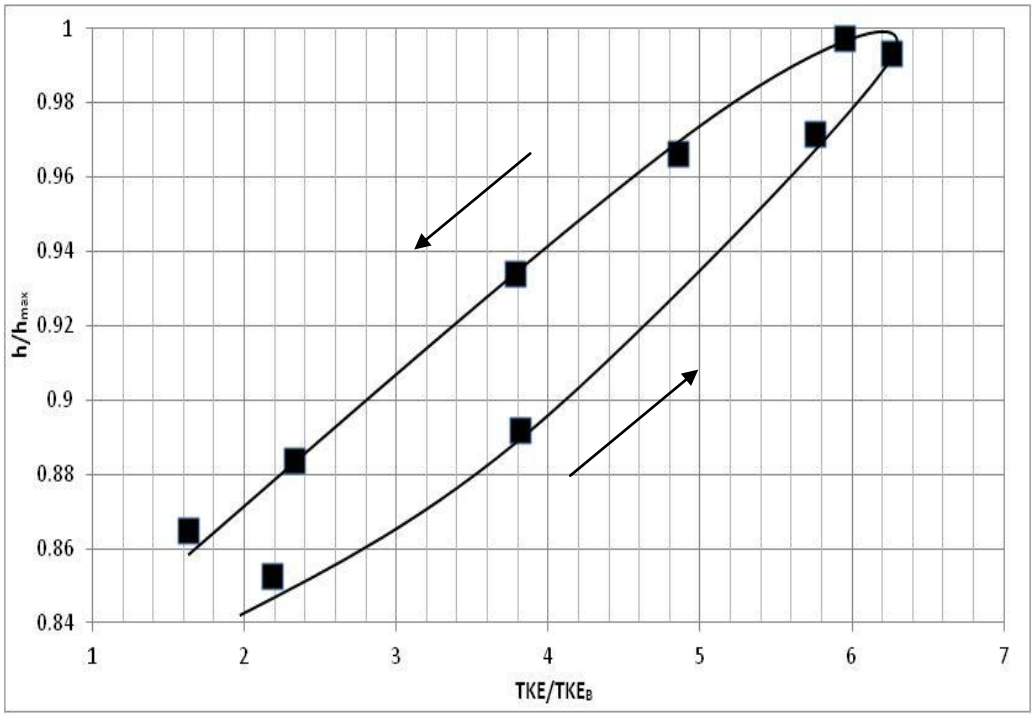

Figure E.4 : The Variation of Dimensionless Turbulence Kinetic Energy (TKE/TKE_B) with respect to Dimensionless Water Depth (h/h_{max}) During the Passage of an Unsteady Flow for Set-1 (d=20 cm) h_1=1.04 cm, Γ=0.0401.

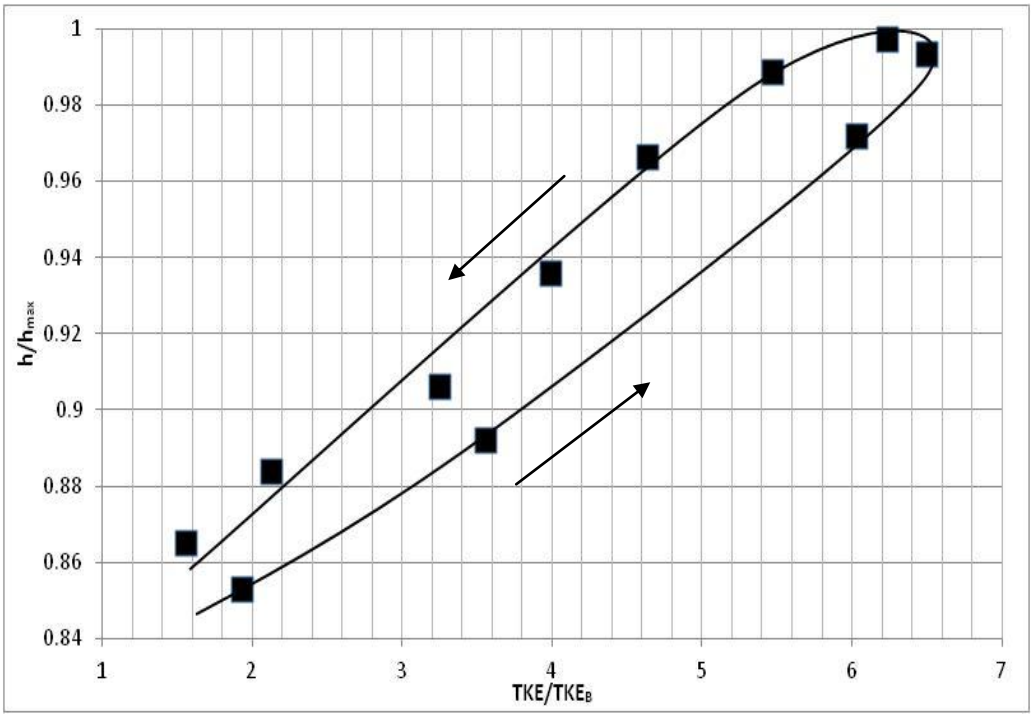

Figure E.5 : The Variation of Dimensionless Turbulence Kinetic Energy (TKE/TKE_B) with respect to Dimensionless Water Depth (h/h_{max}) During the Passage of an Unsteady Flow for Set-1 (d=20 cm) h_1=3.00 cm, Γ=0.0401.

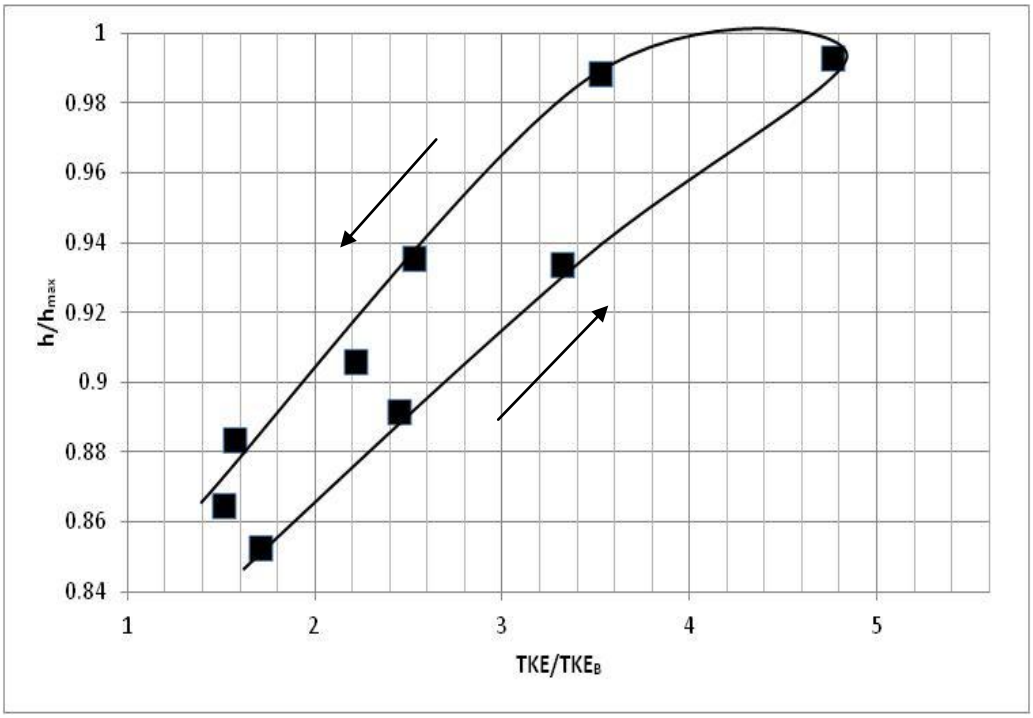

Figure E.6 : The Variation of Dimensionless Turbulence Kinetic Energy (TKE/TKE_B) with respect to Dimensionless Water Depth (h/h_{max}) During the Passage of an Unsteady Flow for Set-1 (d=20 cm) h_1=19.90 cm, Γ=0.0401.

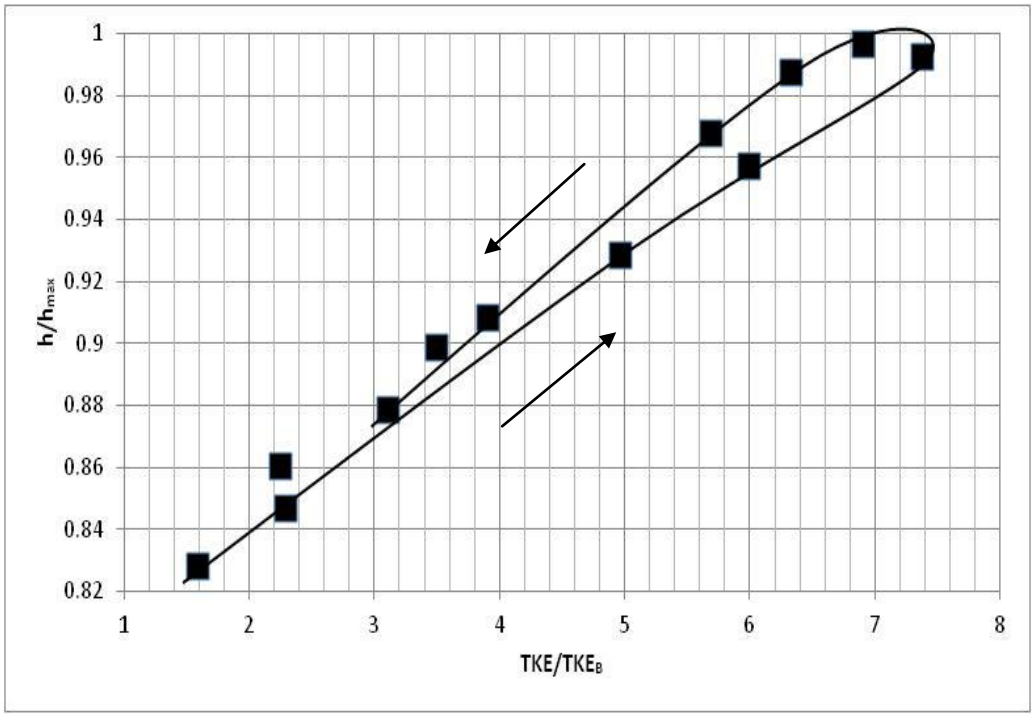

Figure E.7 : The Variation of Dimensionless Turbulence Kinetic Energy (TKE/TKE_B) with respect to Dimensionless Water Depth (h/h_{max}) During the Passage of an Unsteady Flow for Set-1 (d=20 cm) h_1=1.04 cm, Γ=0.0256.

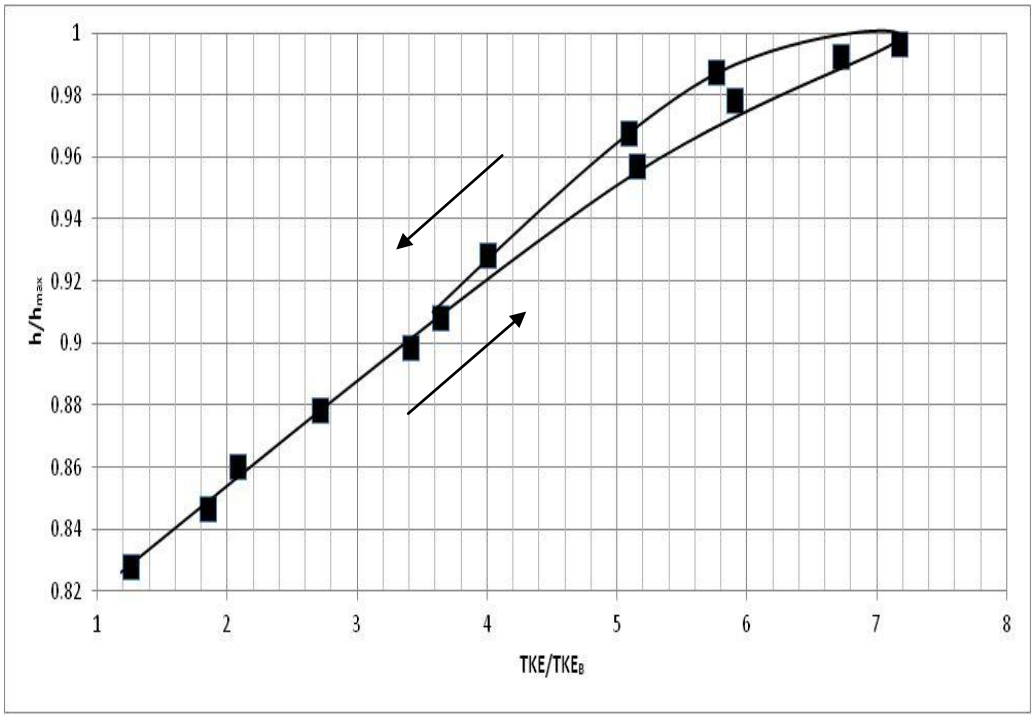

Figure E.8 : The Variation of Dimensionless Turbulence Kinetic Energy (TKE/TKE_B) with respect to Dimensionless Water Depth (h/h_{max}) During the Passage of an Unsteady Flow for Set-1 (d=20 cm) h_1=3.00 cm, Γ=0.0256.

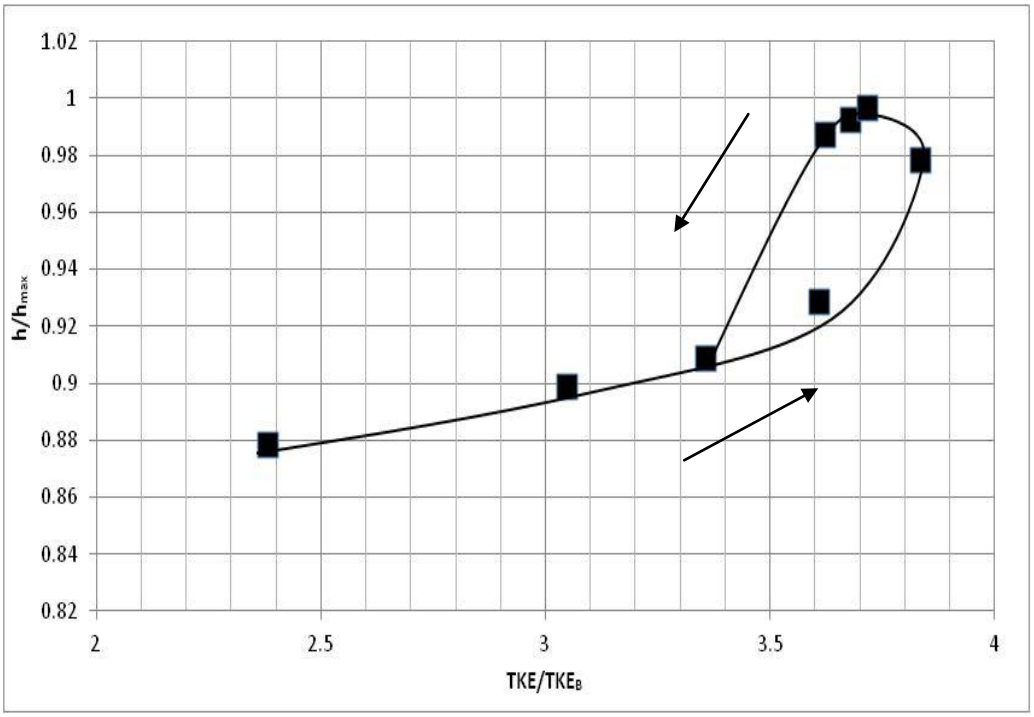

Figure E.9 : The Variation of Dimensionless Turbulence Kinetic Energy (TKE/TKE_B) with respect to Dimensionless Water Depth (h/h_{max}) During the Passage of an Unsteady Flow for Set-1 (d=20 cm) h_1=19.90 cm, Γ=0.0256. .....

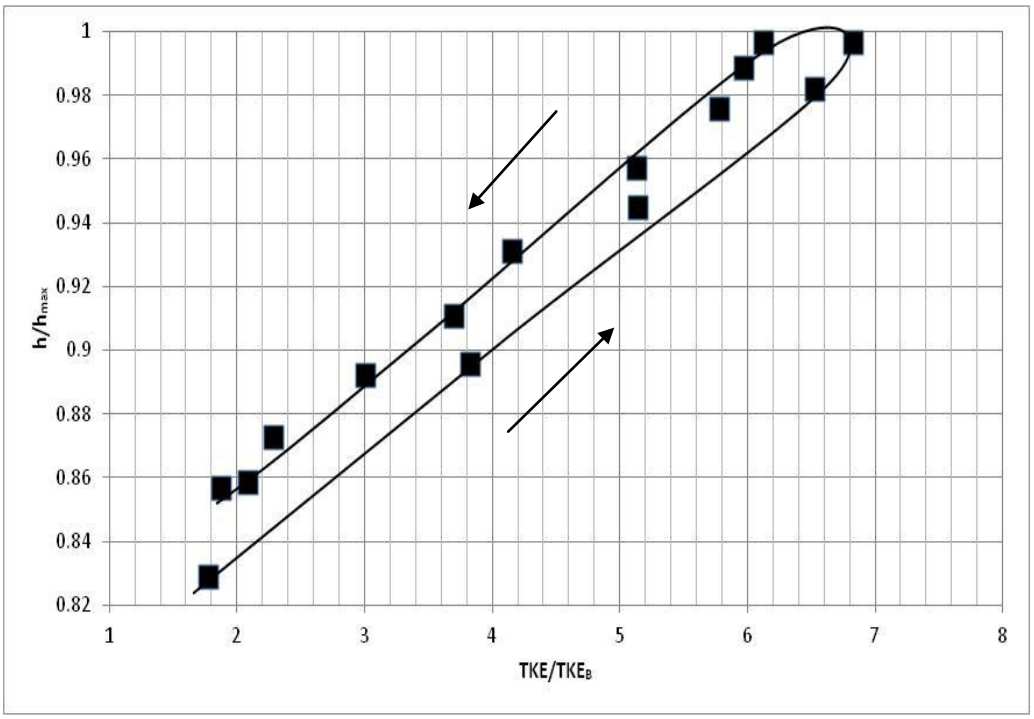

Figure E.10 : The Variation of Dimensionless Turbulence Kinetic Energy (TKE/TKE_B) with respect to Dimensionless Water Depth (h/h_{max}) During the Passage of an Unsteady Flow for Set-1 (d=20 cm) h_1=1.04 cm, Γ=0.0250.

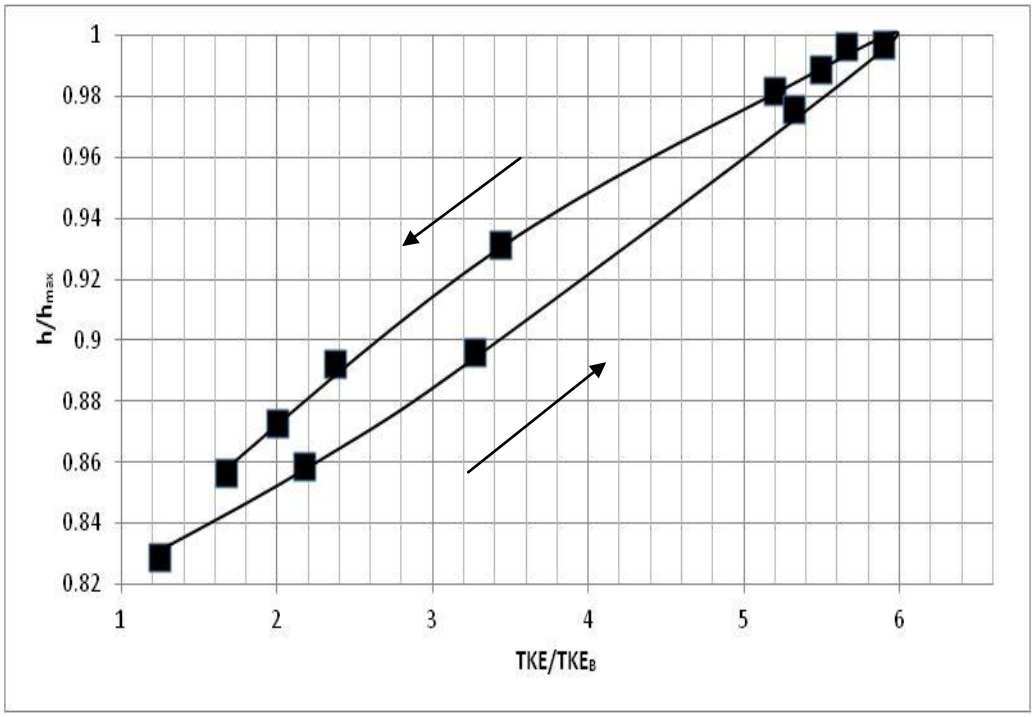

Figure E.11 : The Variation of Dimensionless Turbulence Kinetic Energy (TKE/TKE_B) with respect to Dimensionless Water Depth (h/h_{max}) During the Passage of an Unsteady Flow for Set-1 (d=20 cm) h_1=3.00 cm, Γ=0.0250.

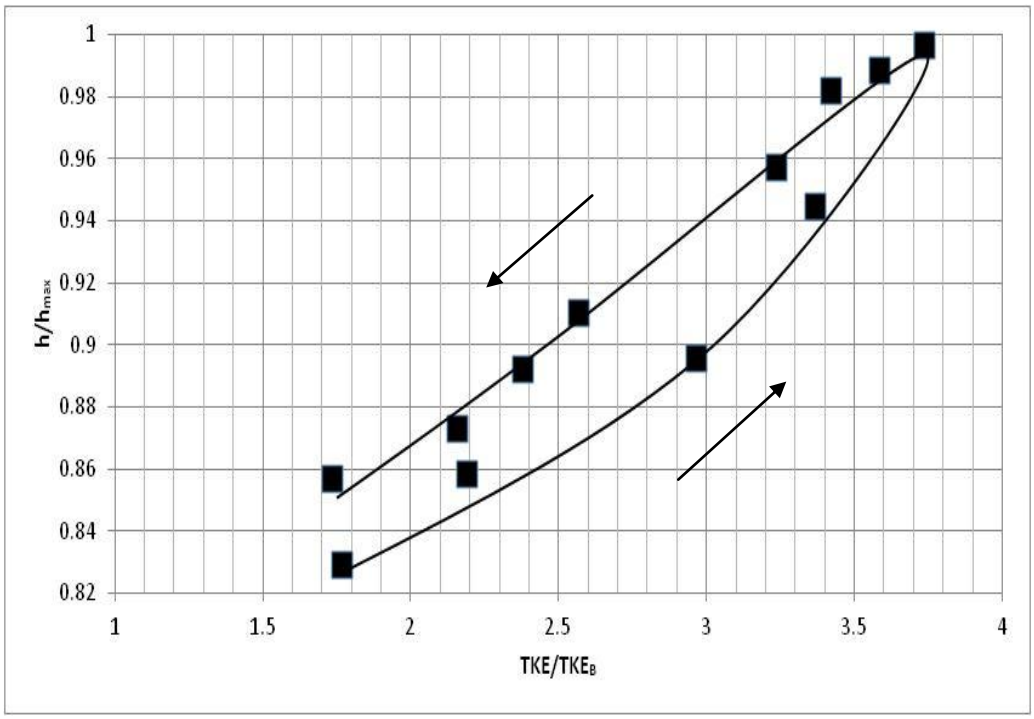

Figure E.12 : The Variation of Dimensionless Turbulence Kinetic Energy (TKE/TKE_B) with respect to Dimensionless Water Depth (h/h_{max}) During the Passage of an Unsteady Flow for Set-1 (d=20 cm) h_1=3.00 cm, Γ=0.0250.

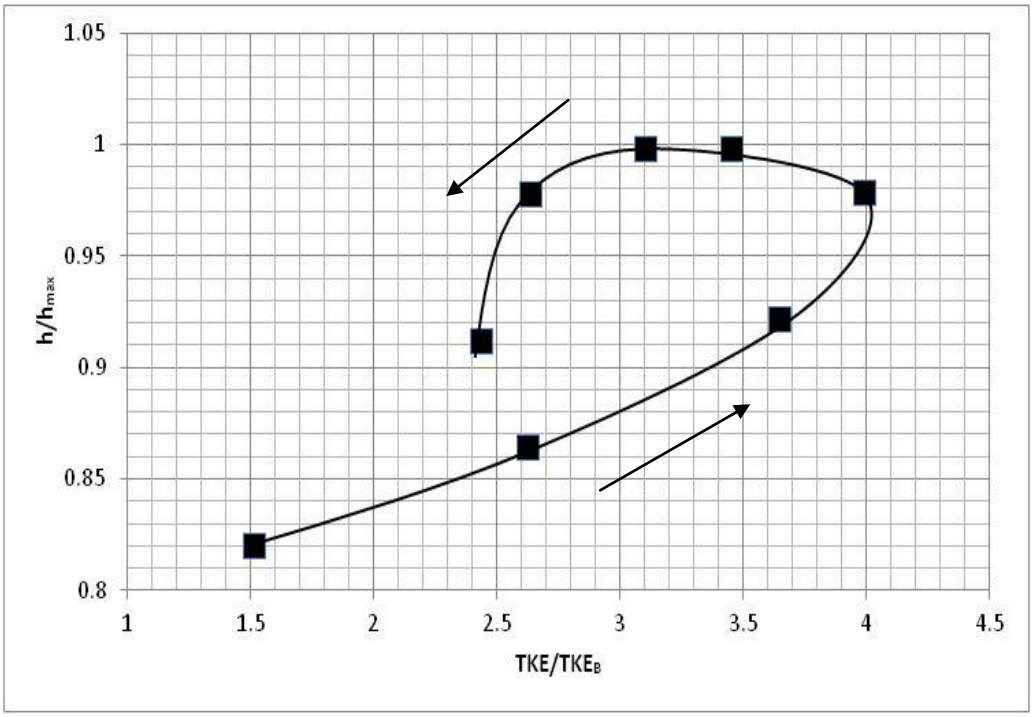

Figure E.13 : The Variation of Dimensionless Turbulence Kinetic Energy (TKE/TKE_B) with respect to Dimensionless Water Depth (h/h_{max}) During the Passage of an Unsteady Flow for Set-2 (d=14 cm) h_1=1.30 cm, Γ=0.0445.

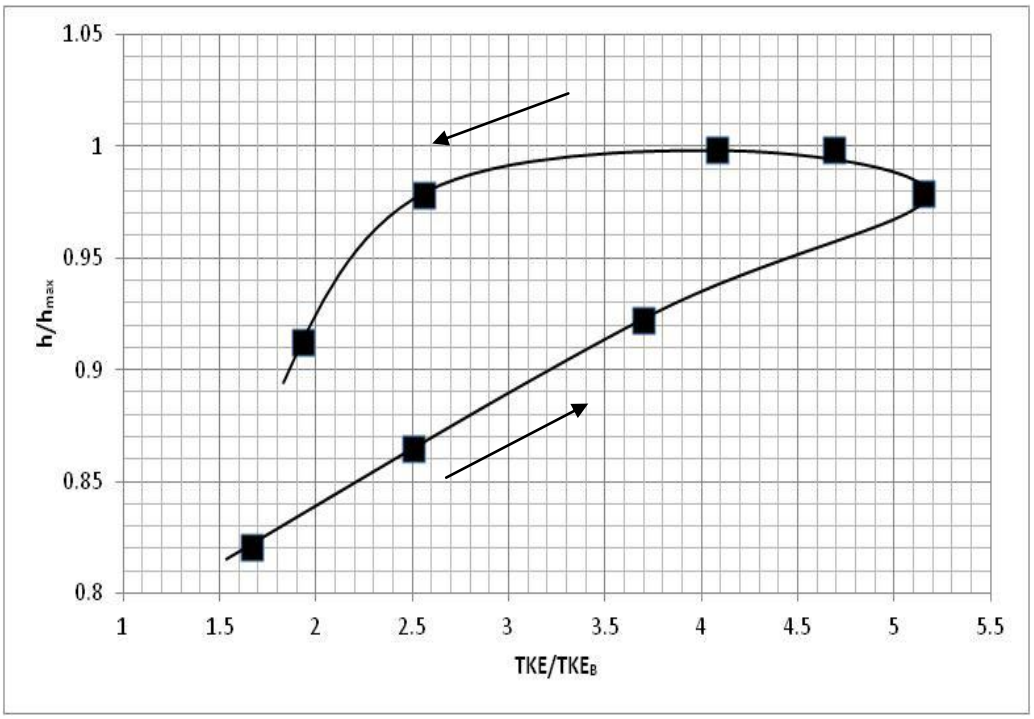

Figure E.14 : The Variation of Dimensionless Turbulence Kinetic Energy (TKE/TKE_B) with respect to Dimensionless Water Depth (h/h_{max}) During the Passage of an Unsteady Flow for Set-2 (d=14 cm) h_1=2.10 cm, Γ=0.0445.

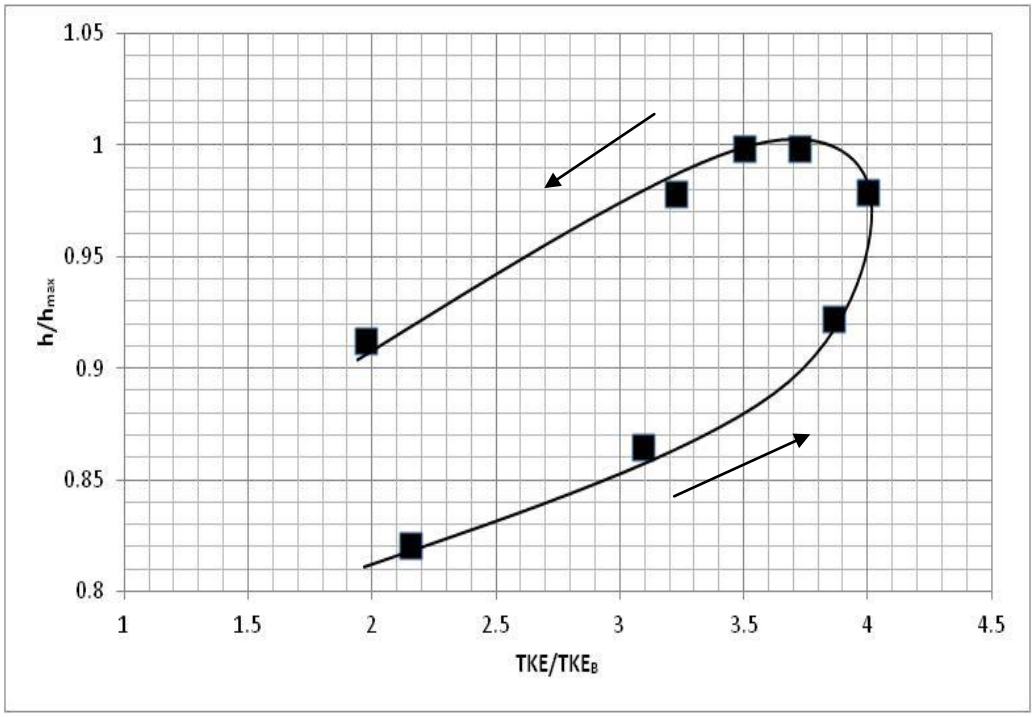

Figure E.15 : The Variation of Dimensionless Turbulence Kinetic Energy (TKE/TKE_B) with respect to Dimensionless Water Depth (h/h_{max}) During the Passage of an Unsteady Flow for Set-2 (d=14 cm) h_1=3.10 cm, Γ=0.0445.

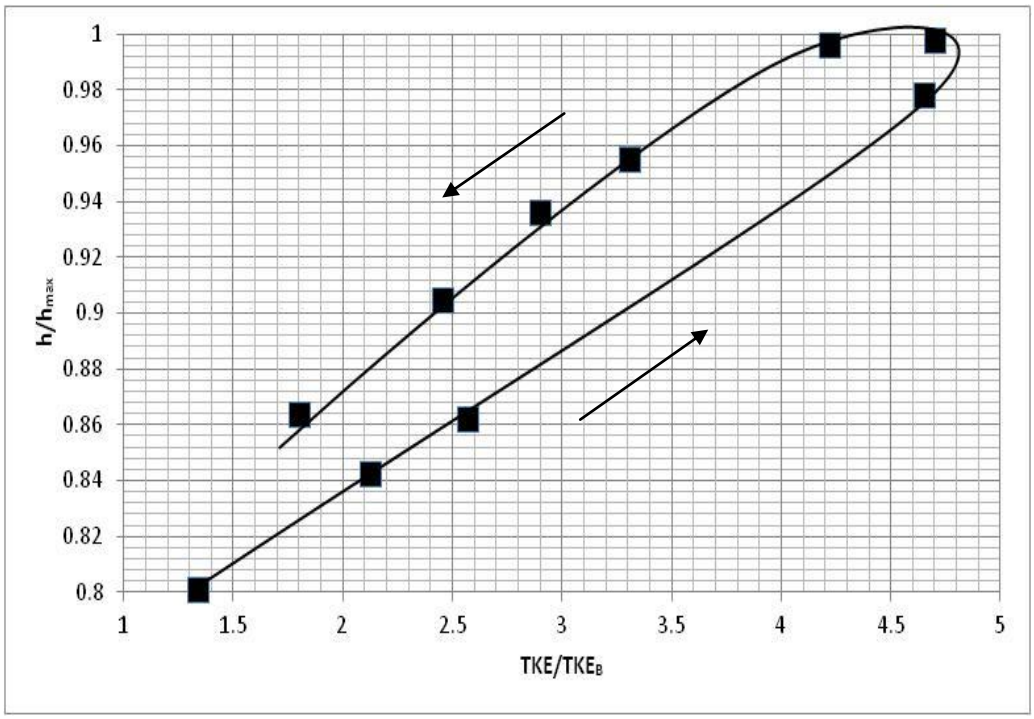

Figure E.16 : The Variation of Dimensionless Turbulence Kinetic Energy (TKE/TKE_B) with respect to Dimensionless Water Depth (h/h_{max}) During the Passage of an Unsteady Flow for Set-2 (d=14 cm) h_1=1.30 cm, Γ=0.0181.

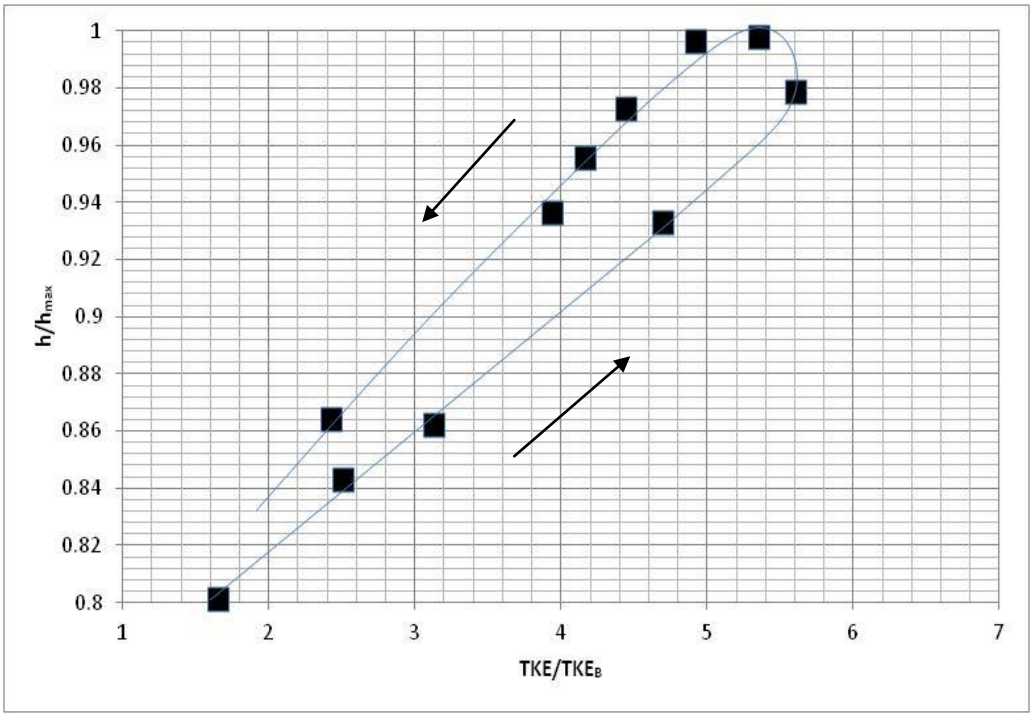

Figure E.17 : The Variation of Dimensionless Turbulence Kinetic Energy (TKE/TKE_B) with respect to Dimensionless Water Depth (h/h_{max}) During the Passage of an Unsteady Flow for Set-2 (d=14 cm) h_1=2.10 cm, Γ=0.0181. .....

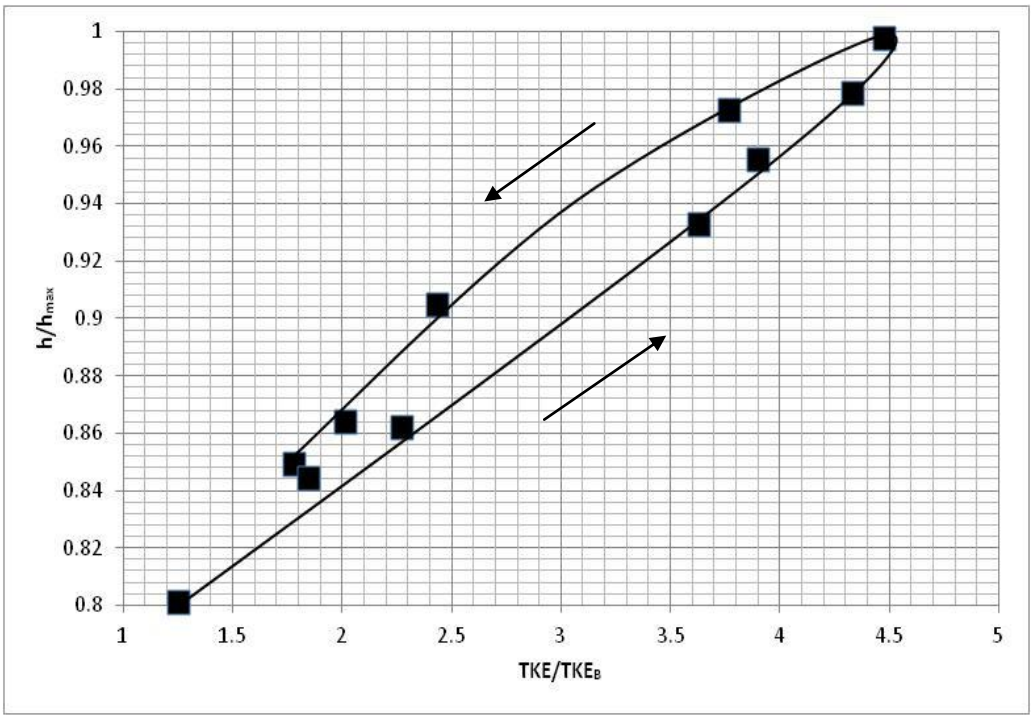

Figure E.18 : The Variation of Dimensionless Turbulence Kinetic Energy (TKE/TKE_B) with respect to Dimensionless Water Depth (h/h_{max}) During the Passage of an Unsteady Flow for Set-2 (d=14 cm) h_1=3.10 cm, Γ=0.0181.

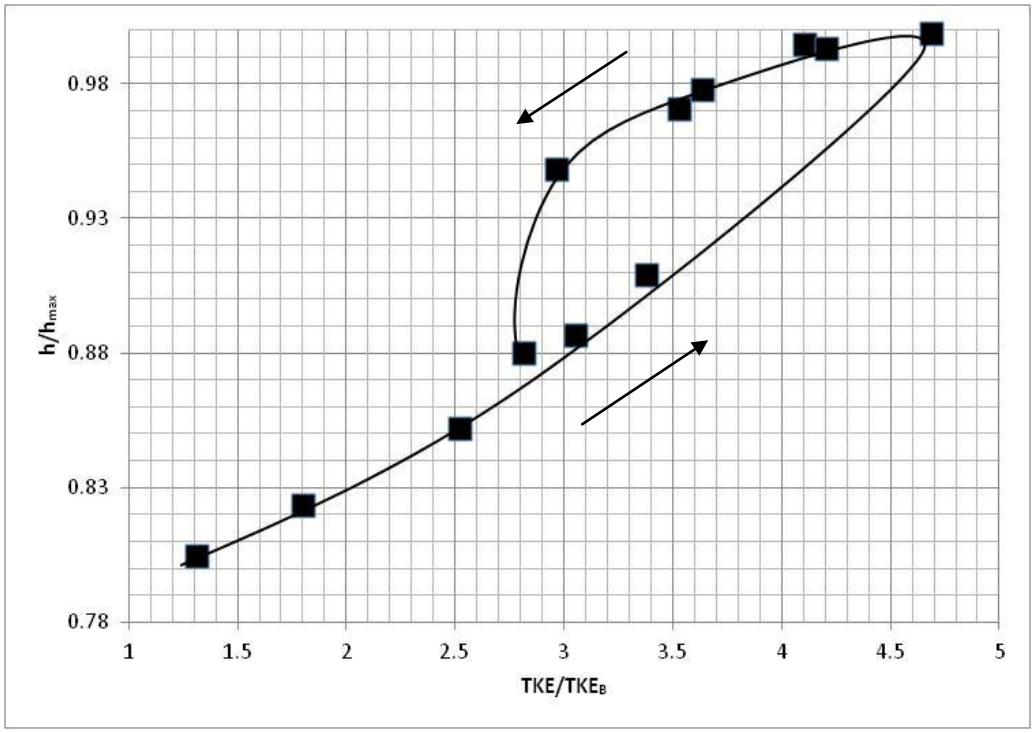

Figure E.19 : The Variation of Dimensionless Turbulence Kinetic Energy (TKE/TKE_B) with respect to Dimensionless Water Depth (h/h_{max}) During the Passage of an Unsteady Flow for Set-2 (d=14 cm) h_1=1.30 cm, Γ=0.0134.

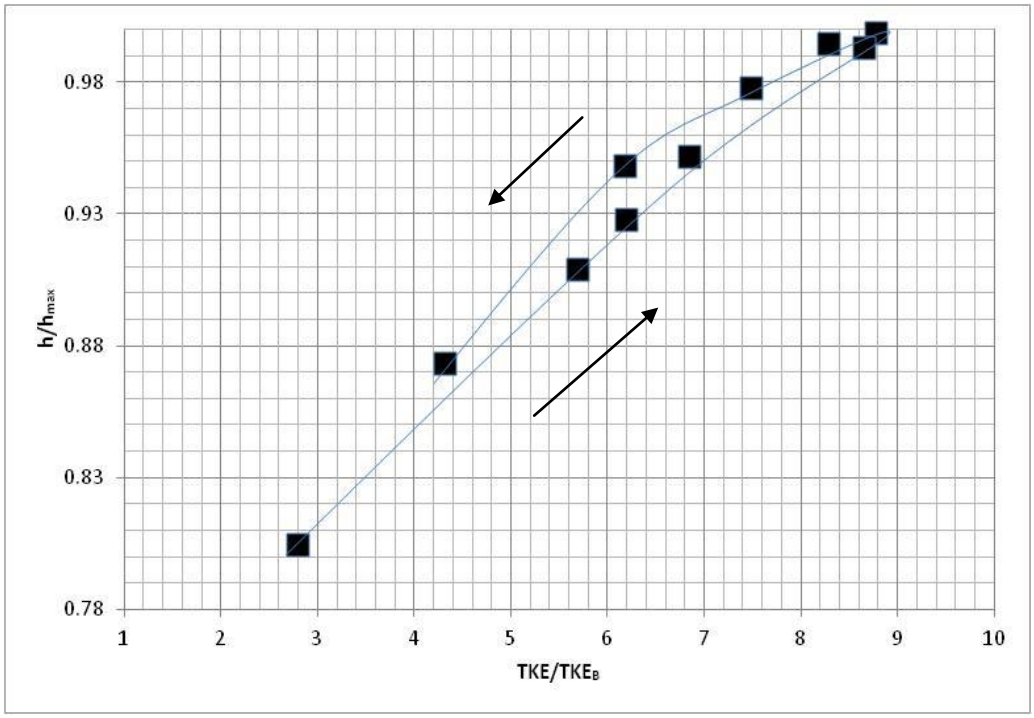

Figure E.20 : The Variation of Dimensionless Turbulence Kinetic Energy (TKE/TKE_B) with respect to Dimensionless Water Depth (h/h_{max}) During the Passage of an Unsteady Flow for Set-2 (d=14 cm) h_1=2.10 cm, Γ=0.0134.

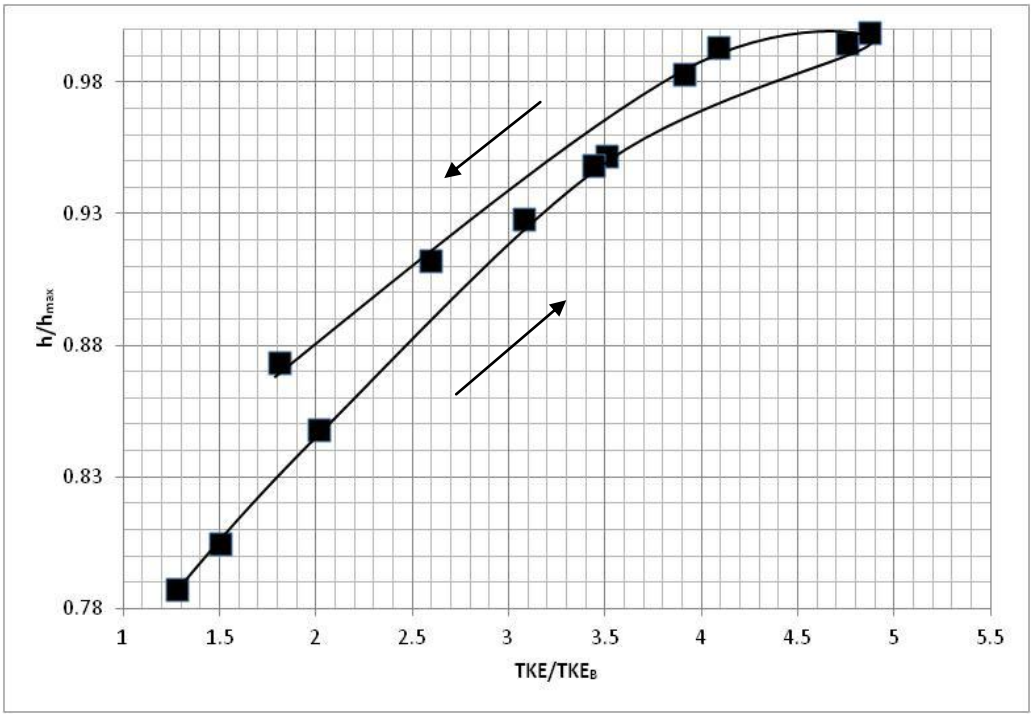

Figure E.21 : The Variation of Dimensionless Turbulence Kinetic Energy (TKE/TKE_B) with respect to Dimensionless Water Depth (h/h_{max}) During the Passage of an Unsteady Flow for Set-2 (d=14 cm) h_1=3.10 cm, Γ=0.0134.

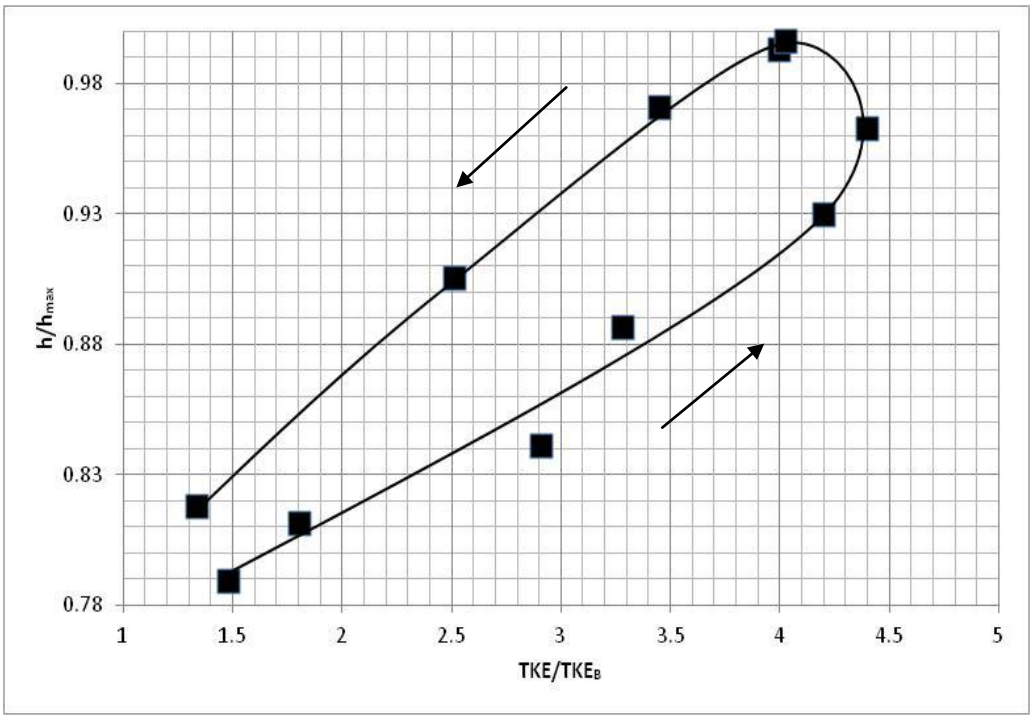

Figure E.22 : The Variation of Dimensionless Turbulence Kinetic Energy (TKE/TKE_B) with respect to Dimensionless Water Depth (h/h_{max}) During the Passage of an Unsteady Flow for Set-2 (d=14 cm) h_1=1.30 cm, Γ=0.0201.

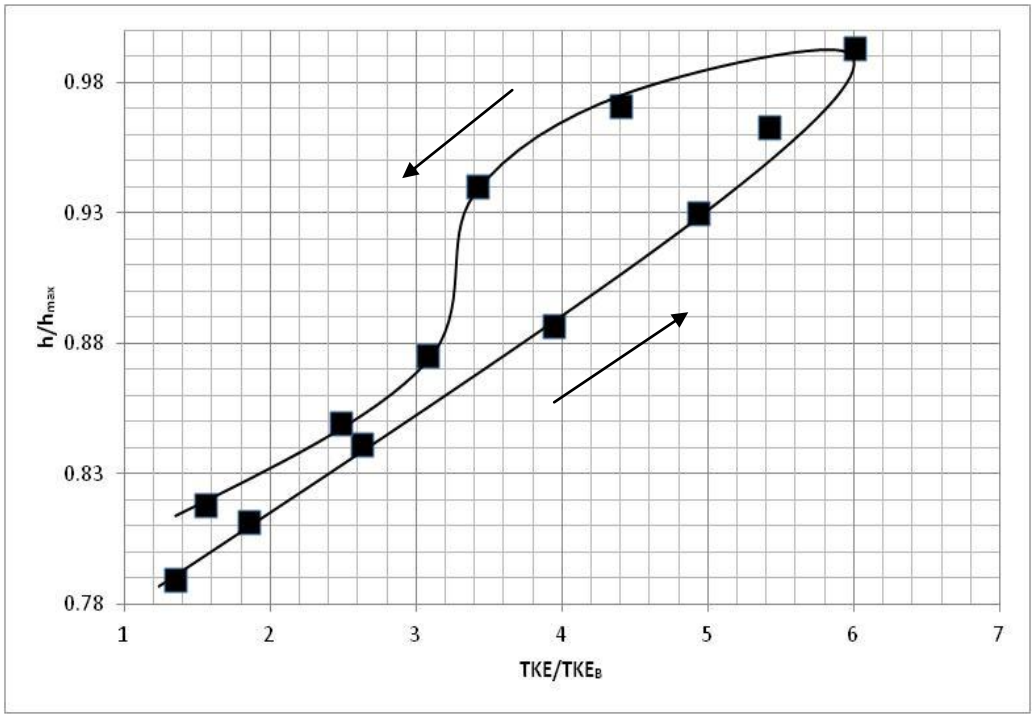

Figure E.23 : The Variation of Dimensionless Turbulence Kinetic Energy (TKE/TKE_B) with respect to Dimensionless Water Depth (h/h_{max}) During the Passage of an Unsteady Flow for Set-2 (d=14 cm) h_1=2.10 cm, Γ=0.0201.

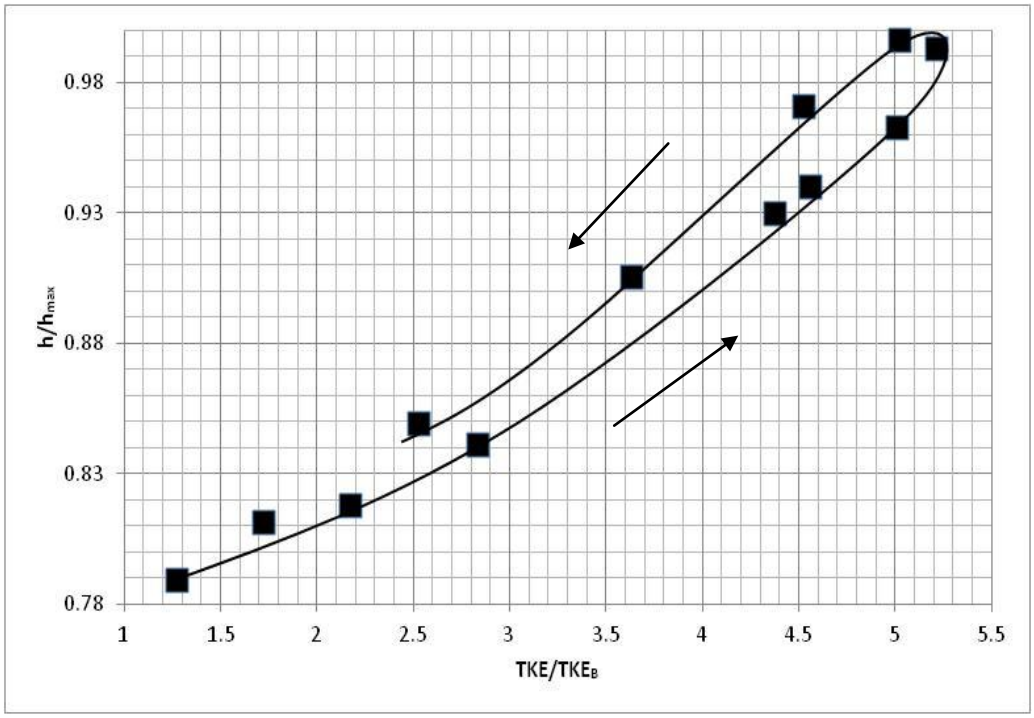

Figure E.24 : The Variation of Dimensionless Turbulence Kinetic Energy (TKE/TKE_B) with respect to Dimensionless Water Depth (h/h_{max}) During the Passage of an Unsteady Flow for Set-2 (d=14 cm) h_1=3.10 cm, Γ=0.0201.

APPENDIX F

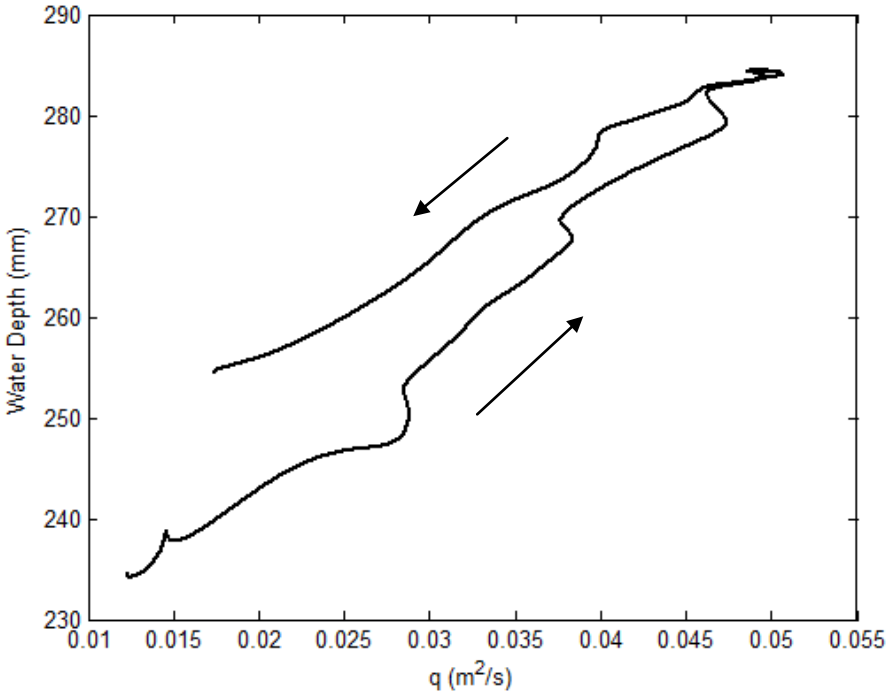

Figure F.1 : The Variation Flowrate (*q*) with respect to Water Depth (*h*) during the passage of unsteady flow for Set-1 (d=20 cm), Γ=0.0526.

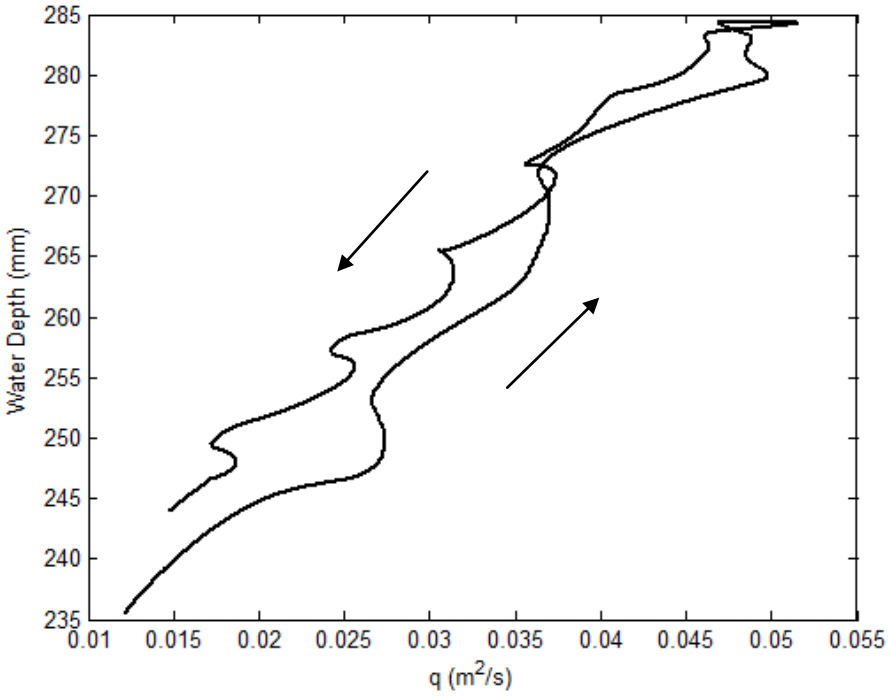

Figure F.2 : The Variation Flowrate (*q*) with respect to Water Depth (*h*) during the passage of unsteady flow for Set-1 (d=20 cm), Γ=0.0401.

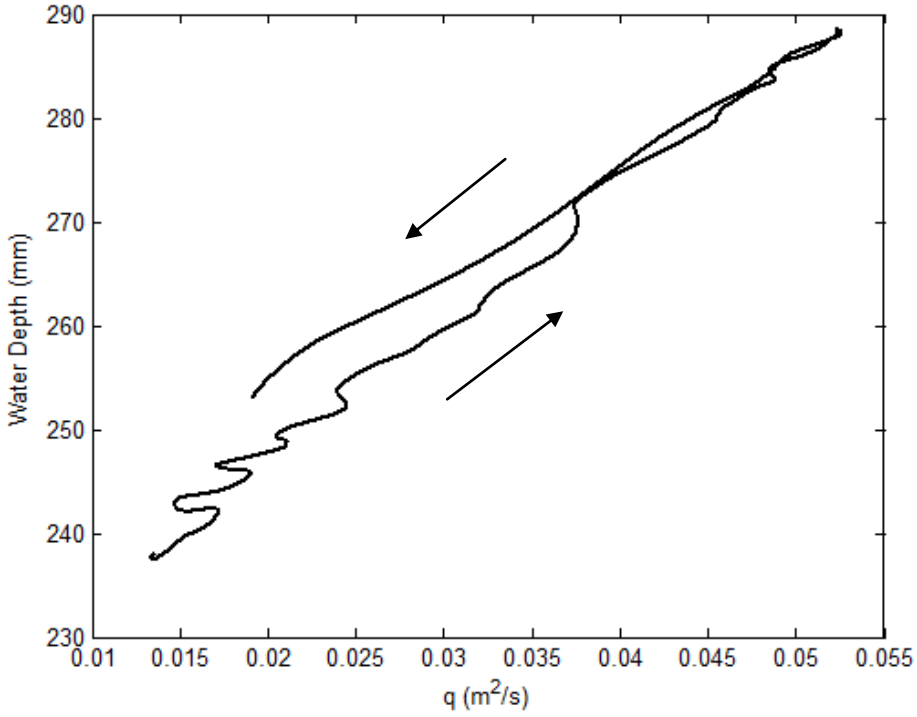

Figure F.3 : The Variation Flowrate (*q*) with respect to Water Depth (*h*) during the passage of unsteady flow for Set-1 (d=20 cm), Γ=0.0256.

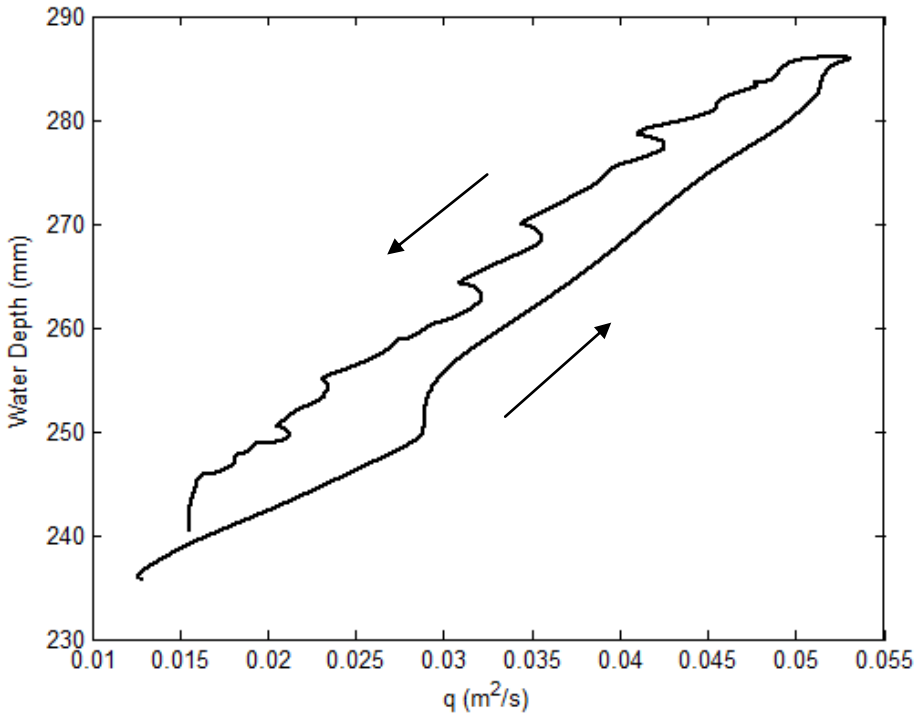

Figure F.4 : The Variation Flowrate (*q*) with respect to Water Depth (*h*) during the passage of unsteady flow for Set-1 (d=20 cm), Γ=0.0250.

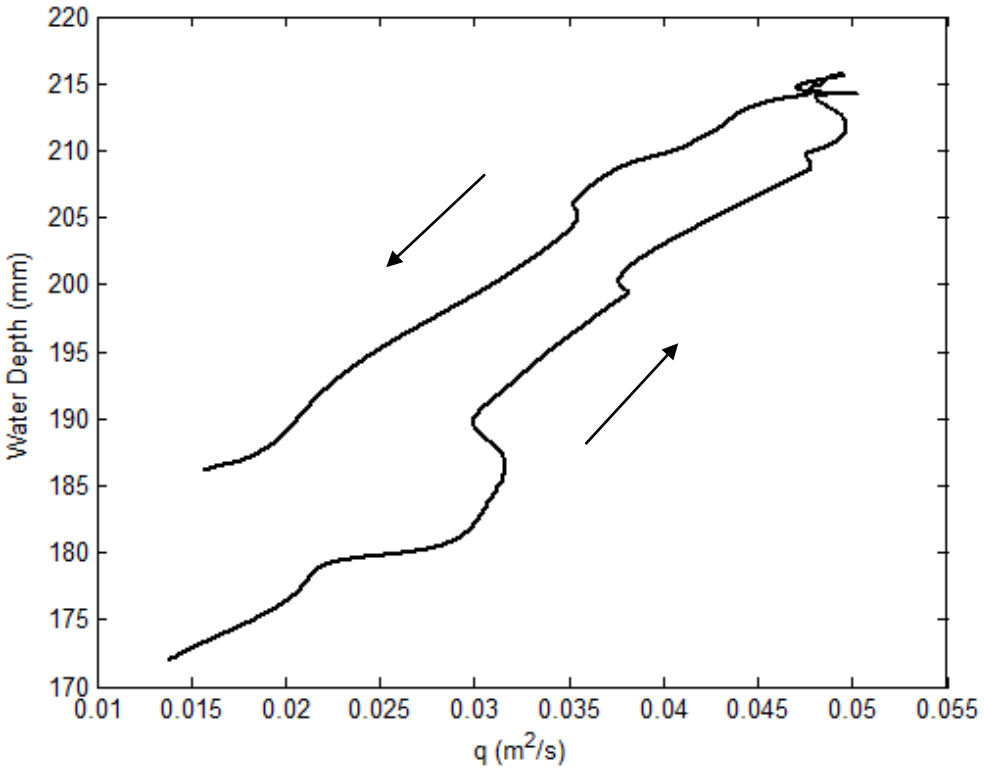

Figure F.5 : The Variation Flowrate (*q*) with respect to Water Depth (*h*) during the passage of unsteady flow for Set-2 (d=14 cm), Γ=0.0445.

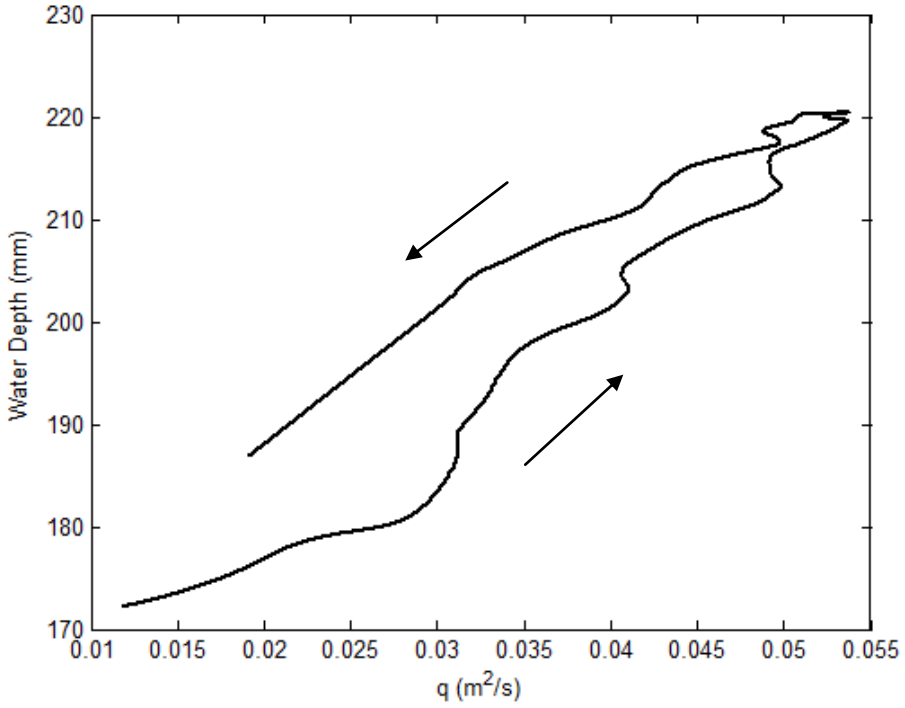

Figure F.6 : The Variation Flowrate (*q*) with respect to Water Depth (*h*) during the passage of unsteady flow for Set-2 (d=14 cm), Γ=0.0376.

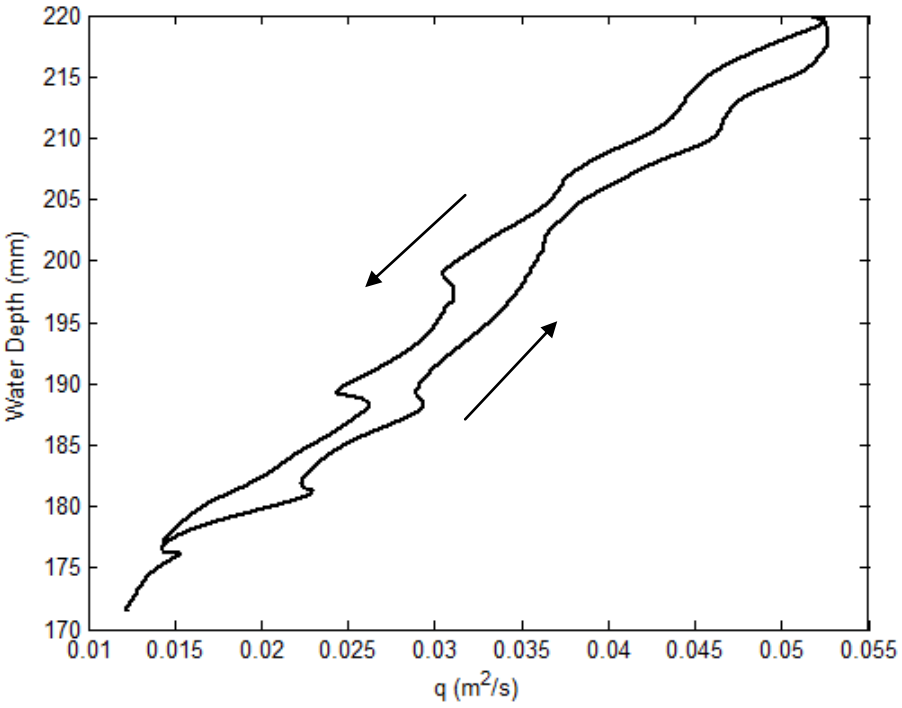

Figure F.7 : The Variation Flowrate (*q*) with respect to Water Depth (*h*) during the passage of unsteady flow for Set-2 (d=14 cm), Γ=0.0201.

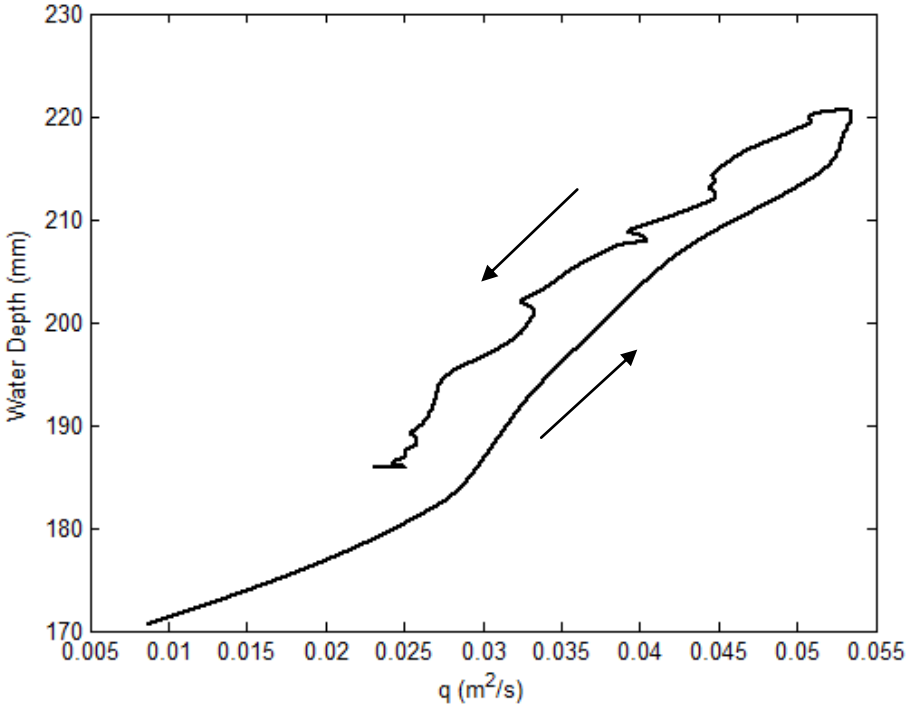

Figure F.8 : The Variation Flowrate (*q*) with respect to Water Depth (*h*) during the passage of unsteady flow for Set-2 (d=14 cm), Γ=0.0181.

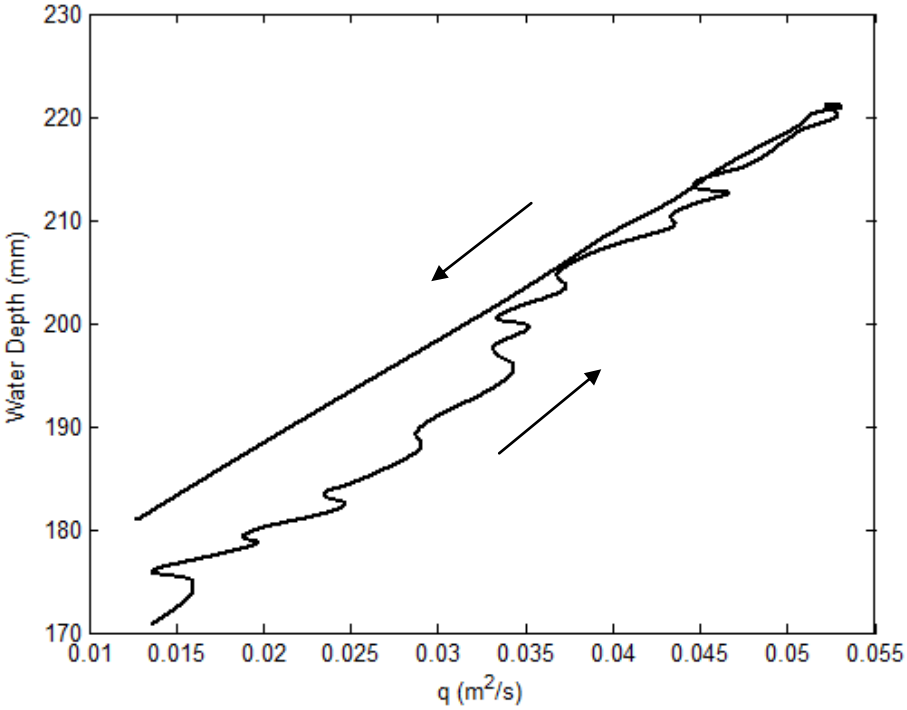

Figure F.9 : The Variation Flowrate (q) with respect to Water Depth (h) during the passage of unsteady flow for Set-2 (d=14 cm), Γ=0.0134.

APPENDIX G

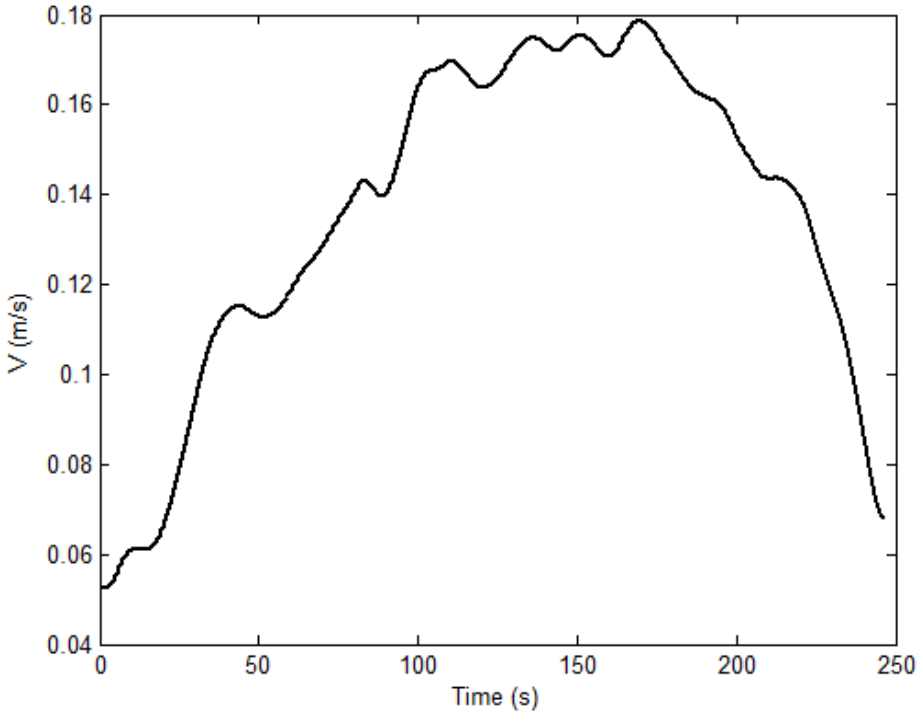

Figure G.1 : The Time Seris of Depth Averaged Velocity (V) During the Passage of Unsteady Flow Set-1 (d=20 cm) Γ=0.0526.

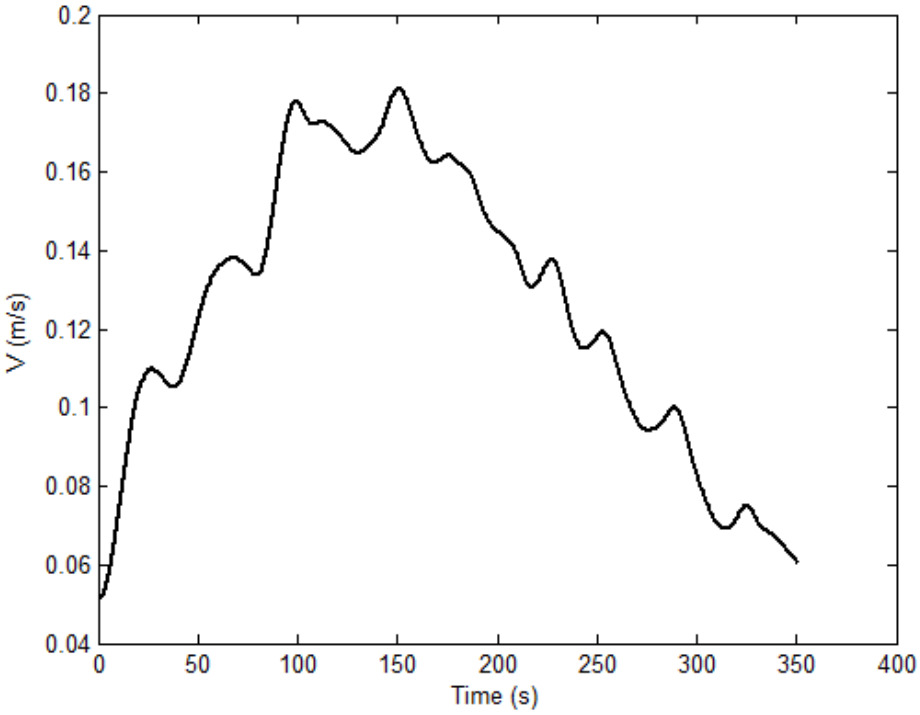

Figure G.2 : The Time Series of Depth Averaged Velocity (V) During the Passage of Unsteady Flow for Set-1 (d=20 cm) Γ=0.0401.

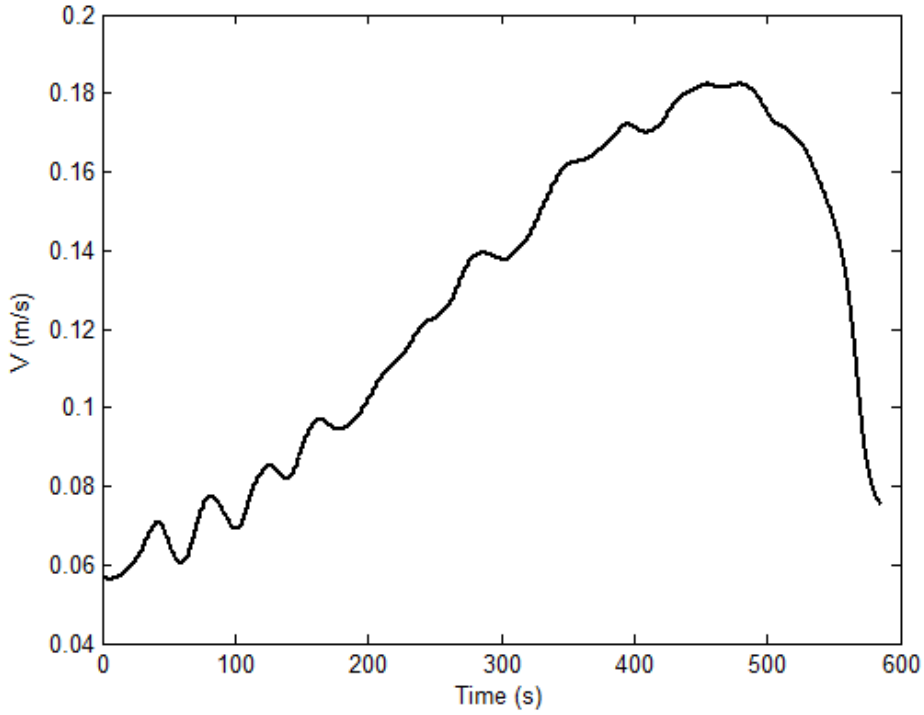

Figure G.3 : The Time Series of Depth Averaged Velocity (V) During the Passage of Unsteady Flow for Set-1 (d=20 cm) Γ=0.0256.

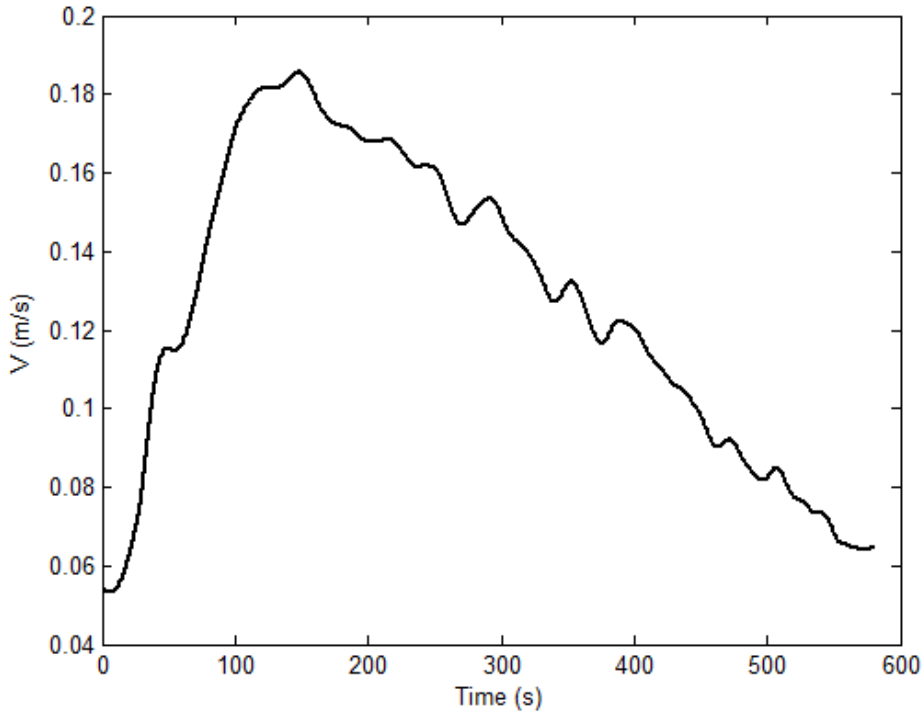

Figure G.4 : The Time Series of Depth Averaged Velocity (V) During the Passage of Unsteady Flow for Set-1 (d=20 cm) Γ=0.0250.

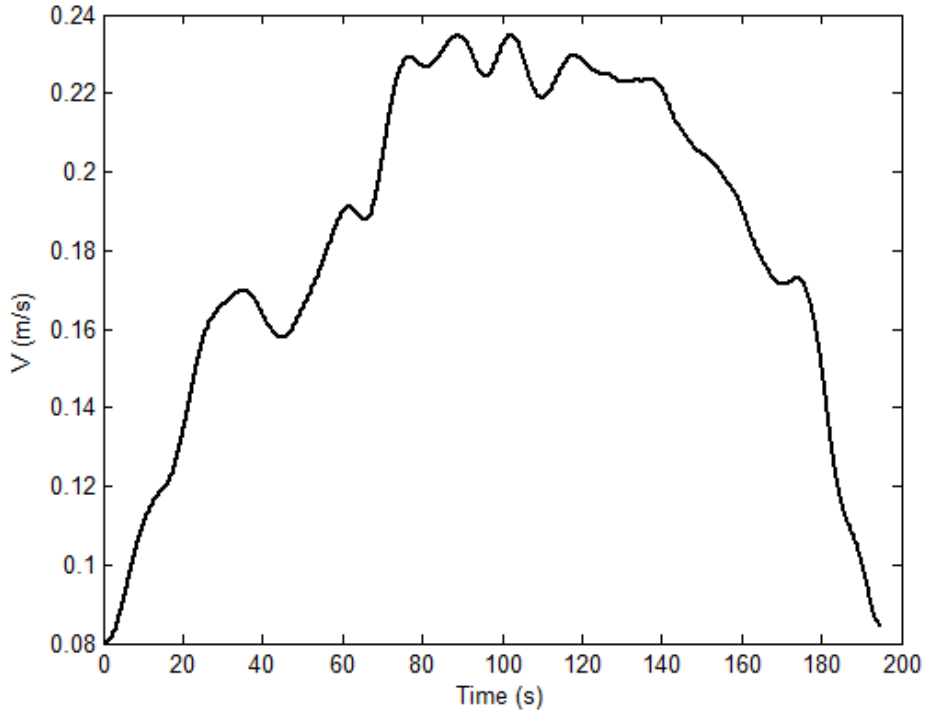

Figure G.5 : The Time Series of Depth Averaged Velocity (V) During the Passage of Unsteady Flow for Set-2 (d=14 cm) Γ=0.0445.

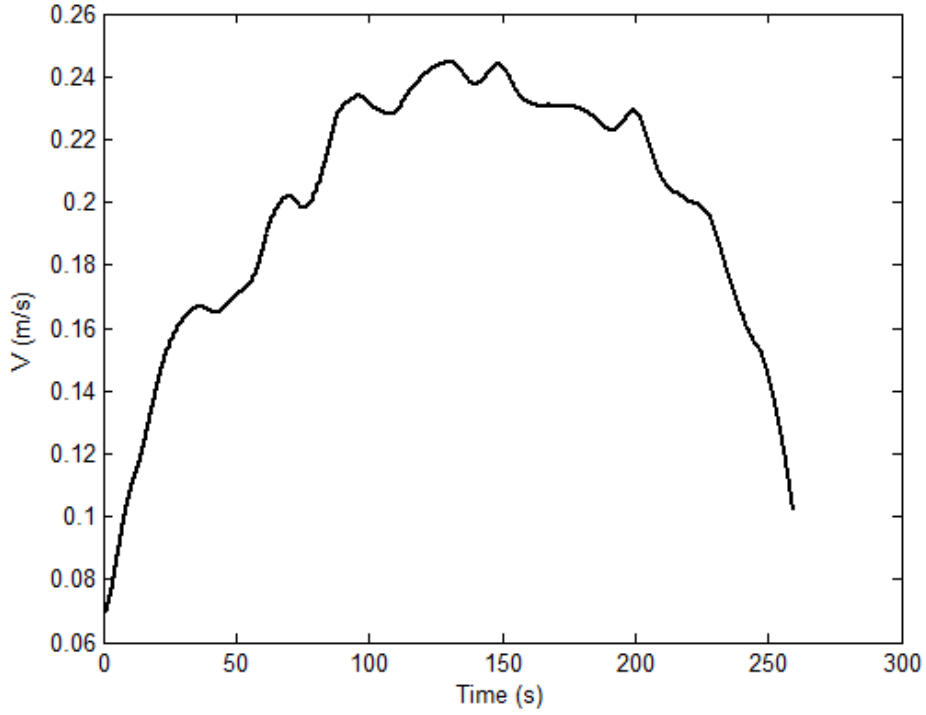

Figure G.6 : The Time Series of Depth Averaged Velocity (V) During the Passage of Unsteady Flow for Set-2 (d=14 cm) Γ=0.0376.

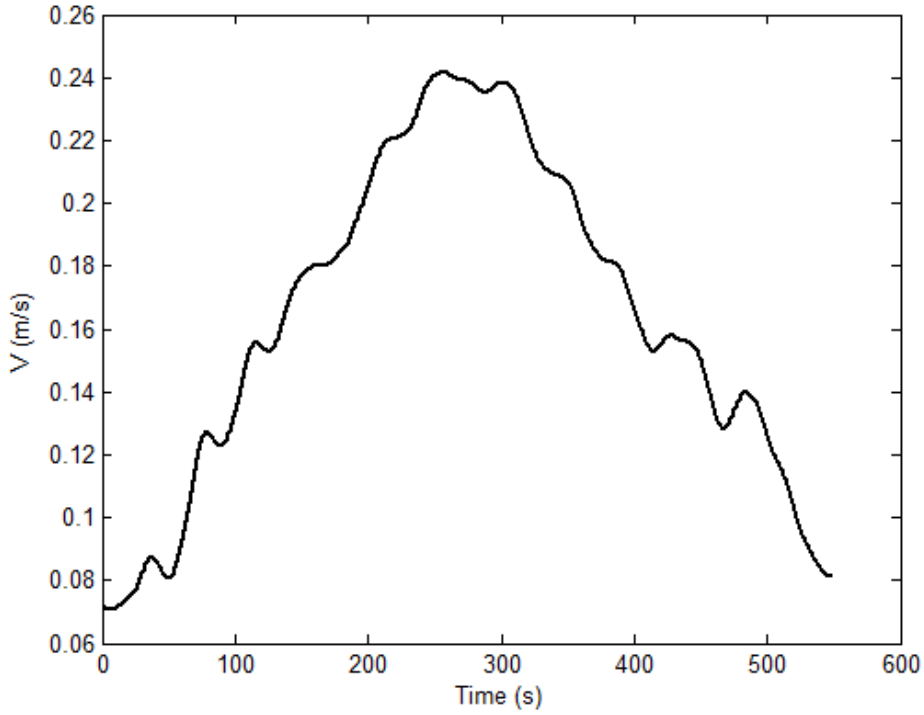

Figure G.7 : The Time Series of Depth Averaged Velocity (V) During the Passage of Unsteady Flow for Set-2 (d=14 cm) Γ=0.0201.

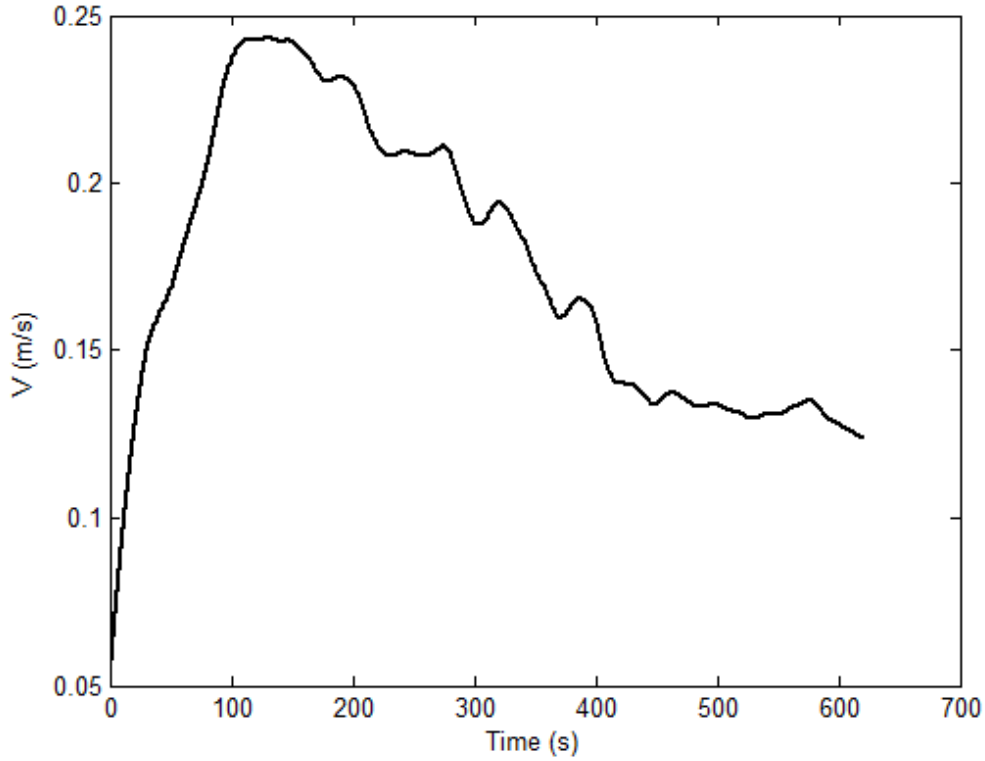

Figure G.8 : The Time Series of Depth Averaged Velocity (V) During the Passage of Unsteady Flow for Set-2 (d=14 cm) Γ=0.0181.

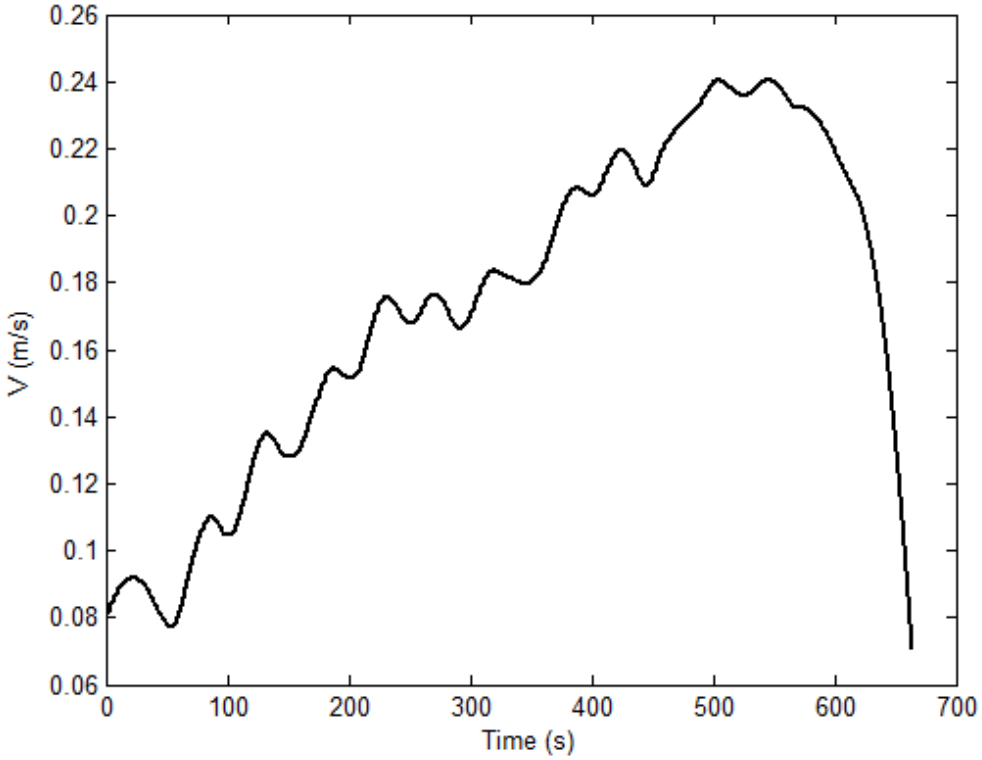

Figure G.9 : The Time Series of Depth Averaged Velocity (V) During the Passage of Unsteady Flow for Set-2 (d=14 cm) Γ=0.0134.

APPENDIX H

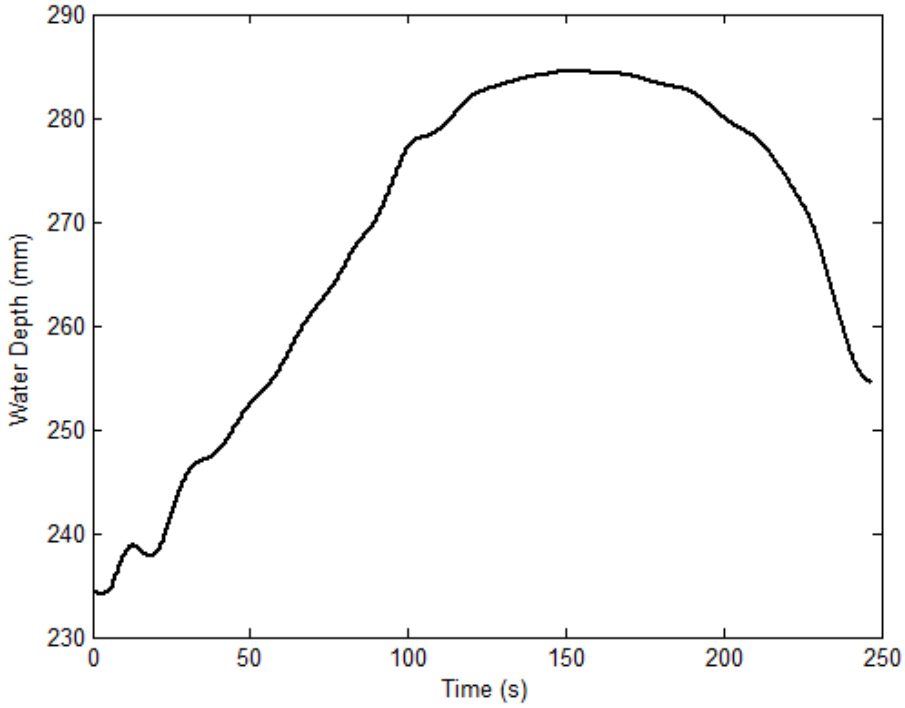

Figure H.1 : The Time Series of Water Depth During the Passage of Unsteady Flow for Set-1 (d=20 cm) Γ=0.0526.

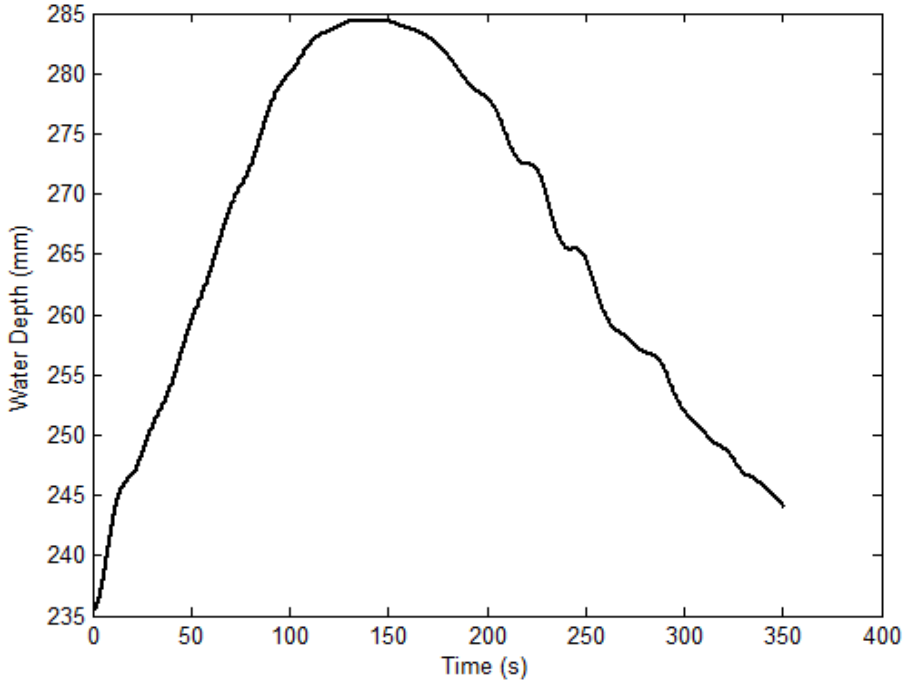

Figure H.2 : The Time Series of Water Depth During the Passage of Unsteady Flow for Set-1 (d=20 cm) Γ=0.0401.

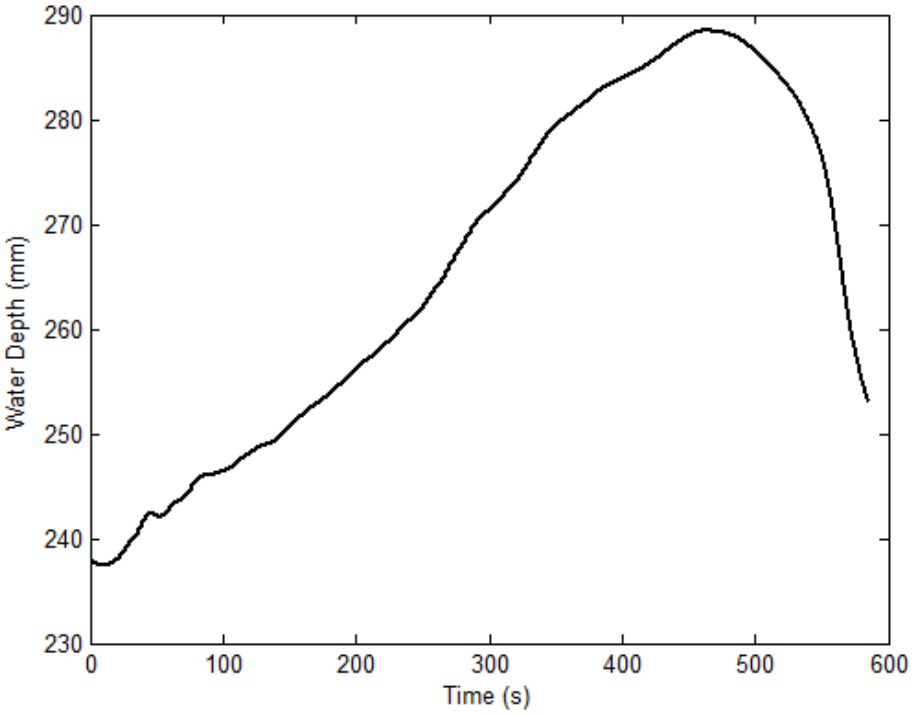

Figure H.3 : The Time Series of Water Depth During the Passage of Unsteady Flow for Set-1 (d=20 cm) Γ=0.0256.

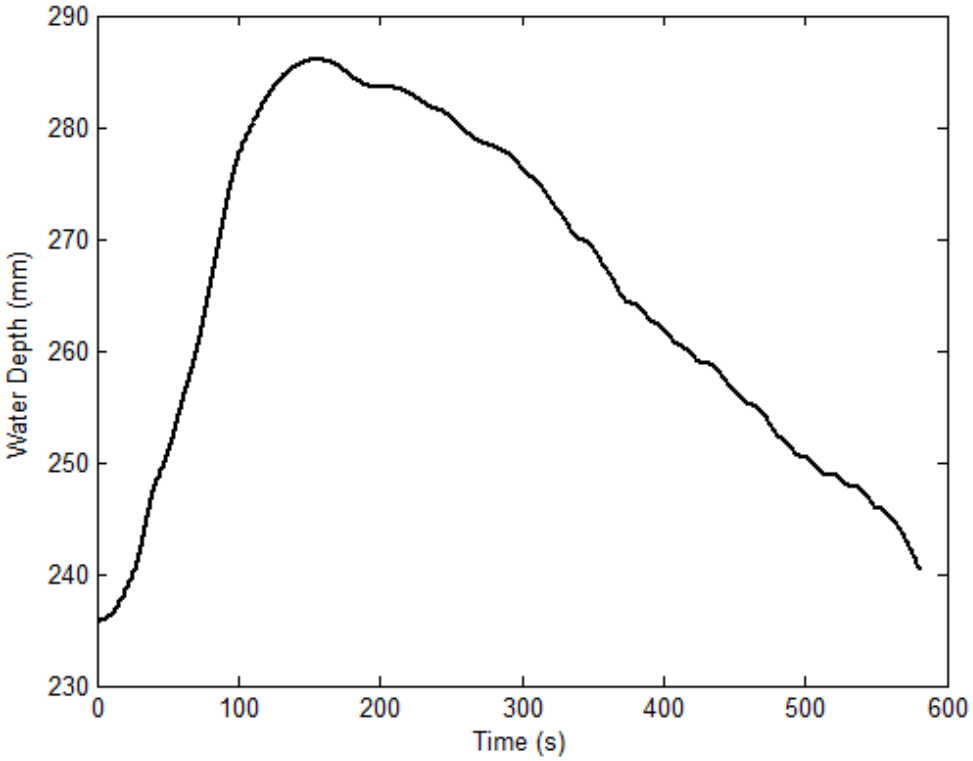

Figure H.4 : The Time Series of Water Depth During the Passage of Unsteady Flow for Set-1 (d=20 cm) Γ=0.0250.

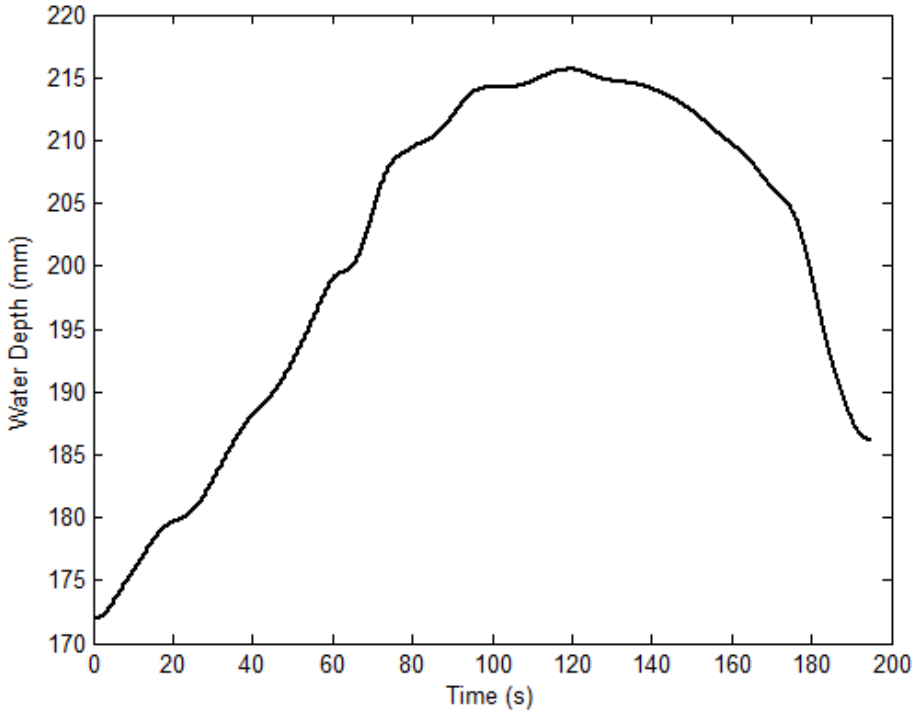

Figure H.5 : The Time Series of Water Depth During the Passage of Unsteady Flow for Set-2 (d=14 cm) Γ=0.0445.

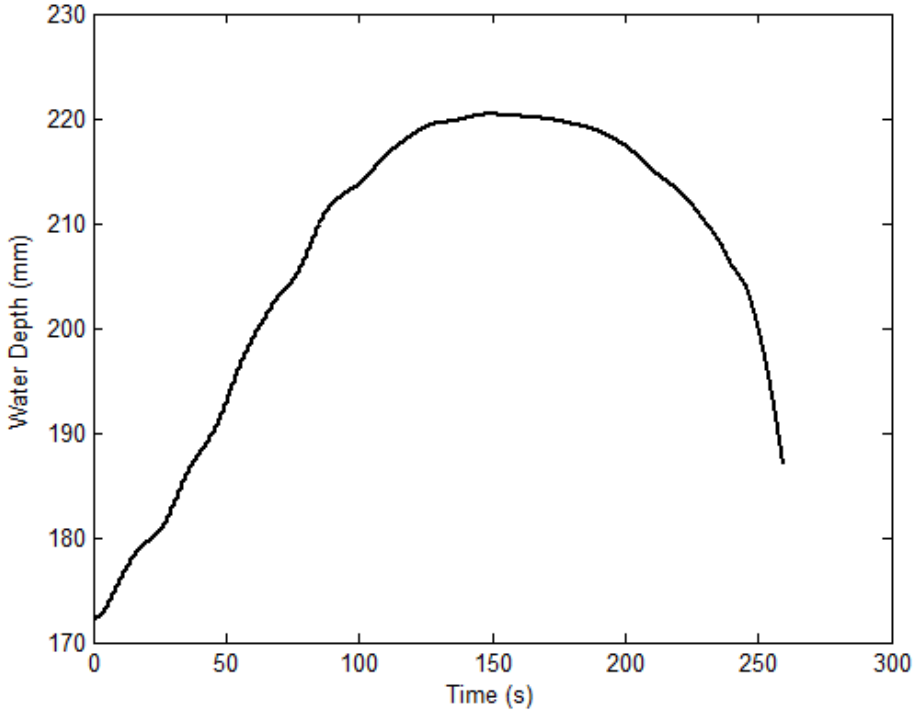

Figure H.6 : The Time Series of Water Depth During the Passage of Unsteady Flow for Set-2 (d=14 cm) Γ=0.0376.

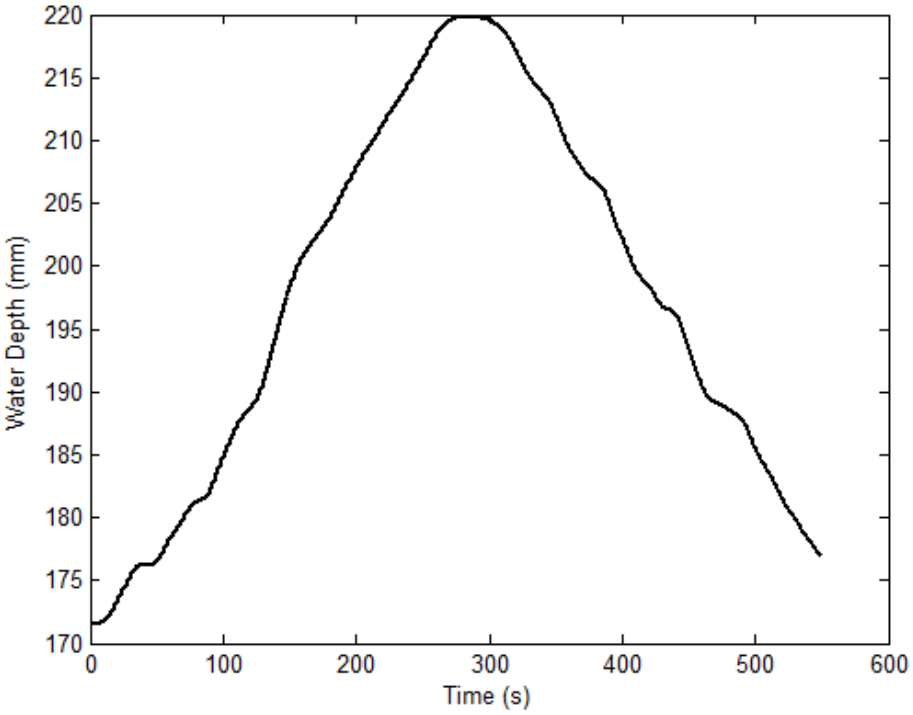

Figure H.7 : The Time Series of Water Depth During the Passage of Unsteady Flow for Set-2 (d=14 cm) Γ=0.0201.

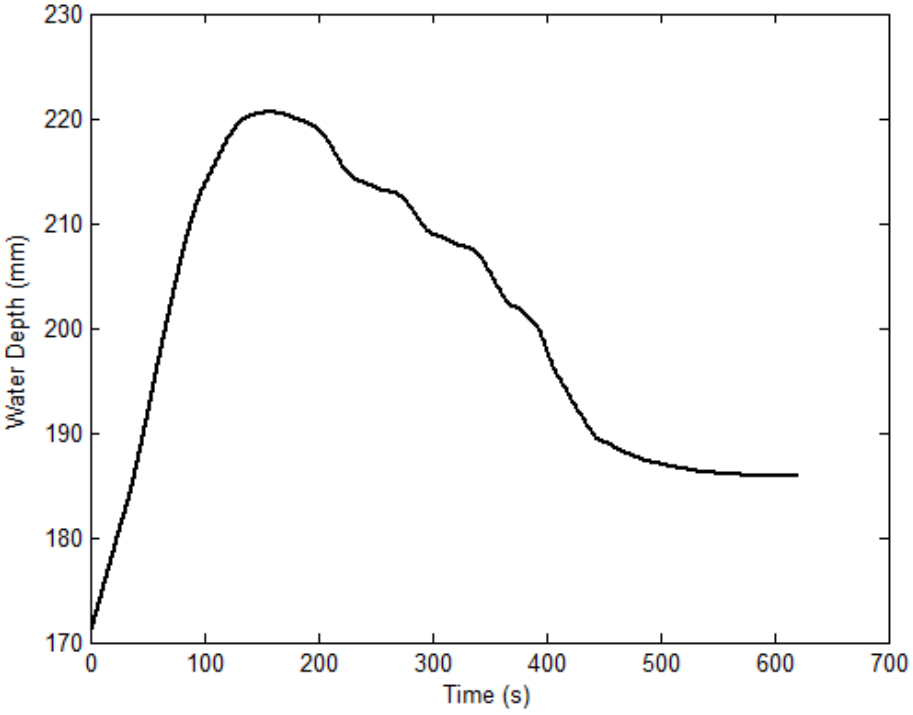

Figure H.8 : The Time Series of Water Depth During the Passage of Unsteady Flow for Set-2 (d=14 cm) Γ=0.0181.

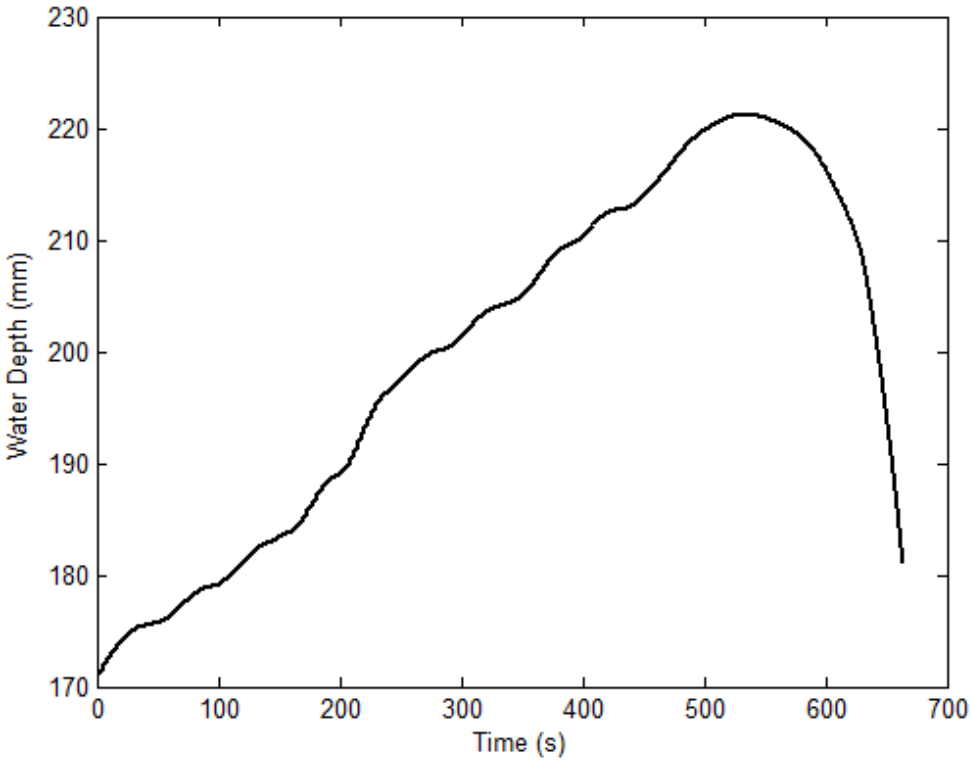

Figure H.9 : The Time Series of Water Depth During the Passage of Unsteady Flow for Set-2 (d=14 cm) Γ=0.0134.

APPENDIX I

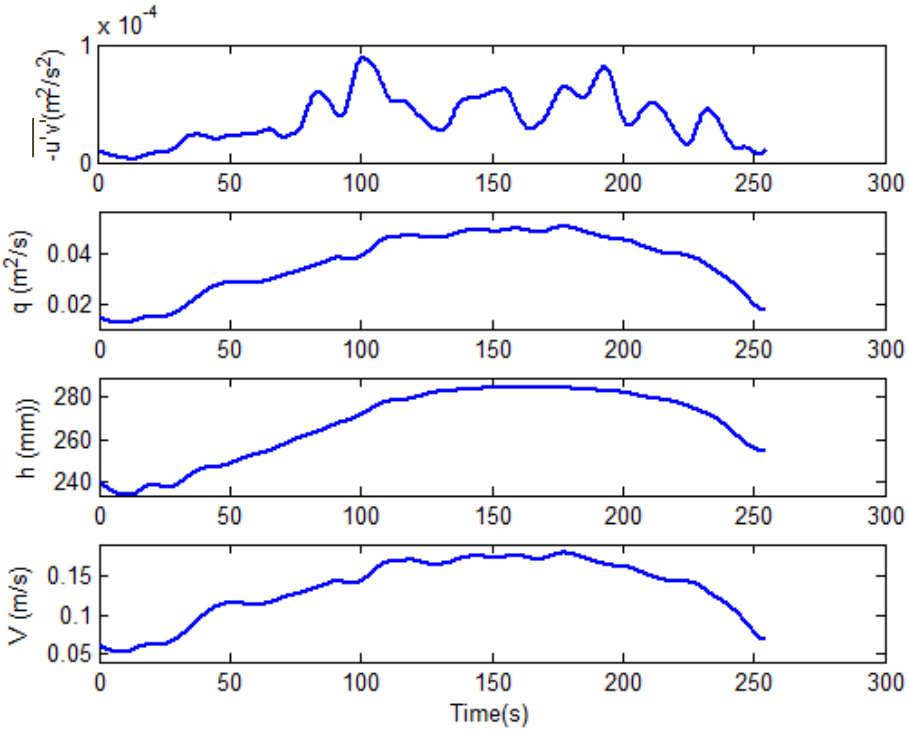

Figure I.1 : Time Variation of Hydraulic Parameters for Set-1 (d=20 cm), Γ=0.0526.

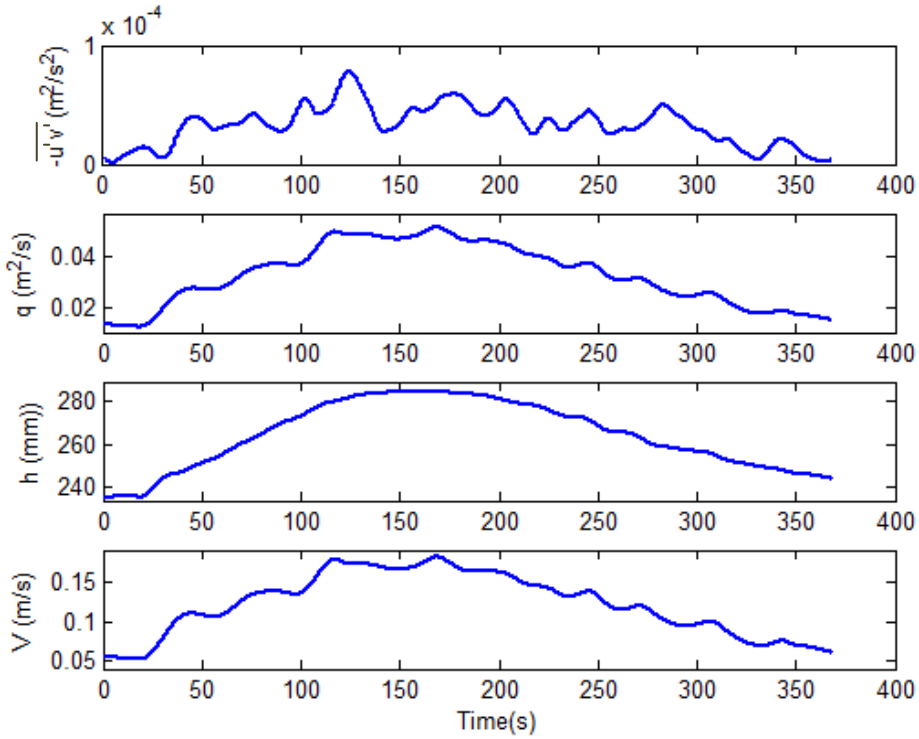

Figure I.2 : Time Variation of Hydraulic Parameters for Set-1 (d=20 cm), Γ=0.0401.

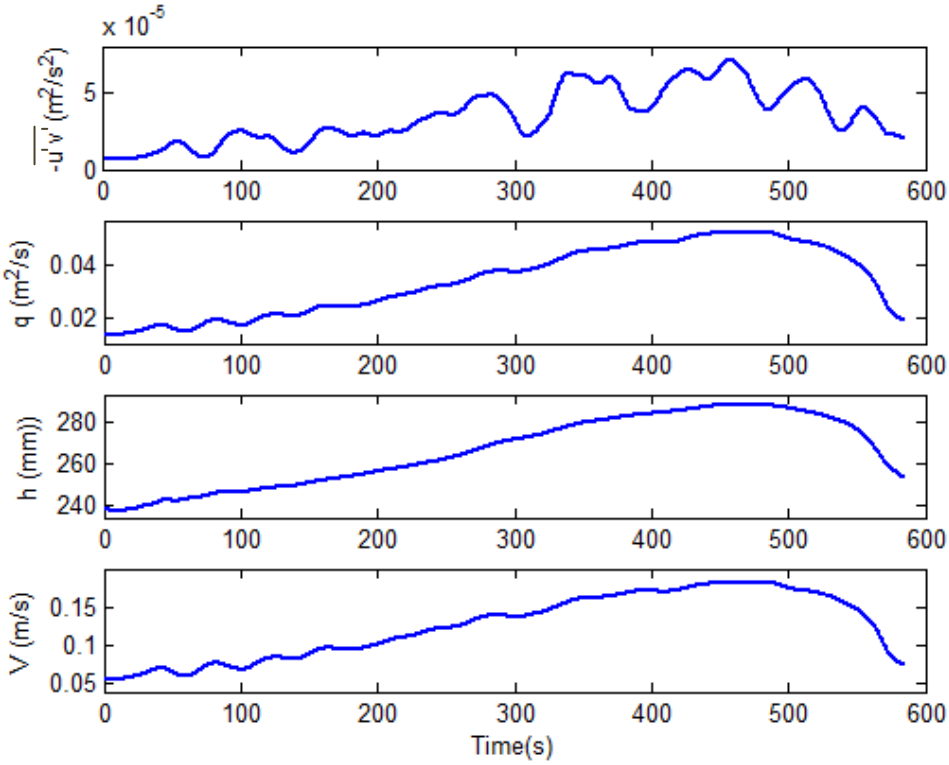

Figure I.3 : Time Variation of Hydraulic Parameters for Set-1 (d=20 cm), Γ=0.0256.

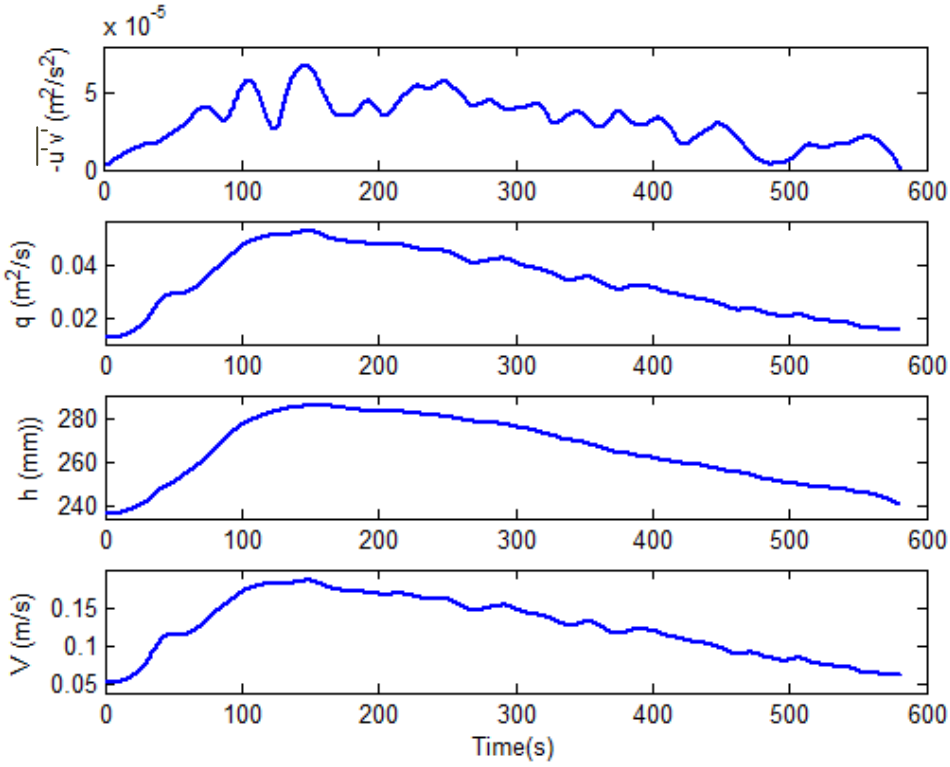

Figure I.4 : Time Variation of Hydraulic Parameters for Set-1 (d=20 cm), Γ=0.0250.

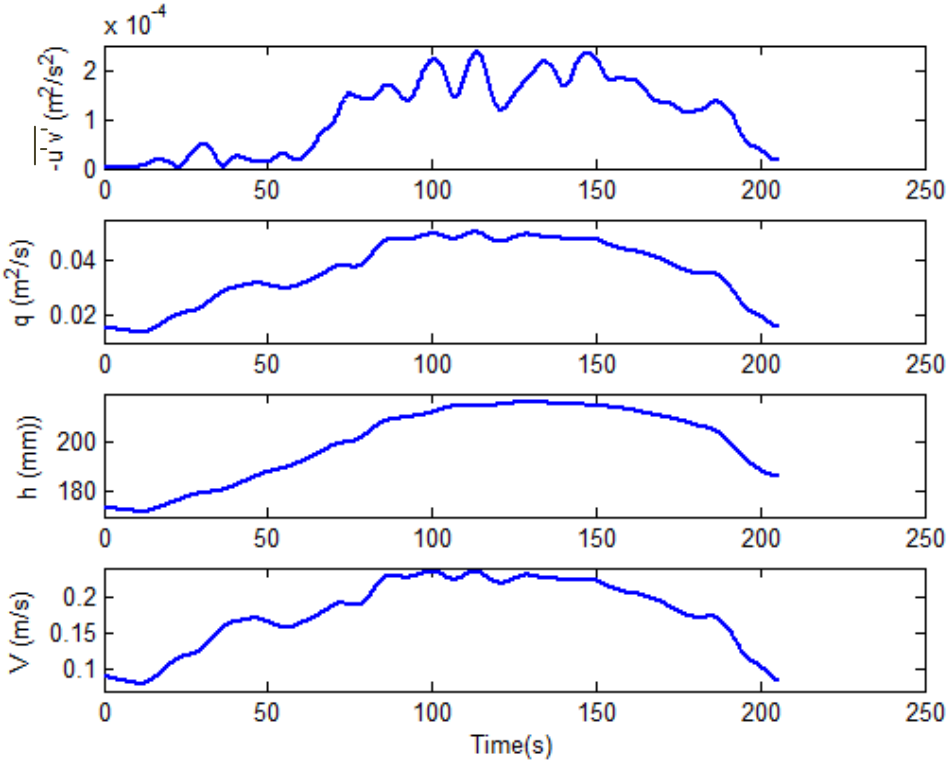

Figure I.5 : Time Variation of Hydraulic Parameters for Set-2 (d=14 cm), Γ=0.0445.

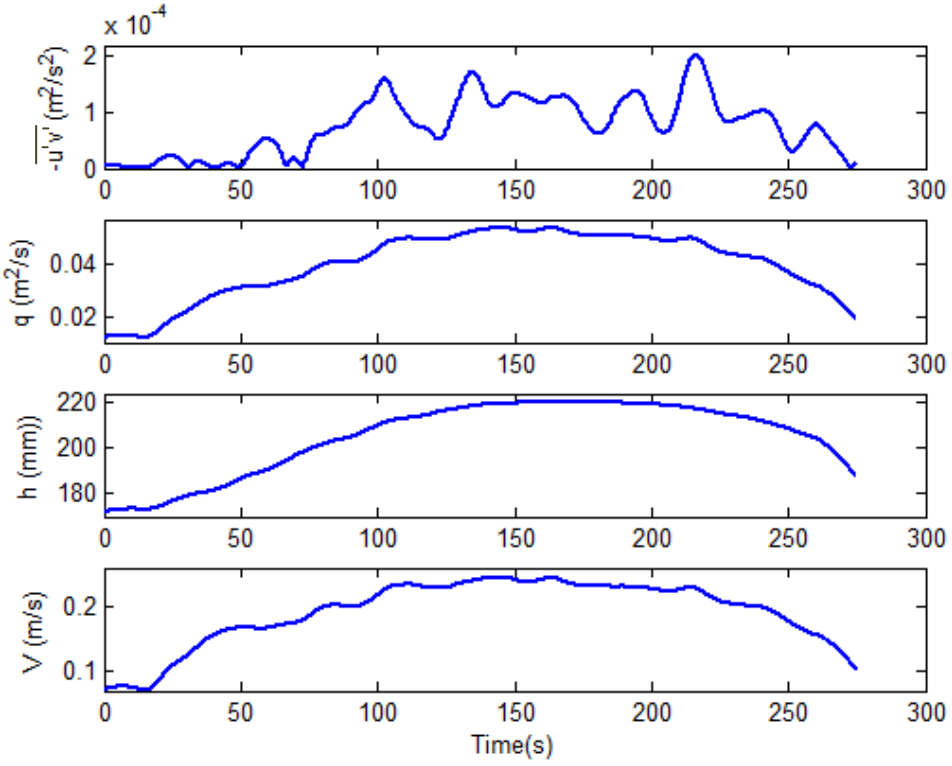

Figure I.6 : Time Variation of Hydraulic Parameters for Set-2 (d=14 cm), Γ=0.0376.

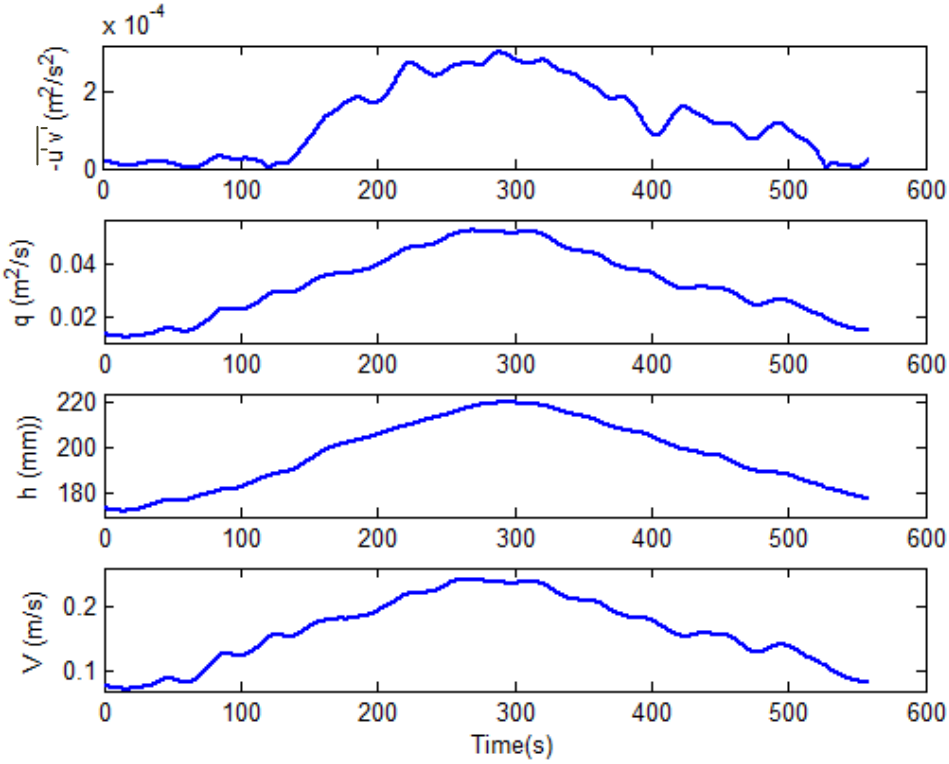

Figure I.7 : Time Variation of Hydraulic Parameters for Set-2 (d=14 cm), Γ=0.0201.

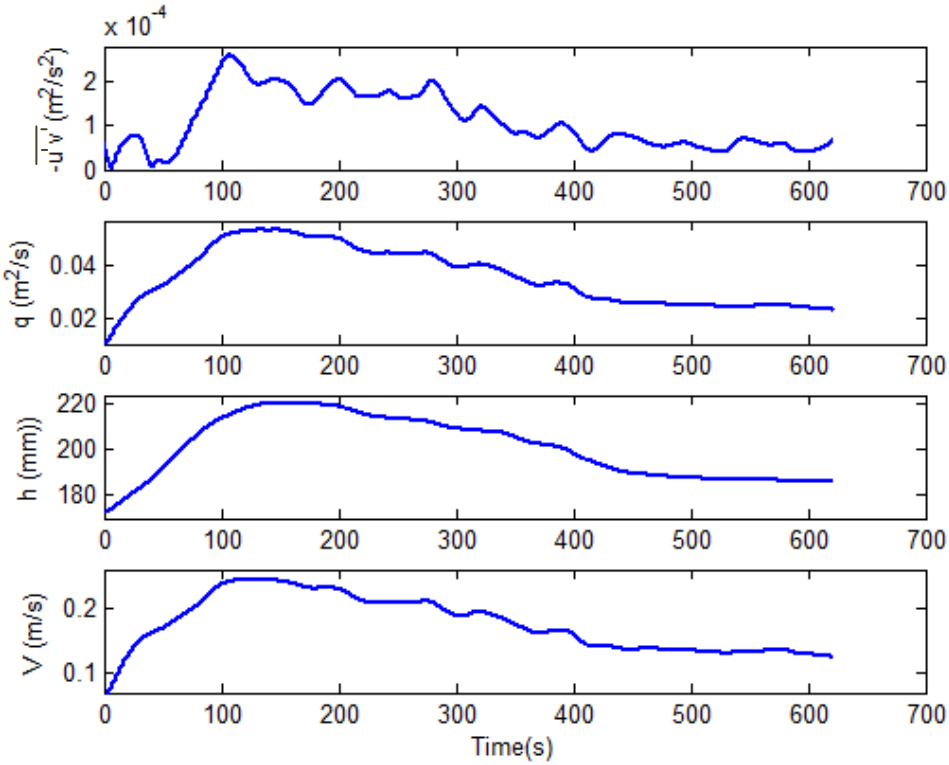

Figure I.8 : Time Variation of Hydraulic Parameters for Set-2 (d=14 cm), Γ=0.0181.

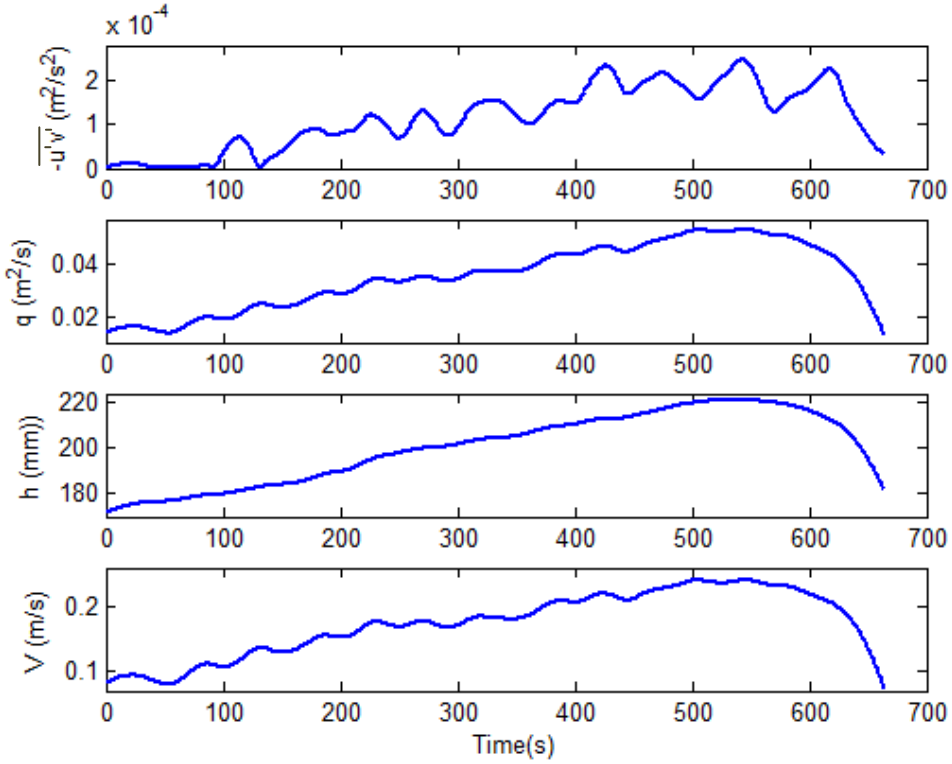

Figure I.9 : Time Variation of Hydraulic Parameters for Set-2 (d=14 cm), Γ=0.0134.

CURRICULUM VITAE

Name Surname: Eryılmaz Erdog

Place and Date of Birth: İzmir/21.11.1989

Address: Levent/ISTANBUL

E-Mail: eryilmazerdog@gmail.com

B.Sc.: Civil Engineering

Professional Experience and Rewards: Technical Office Engineer

List of Publications and Patents: -